Control of Multi-Input Converter for Hybrid Wind-Solar-Battery based System

1. (a) Name of the Principal Investigator : Dr. TAPAS KUMAR SAHA

Designation : Professor, EE Deptt.

Name of institution :National Institute of Technology Durgapur

Address : Department of Electrical Engineering,
N. I. T. Durgapur,
Durgapur, West Bengal- 713209

Contact details:
Tel. No / Mobile : 9434788171
Email : tapassahanit@gmail.com,tapas.saha@ee.nitdgp.ac.in

2. (b)Other Investigators:
Name of Co-Principal Investigator : Dr. JAYATI DEY

Designation : Associate Professor, EE Deptt.

Name of institution : National Institute of Technology Durgapur

Address : Department of Electrical Engineering,
N. I. T. Durgapur,
Durgapur, West Bengal- 713209

Contact details:
Tel. No / Mobile : 9434788173
Email : deybiswasjayati@gmail.com, jayati.dey@ee.nitdgp.ac.in

CONTENTS

Chapter1: Introduction

It is very much necessary to control the multi-input DC/DC converter connected hybrid wind-solar- storage based energy conversion system to fulfil certain objectives. The considered work will have the following advantages: 1) power from the wind turbine or the PV array can be delivered to the utility grid/stand-alone load individually or simultaneously, 2) MPPT feature can be realized for both wind energy and, PV, 3) a large range of input voltage variation caused by different wind speed, insolation and battery charge can be acceptable, and 4) state of charge (SOC) based smoothing of the output fluctuation of a wind power and PV hybrid generation system can be achieved. The controlled hybrid system can be considered as an adaptive cognition micro-units of the grid, with context awareness and fault tolerance.

The research and development in the DC/DC converter and controller will necessarily improve the wind turbine contribution of power in the system. The power supply topology with theoretical controller development will be implemented in both simulation and experimental platforms. The real time performance analysis will build the confidence to prepare a prototype for any site in India to meet the demand from its own resources.

1.1 Literature review

Yaow-Ming Chen et al. (2002) have presented a circuit topology in which two isolated dc sources are producing ac power to feed the multi input single output transformer.

There are following features in this topology

1. Magnitude of the dc voltage source can be different.
2. It ensures the voltage regulation during the failure of one source.
3. It can provide electrical isolation.
4. Authors have presented the conduction time based control of the multi input single output control utilizing phased shifted control technique

The work has been upgraded and finally presented by the same author in 2009. **Yuan-Chuan Liu et al. (2009)** synthesizes multi input converter (MIC) using basic PWM converters (like buck, boost, sepic etc.) and pulsating source cell (PSC).

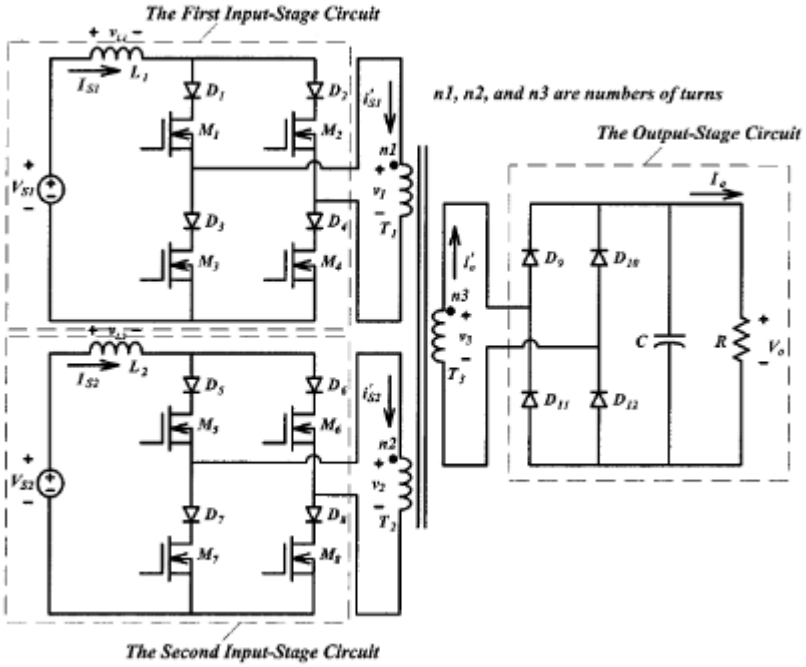

Fig. 1.1. Circuit topology of the proposed two-input current-fed full-bridge dc/dc converter [Yaow-Ming Chen et al. (2002)]

These pulsating source converters are of two types 1.PVSC and 2.PCSC

PVSC It is connected in series with any branch . and a parallel diode is connected

PCSC It is connected in parallel with any branch and a diode in series to block voltage

Quasi-MIC If any PSC is not able to transfer power from source to load but to energy buffer portion .then these type of PSC can be levelled as Quasi-MIC

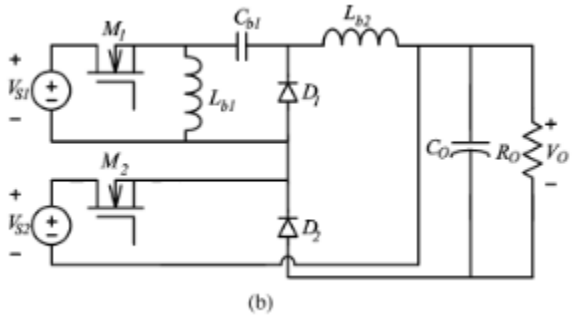

Fig. 1.2. MICs synthesized by the zeta-type PVSC with different prime converters| (b) buck boost converter. [Yaow-Ming Chen et al. (2009)]

Y. Jiao et. al. (2010) proposed a super-lift converter to achieve high voltage gains. Total "n" number of super-lift cell connected to form n-cell super-lift dc-dc converters. The operation is transformer less. It has been explained clearly that there is limitation in small signal modelling because the dynamic response is limited because high frequency component average out. In that case Sliding mode control is very helpful. Sliding surface can be chosen either from error, its integrals, double integrals but this requires comparatively larger time for system representing point to reach steady state point. This results in large current and voltage overshoot. This problem can be reduced by preparing a sliding surface consists of state variable and their error from sliding surface. This will increase the complexity in designing the controller.

Here sliding surface is chosen as

$$S = i_L + aV_o + b\int(\lambda V_o - V_{ref})dt + m\iint\left((\lambda V_o - V_{ref})d\tau\right)dt$$

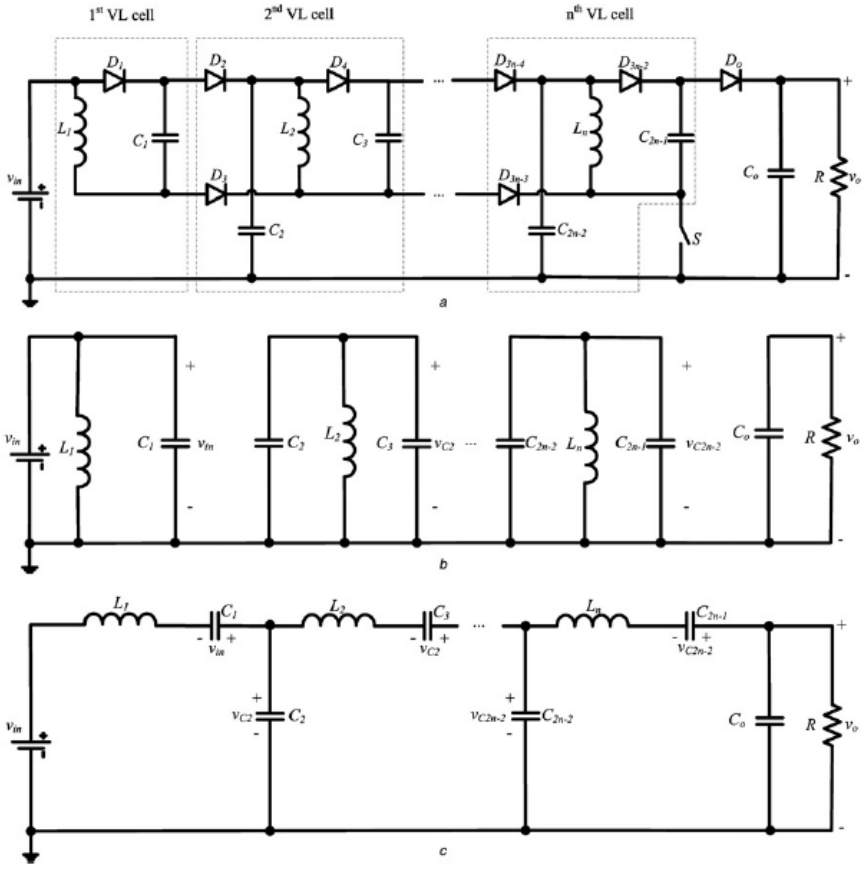

Fig. 1.3. Generalised circuit of the super-lift converters with n-cell cascaded structure [Y. Jiao et. al. (2010)]

Saeed Danyali et al. (2014) later propose new topology in multi input source system. This topology has a features of single stage power conversion. This unique feature has the ability to achieve upper hand in power loss, size. The topology is presented in Fig. 4. The middle boost converters are current bidirectional and connected to the dc-link of the common battery, while the other ones (i.e., i = 3, ..., n)are current unidirectional and fed from separate input dc sources (i.e., Vi3, ... Vin). The first aim of using the battery storage is to supply or absorb the power difference between the total generated dc power by the input dc sources and the load power. In this hybrid system, all kind of rechargeable batteries and also ultra-capacitors are applicable.

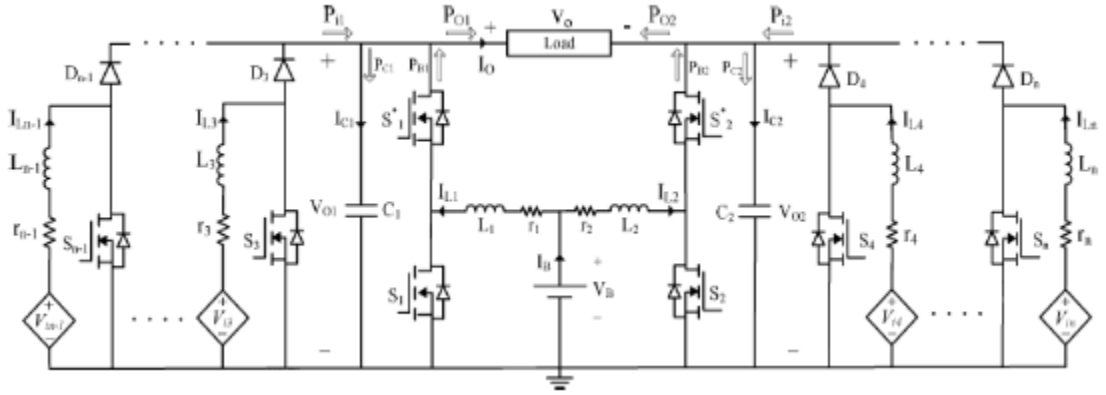

Fig.1. 4. Proposed converter structure. [Saeed Danyali et al. (2014)]

The AC signal is achieved by applying the phase shift in ripple voltage at two pole through switching sequence. C1 and C2 are value 47 μF. Small signal analysis in the system modelling has been done to achieve the control law. Control is done through pole placement control method

In overall efficiency of the system is more 90% under experimental environment.

Independent control for each input can be done with proper decoupling on the dynamics. **Mohammad Reza Banaei et. al. (2014)** has said that the topology reduces the current stress and provides the high voltage gain which is higher than the summation of input voltages. This paper also represents the total loss that occurs during the power conversion.

Proposed scheme verified against the double input converter system. In which inner converter is basically a buck-boost converter and outer one is the boost converter.

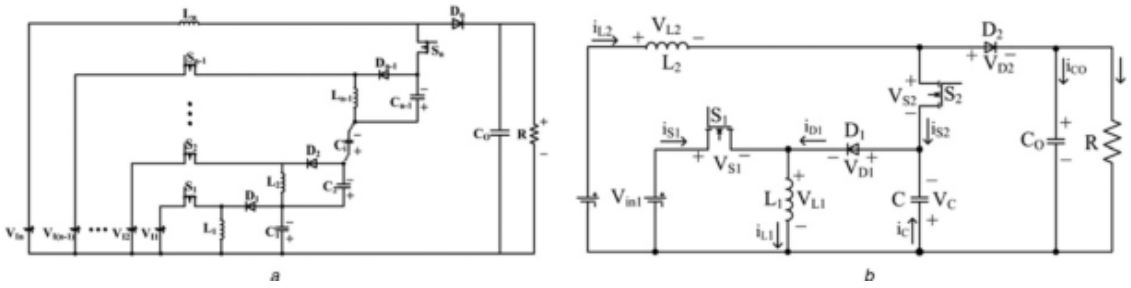

Fig. 1.5. Circuit of the proposed multi-input DC/DC converter [Mohammad Reza Banaei et. al. (2014)]

B. Mangu et. al. (2016) proposed a topology with following characters:

• Exploring a multi-objective control scheme for optimal charging of the battery using multiple sources.

• Supplying un-interruptible power to loads.

• Ensuring evacuation of surplus power from renewable sources to the grid, and charging the battery from grid as and when required.

Therefore, the MPP operation is assured by controlling IL, while maintaining proper battery charge level. IL is used as inner loop control parameter for faster dynamic response while for outer loop, capacitor voltage across PV source is used for ensuring MPP voltage. An incremental conductance method is used for MPPT.

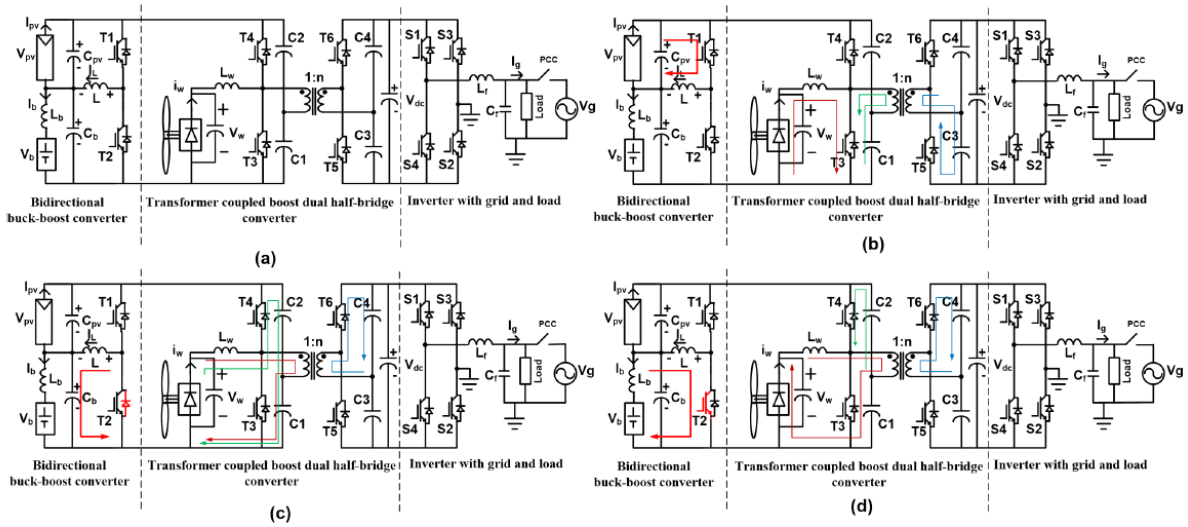

Fig. 1.6. Operating modes of proposed multi-input transformer coupled bidirectional dc-dc converter. (a) Proposed converter configuration. (b) Operation when switch T3 is turned ON. (c) Operation when

switch T4 ON, charging the capacitor bank. (d) Operation when switch T4 ON, capacitor C2 discharging [B. Mangu et. al. (2016)].

Mahdi Azizi et. al. (2016) proposed a novel converter with considerations as one of the inputs must be a battery pack, and three power switches per leg., as shown in Fig. 7. This is able to reduce number of driving circuit. The circuit operates in three mode of operation

Boost mode: lower switches must be on (s3,s6). State of other switches determine by the required output voltages. Turning off lower switches causes current to flow through antiparallel diode of lower and upper switches.

Buck mode: only the energy storage element can operate under buck mode. when middle and upper switches of the leg are conducting the energy following through inductor and battery. In the second interval that lasts for $(1 - d1)Ts$, lower switches are ON and middle and upper switches are switched ON/OFF according to the required output voltage vector.

Inverter mode: If all the lower switches are on it will deliver any desired voltage within the range. If all the lower switches are off it will only generate two level of voltages.

An S-MIC (semi isolated multi-input converter) consists of a forward-type I-PVSC(isolated pulsating voltage source cell) and a buck–boost prime converter is proposed for the hybrid PV/wind power charger system to realize the MPPT function for each PV/wind source by **Cheng-Wei Chen et. al. (2015)**. High voltage power source with large magnitude fluctuating at high rate is fed at isolated power source while small power source is fed in non-isolated manner. The scheme is shown in Fig. 8.

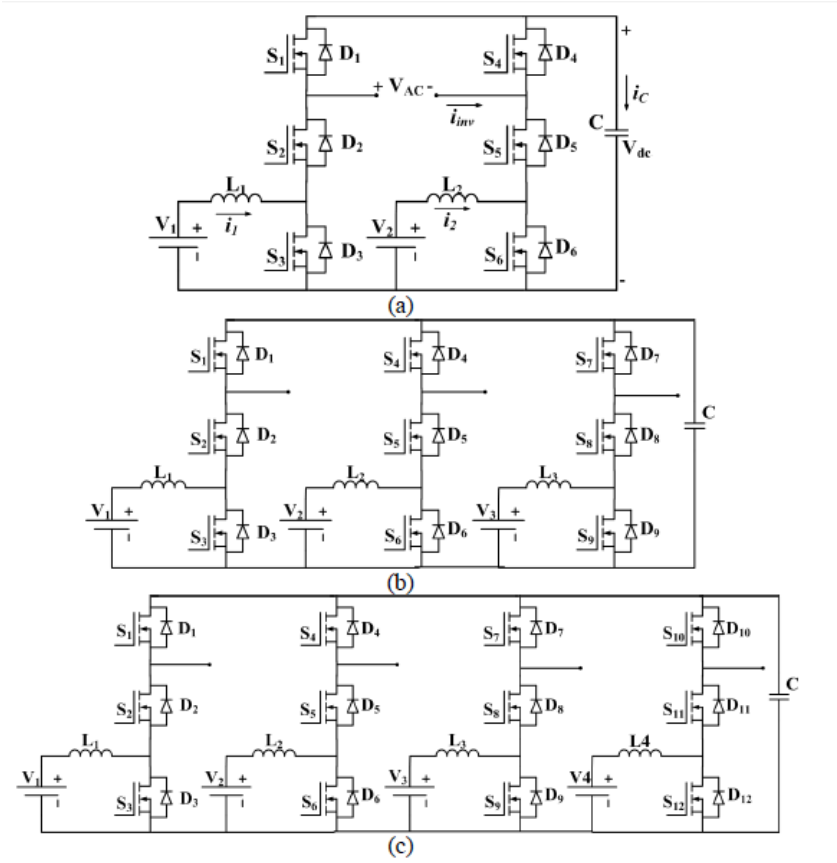

Fig.1.7. Proposed multi-input converters (a) two input converter, (b) three input converter and (c) four input converter [Mahdi Azizi et. al. (2016)]

mode	State of the switches	
I	S1 on; S2 on	D2,D3;D4 turned off; both supply energy storage component L1
II	S1 on; S2 off	D1;D3 reverse biased; wind supply the energy to inductor L1 and also to the battery
III	S1 off; S2 on	PV power source will charge the inductor L1 and energy stored in the transformer will free wheel through the source
IV	S1 off; S2 off	D2,D4 are forward biased; transformer will be reset and energy stored in the inductor will charge the battery

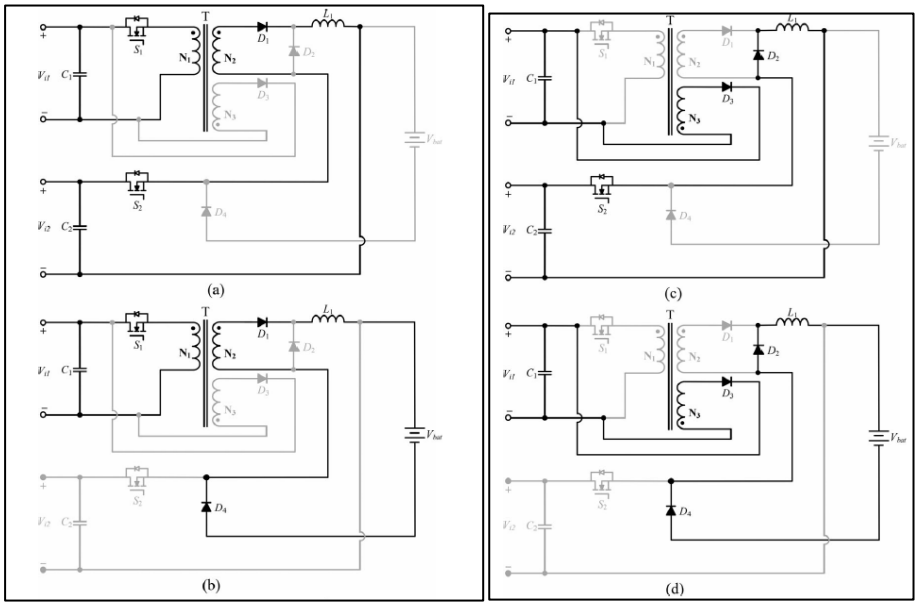

Fig. 1.8. Operation modes and equivalent circuits of the proposed hybrid PV/Wind battery charger. (a) Mode I. (b) Mode II. (c) Mode III. (d) Mode IV [Cheng-Wei Chen et. al. (2015)].

Some DC renewable energy sources are integrated to 3 level DC-DC converter by **Serkan Dusmez et. al. (2016)**. The transformer is isolating the input and output

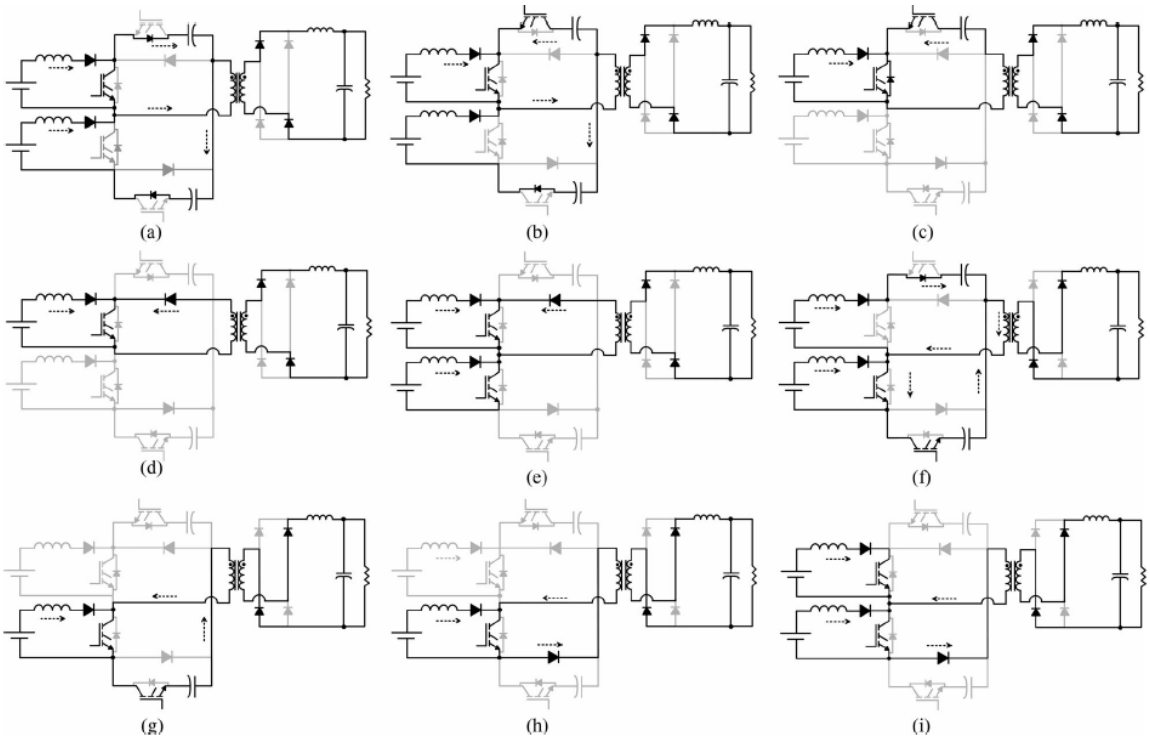

Fig. 1.9. Operation intervals of the converter. (a) Interval 1:$t < t0$. (b) Interval 2: $t0 < t < t1$. (c) Interval 3: $t1 < t < t2$. (d) Interval 4: $t2 < t < t3$. (e) Interval5: $t3 < t < t4$. (f) Interval 6: $t4 < t < t5$. (g) Interval 7: $t5 < t < t6$. (h) Interval 8: $t6 < t < t7$. (i) Interval 9: $t7 < t < t8$ [Serkan Dusmez et. al. (2016)].

Design of different component is given. Also for stable operation duty ration expressed.

Rui Ling et. al. (2016) described the synchronous buck converter is basically a buck converter with the diode replaced by the semiconductor switch. Here second order sliding mode control is presented with the help of improved sub-optimal algorithm. Sliding surface consists of only voltage error. State machine realization of sliding mode control is also described.

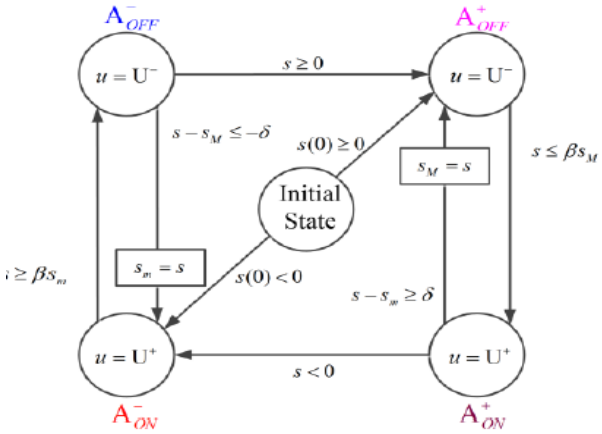

Fig.1.10. State-machine controller based on the improved suboptimal algorithm [Rui Ling et. al. (2016)]

Sliding mode dynamic controller is presented by **S. Zerkaoui et. al. (2009).**

Sliding surface chosen as $\delta_i(t) = e_i(t) + \alpha \int_0^t e_i(\tau)\, d\tau$

Where $e_i(t) = K_i\left[I_{Li} - I_{Li-ref}\right] + K_3[V_{bus} - V_{bus-ref}]$

Authors propose a non-linear switching control input $\psi_{si}(t) = -\frac{\gamma_i(t)}{H_i(t)} sign(\delta_i(t))$

This helps to estimate the upper bound of the uncertainties and external disturbance. In order to reduce the chattering 'sign' function replaced by saturation function

$$sat(\delta(t), \zeta) = \begin{cases} sign(\delta), |\delta| > 0 \& \zeta > 0 \\ \frac{\delta}{\zeta}, |\delta| \leq \zeta \end{cases}$$

Ultimately equivalent SMDC rule can be designed as $\phi_i(t) = \phi_{eqi}(t) - \frac{\gamma_i(t)}{H_i(t)} sat(\delta(t), \zeta)$

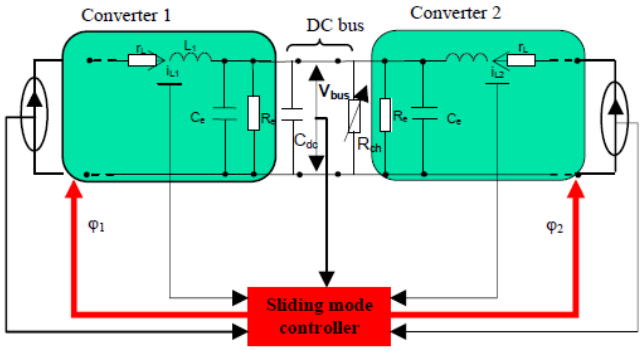

Fig. 1.11: MIMO sliding mode robust control scheme [S. Zerkaoui et. al. (2009)]

Lin Xu et al. (2016) proposed an improved optimal sizing method for WEB-HPS, which can take the following factor into the account

(i) the operating reserve capacity, (ii) the battery charge/discharge current, (iii) the charge/discharge rates and (iv) the charge/ discharge cycle.

Three important parameters are taking into account while optimizing the size.

1. loss of power supply probability (LPSP)

$$\mathrm{LPSP} = \frac{\sum_{i=1}^{N} [P_L(t_i) - (P_{\mathrm{wt}}(t_i) + P_{\mathrm{pv}}(t_i) + P_{\mathrm{bs\_dch}}(t_i)]}{\sum_{i=1}^{N} P_L(t_i)}$$

2. Fluctuaiton rate between solar and wind (D_L)

$$D_L = \frac{1}{\bar{P}_L} \sqrt{\frac{1}{N} \sum_{i=1}^{N} (P_{\mathrm{wt}}(t_i) + P_{\mathrm{pv}}(t_i) - P_L(t_i))^2}$$

3. power fluctuation (D_{gs})and standard deviation (STD)

Pandurangan Shanthi et. al. (2017) employs the circuit topology, consists of two converters, grid side converters and wind side converter. DC bus voltage reference is generated through MPPT controller which is applied on PV system. With the Vref and the output voltages of WSC the error signal fed at SDM (synchronous detecting method) through PI controller. Then there are other two

signal i.e. voltages of wind generator and input current of PMSM are also fed at SDM. From SDM reference current for WSC generated.

Total generated power and grid side current and voltages are fed at GSC side SDM from which reference current for GSC generated .Then hysteresis controller applied on ($I_{tref} - I_{gxyz} - I_{xyz\_gsc}$) .

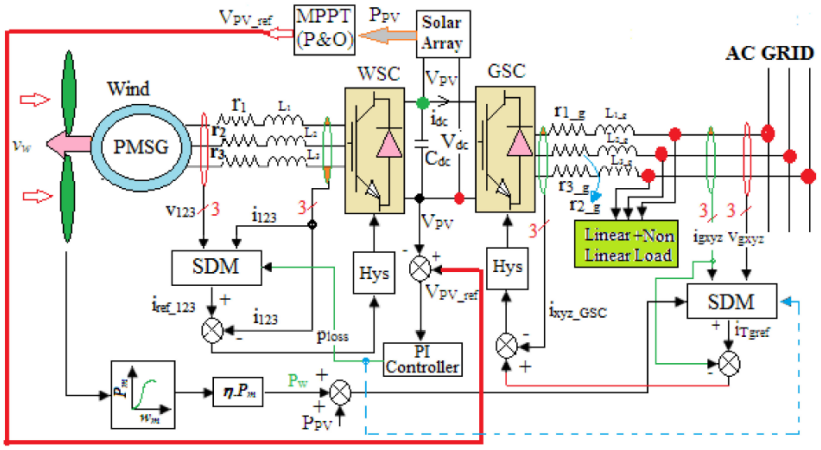

Fig. 1.12. Schematic representation of wind/PV hybrid system [Pandurangan Shanthi et. al. (2017)]

Some other basic controllers are also developed in the literature. Interestingly **Veerachary Mummadi et. al. (2008)** integrated double buck-boost converter in the work. Low voltage source is controlled by current controlled loop while the high voltage source is controlled by voltage controlled current loop. Relationship between states and duty ratio under small signal variation is established.

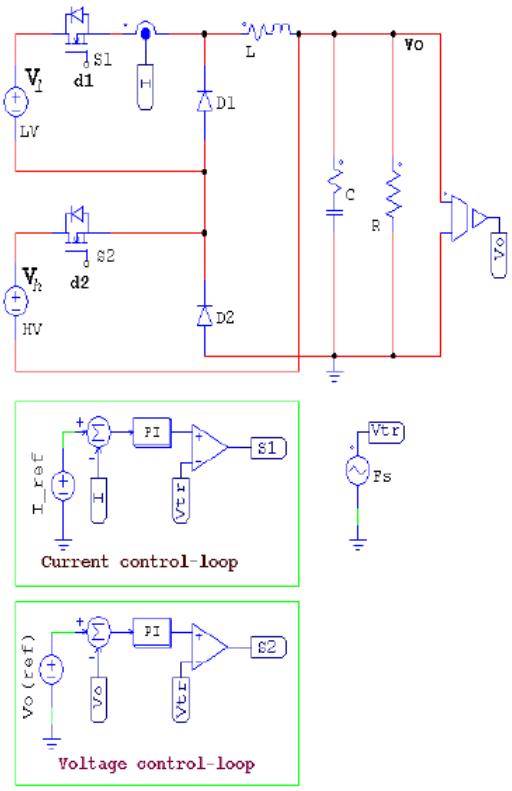

Fig. 1.13. Control of Multi-input Buck-Boost Converter [Veerachary Mummadi et. al. (2008)]

Chapter 2: Modelling of the system

In this work the proposed multi-input dc–dc converter is the fusion of the buck-boost and the buck converter with a battery storage based generation system at the inverter output. Syntheses of the multi-input dc–dc converter will be done by inserting the pulsating voltage source of the buck converter into the buck-boost converter. In order not to hamper the normal operation of the buck-boost converter and to utilize the inductor for the buck converter, the pulsating voltage source of the buck converter must be series-connected with the output inductor.

The system consists of the systems as per the following figure:

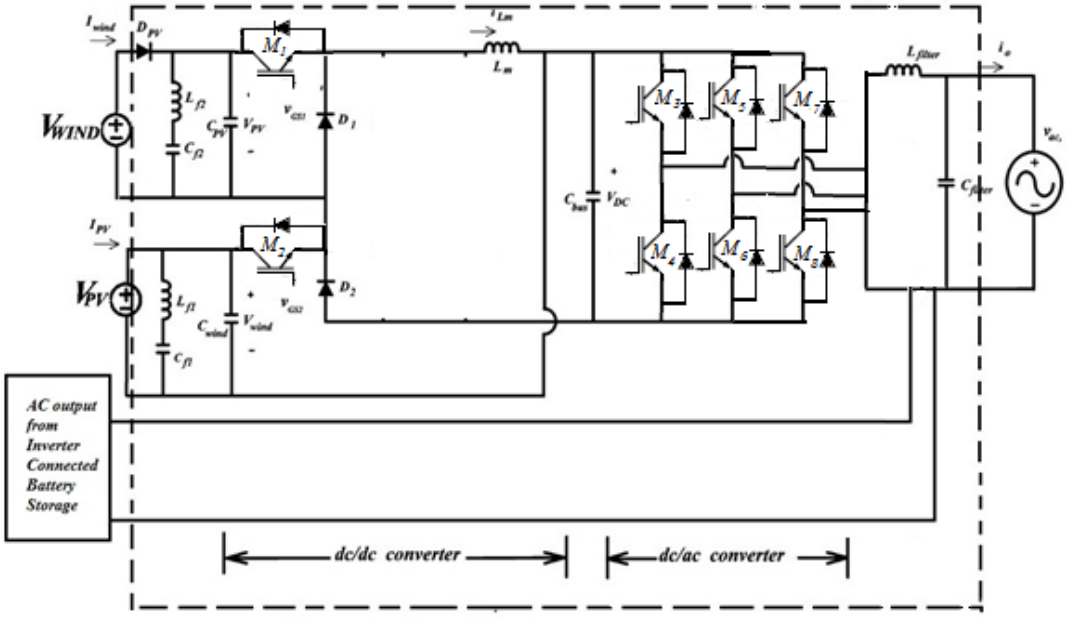

Fig.2.1: The multi-input inverter topology to connect wind-solar-storage based system

Modelling of the system components has been completed. The transfer function of the multi input converter (MIC) is found as:

The transfer function is developed as:

$$[G]=\begin{bmatrix} g_{11} & g_{12} \\ g_{21} & g_{22} \end{bmatrix}=\begin{bmatrix} \frac{\hat{v}_O}{\hat{d}_1} & \frac{\hat{v}_O}{\hat{d}_2} \\ \frac{\hat{i}_{LO}}{\hat{d}_1} & \frac{\hat{i}_{LO}}{\hat{d}_2} \end{bmatrix}=\tilde{C}\left(SI-\tilde{A}\right)^{-1}\tilde{B}+\tilde{D} \qquad (1)$$

Where

$$g_{11}=\frac{\hat{v}_O}{d_1}=\frac{\frac{(1-D_2)V_H}{LC_O}}{S^2+\frac{S}{R_OC_O}+\frac{(1-D_2)^2}{LC_O}},\ g_{12}=\frac{\hat{v}_O}{d_2}=\frac{\frac{(1-D_2)(V_C+V_{LO})}{LC_O}-S\frac{I_L}{C_O}}{S^2+\frac{S}{R_OC_O}+\frac{(1-D_2)^2}{LC_O}}$$

$$g_{21}=\frac{\hat{i}_{LO}}{d_1}=\frac{D_2\left(S+\frac{1}{R_OC_O}\right)\frac{V_H}{L}}{S^2+\frac{S}{R_OC_O}+\frac{(1-D_2)^2}{LC_O}},\quad g_{22}=\frac{\hat{i}_{LO}}{d_2}=\frac{D_2\left(S+\frac{1}{R_OC_O}\right)\left(\frac{V_C+V_{LO}}{L}\right)-\frac{D_2(1-D_2)I_L}{LC_O}}{S^2+\frac{S}{R_OC_O}+\frac{(1-D_2)^2}{LC_O}}+I_L$$

The complete system is simulated in MATLAB SIMULINK environment as follows:

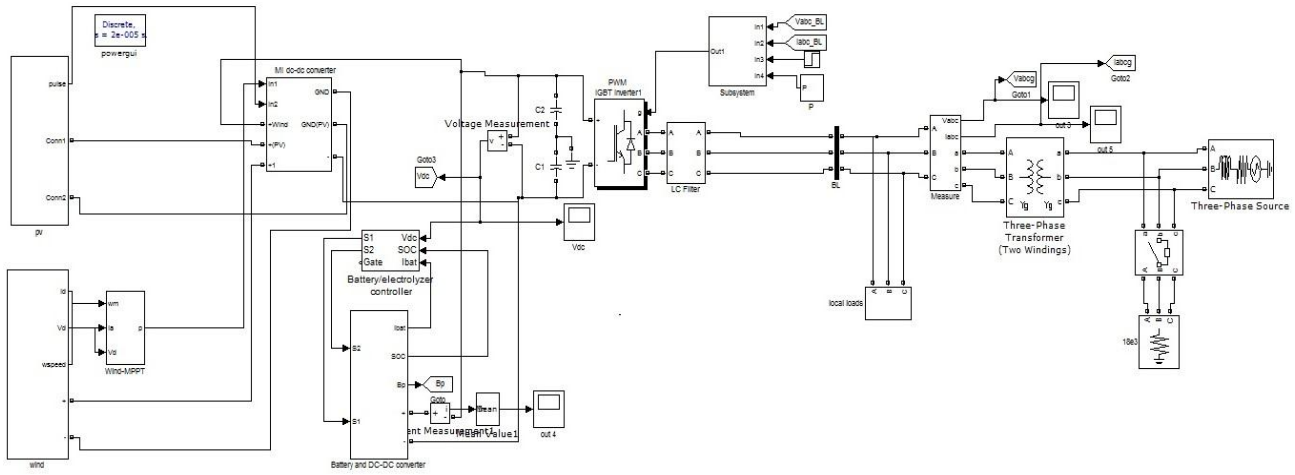

Fig. 2.2: The MIC with proposed PV and WIND system based grid connected simulation model.

The variation in the output voltage with the system is found in open loop as:

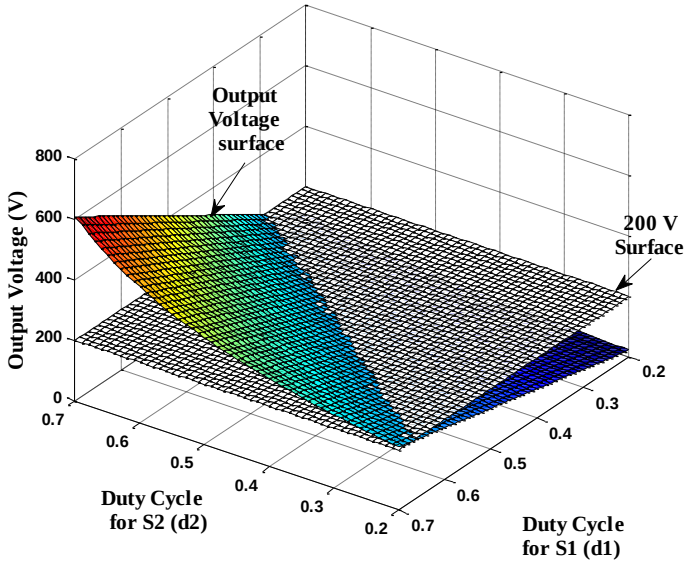

Fig. 2.3: Variation in output voltage for different duty ratio of the devices

2.1 Hardware fabrication of the system

The system shown in Fig. 2.1 is fabricated in hardware and shown in the Fig. 2.4

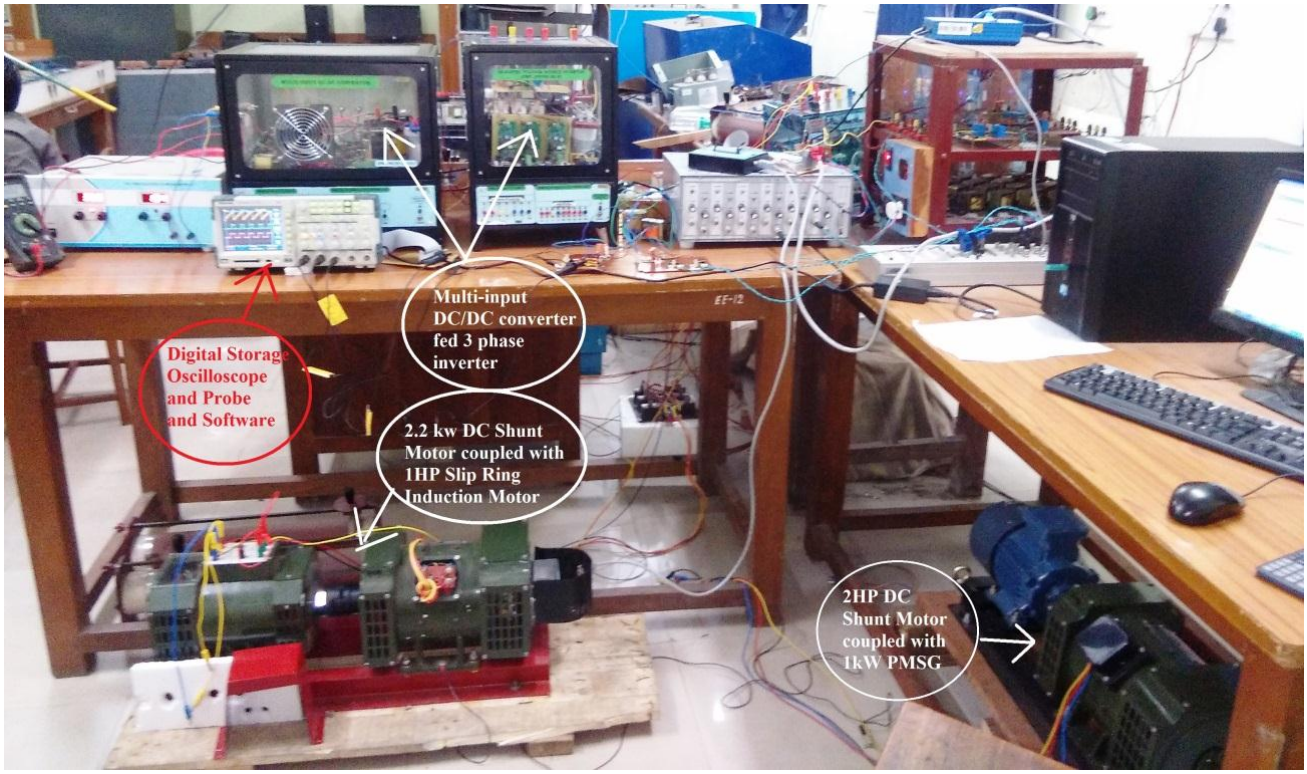

Fig. 2.4: Laboratory prototype of the proposed system

Chapter 3: Bifurcation Analysis of the system

A controller is developed to carry the bifurcation analysis.

A modified hysteresis band based control scheme is used to control the output voltage of the converter. The error signal is amplified in first stage of the controller, and considered as the control signal in next stage. The control signal is compared with a carrier wave signal for generation of PWM signal for S_1.

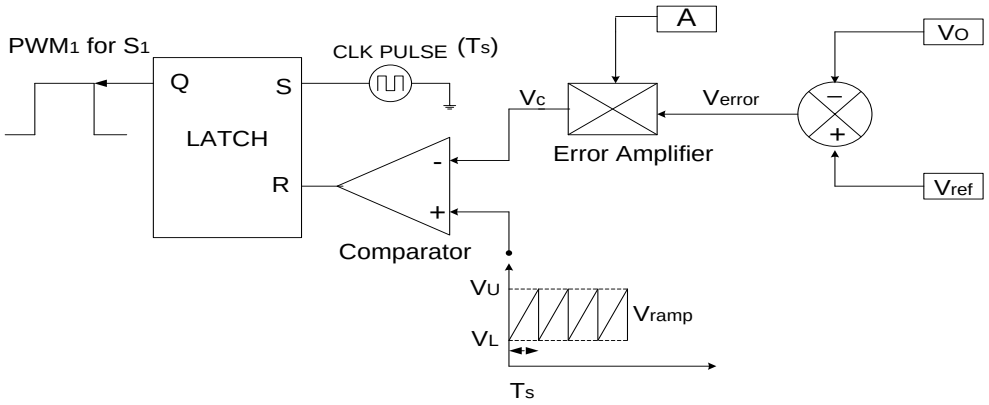

Fig. 3.1: Voltage Mode Controller for PWM1

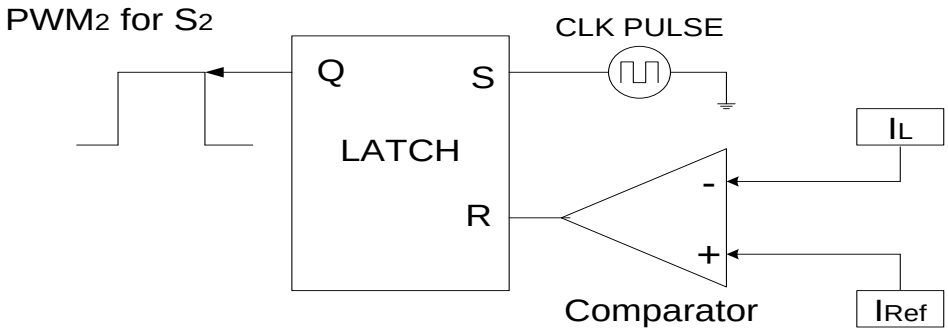

Fig. 3.2: Current Mode Controller for PWM2

The MIC is represented using discrete time mapping model. This model is numerically iterated to develop the bifurcation diagram for this converter. These diagrams convey the information about

bifurcation path of this converter. Bifurcation diagrams are the basic tool to study the change in the system behaviour in response to the variation of control parameters.

Fig 3.3 (a) represents current bifurcation diagram and Fig 3.3 (b) represents voltage bifurcation diagram. From both of these bifurcation diagrams one can infer that,

As the reference current changes, at its value more than 4.25A the converter enters period-2 bifurcation region and after the value of 4.65A the converter enters period-4 bifurcation region.

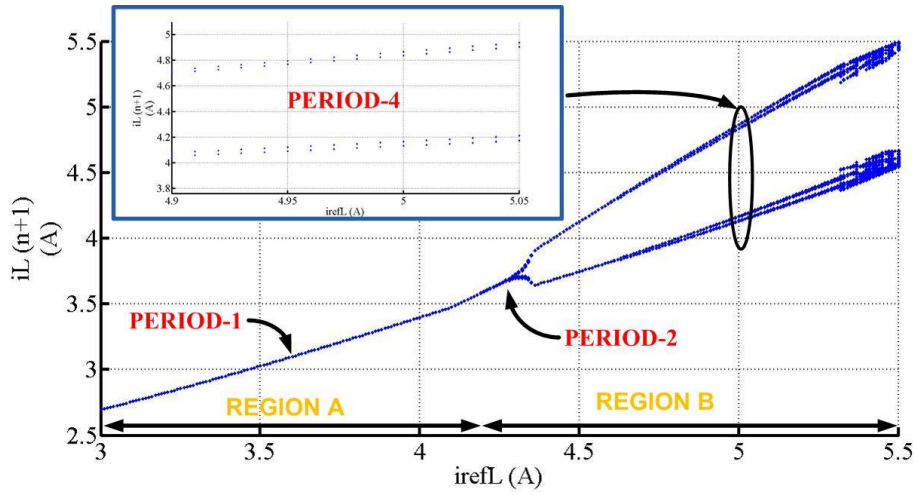

(a)

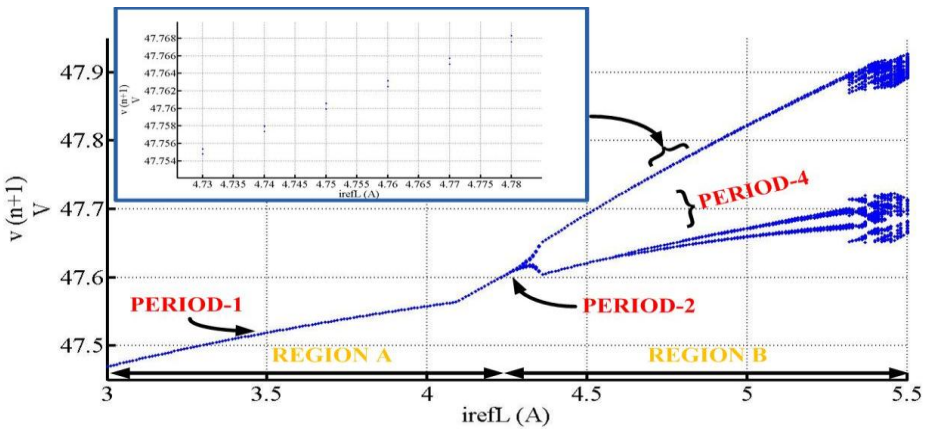

(b)

Fig 3.3 Bifurcation diagram for variation of I_{refL} *with* $V_1 = 60V, V_2 = 30V$ *and* $V_{ref} = 48V$

(a) Current and (b) Voltage Bifurcation diagram.

Implementation of the control in simulation environment has been accomplished successfully.

The period 1, period 2, and period 4 operations are shown for the inductor currents as follows.

Case 1: Inductor current reference is set at 3.6A and voltage reference is kept at 48V

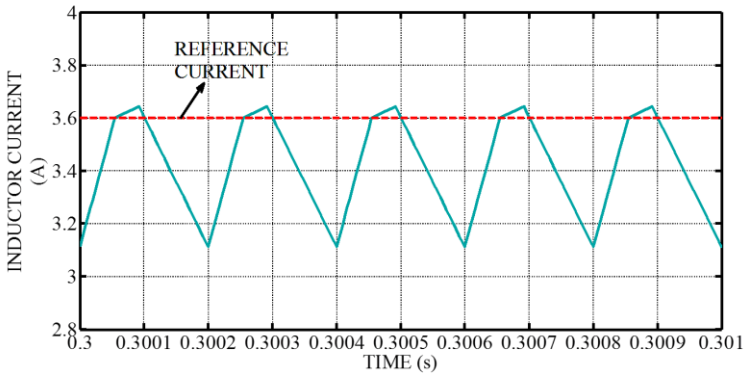

Fig 3.4: Inductor current at $I_{refL} = 3.5A \, and \, V_{ref} = 48V$

Case 2: Inductor current reference is set at 4.6A and output voltage reference is set at 48V

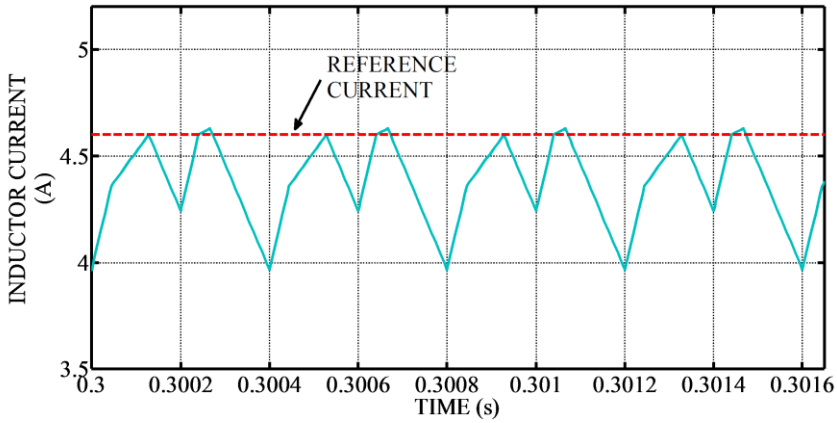

Fig 3.5: Inductor current at $I_{refL} = 4.6A \, and \, V_{ref} = 48V$

Case 3: Inductor current reference is set at 5A and voltage reference is kept at 48V

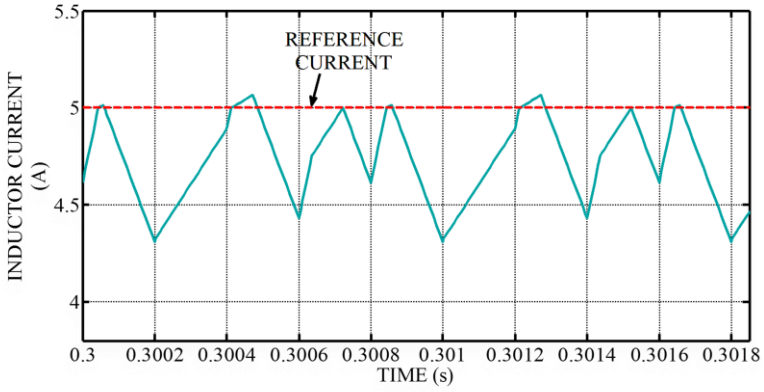

Fig. 3.6: Inductor current at $I_{refL} = 5A \, and \, V_{ref} = 48V$

Investigation of Nonlinear Phenomena of MIC in Real-time Environment

In order to verify the different nonlinear phenomena of the considered converter, an experimental scheme has been adopted.

The hardware results with the same cases are presented here:

Case 1: Inductor current reference is set at 3.65A, reference voltage set at 48V

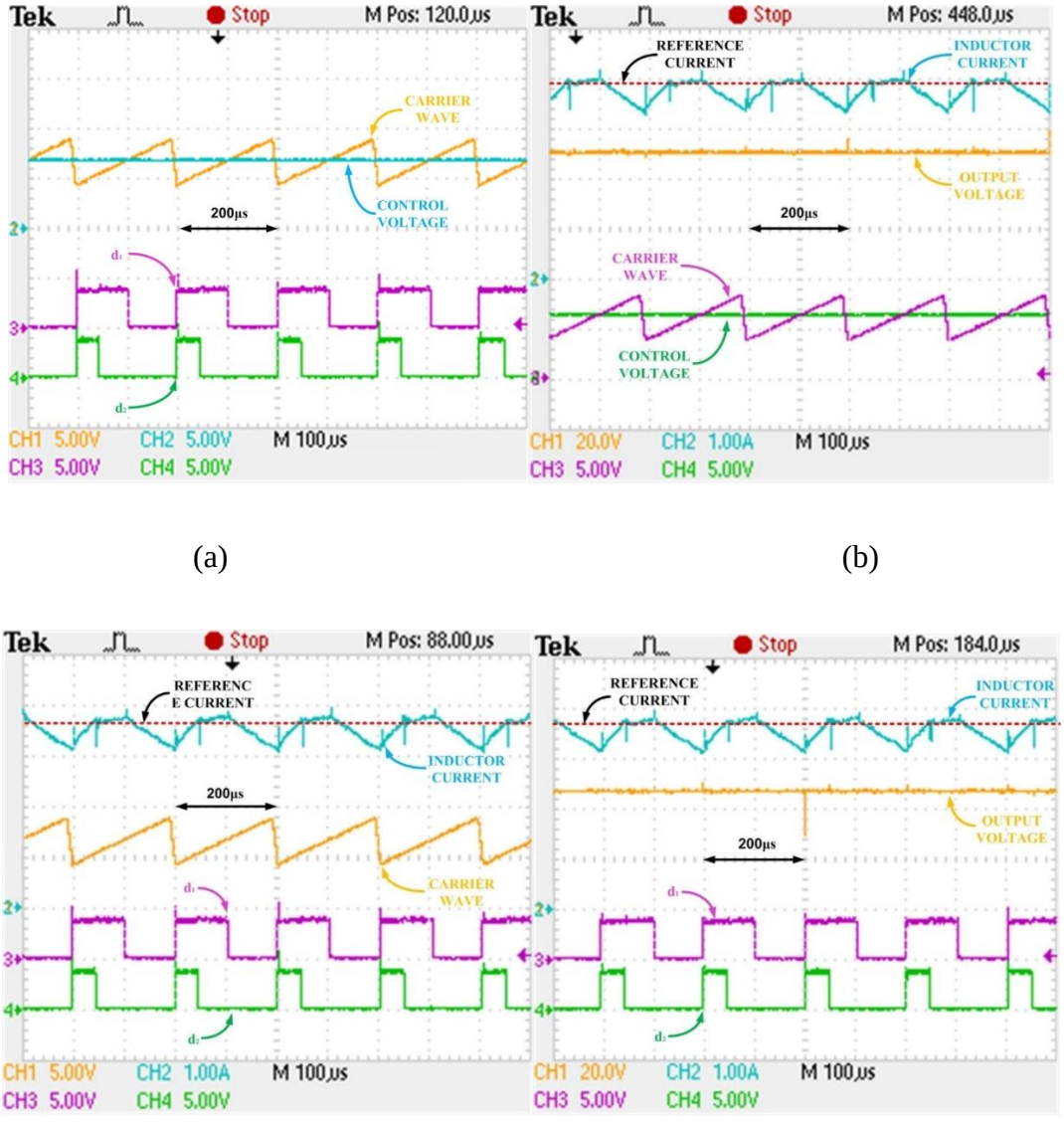

Fig. 3.7: (a), (b), (c) and (d) are hardware results for reference current 3.65A,

Here it can be observed that, for this reference current the converter shows period-1 operation.

Case 2: Inductor current reference is set at 4.64A, reference voltage set at 48V

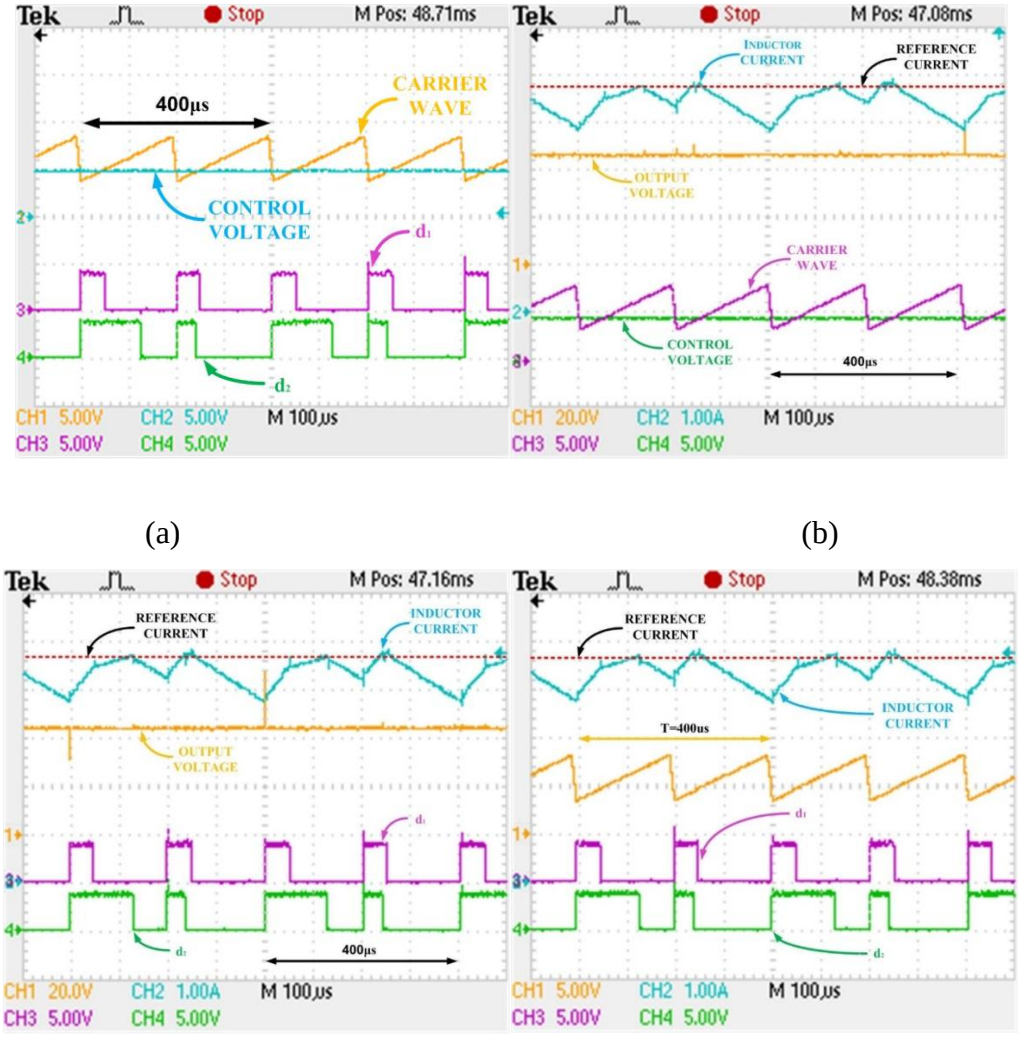

Fig.3.8: (a), (b), (c) and (d) are hardware results for reference current 4.64A

Here it is observed that, for this reference current the converter shows period-2 operation.

Case 3: Inductor current reference is set at 5.25A, reference voltage set at 48V

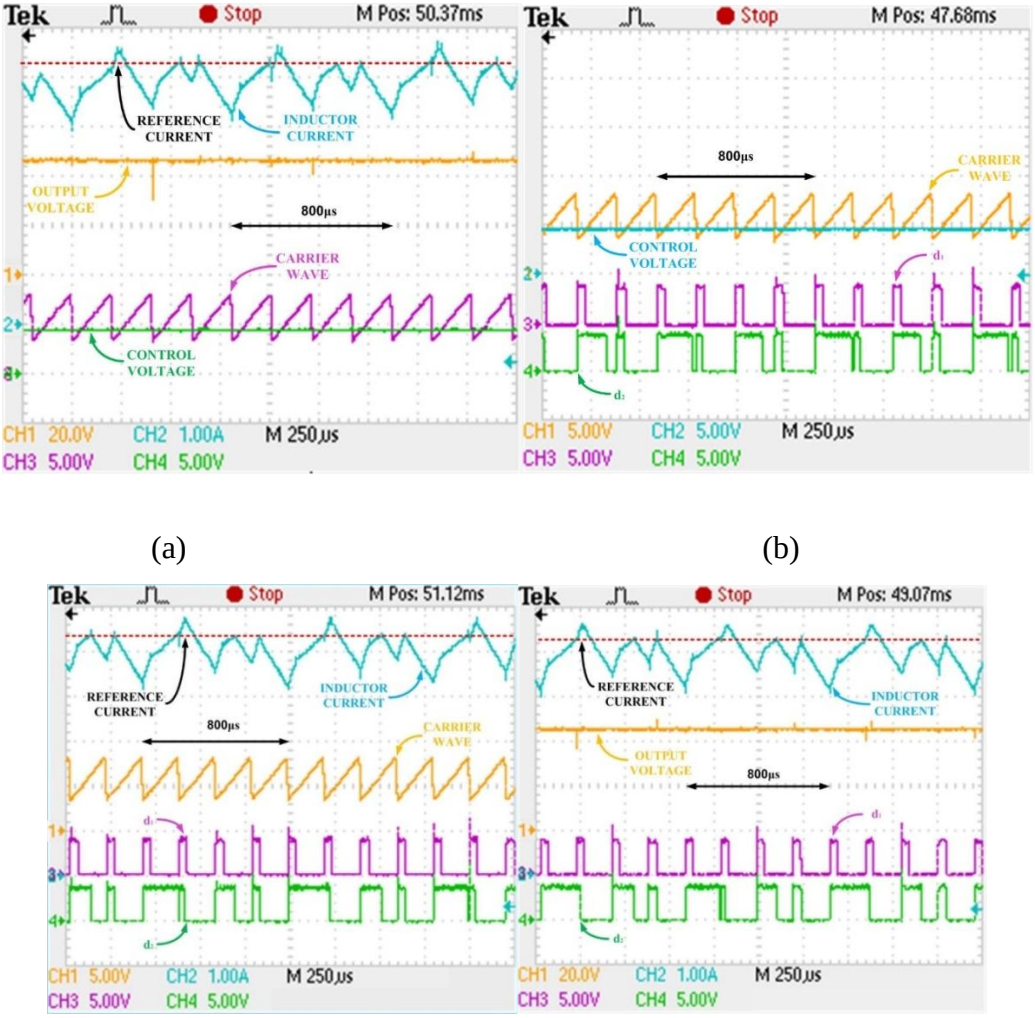

(a) (b)

(c) (d)

Fig.3.9: (a), (b), (c) and (d) are hardware results for reference current 4.64A

Here for this reference current the converter shows period-4 operation.

Chapter 4: Control of the system

4.1 PI Controller

A decoupler based PI controller is developed.
To eliminate the effect of the cross-coupling transfer function the decoupler is proposed and the complete structure is presented in Fig. 4.1.

$$[D]=\begin{bmatrix} d_{11} & d_{12} \\ d_{21} & d_{22} \end{bmatrix}=\begin{bmatrix} -\frac{g_{22}}{g_{21}} & 1 \\ 1 & -\frac{g_{11}}{g_{12}} \end{bmatrix} \quad (4.1)$$

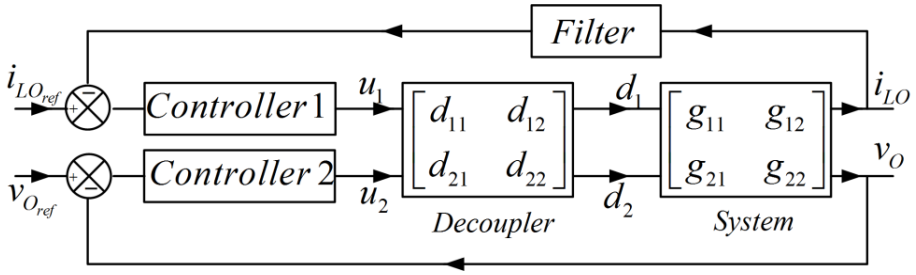

Fig.4.1. Structure of the close loop control of the Multi Input converter

The current controller (k1) is designed with gain cross over frequency 468 rad/sec and phase margin 62.8º. The voltage controller (k2) is designed with gain cross over frequency 300 rad/sec and phase margin 64.2º.

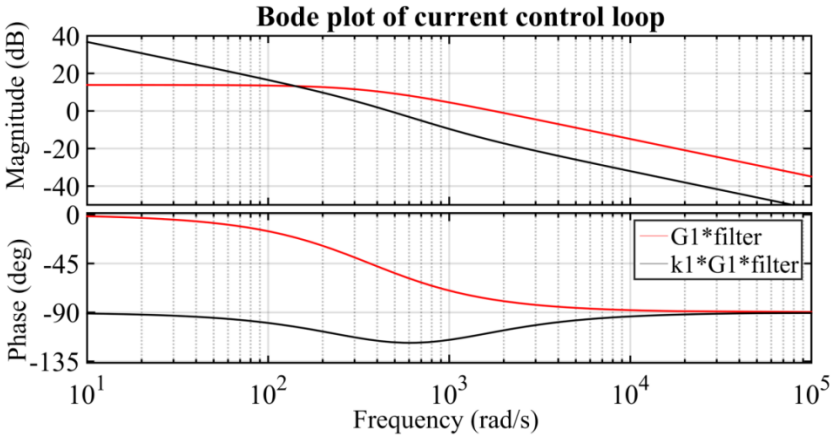

Fig. 4.2. Bode plot of current control loop

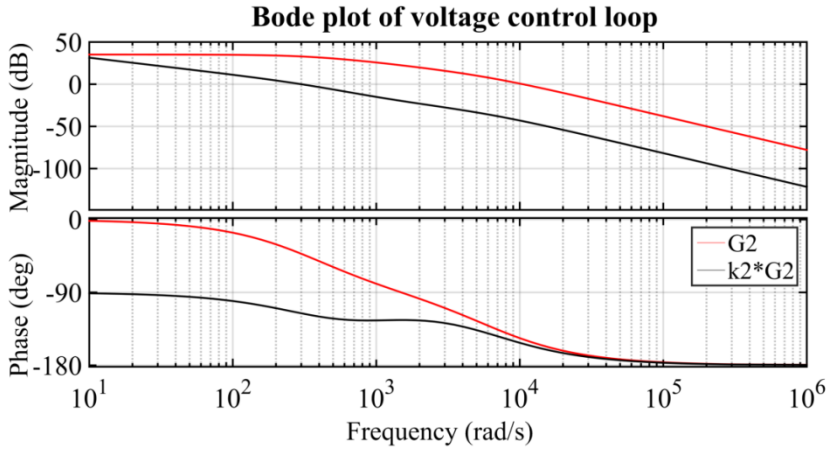

Fig. 4.3. Bode plot of voltage control loop

Implementation in Simulation Environment

The performance of the converter is investigated through implementation in MATLAB-SIMULINK environment. The system parameters are tabulated in TABLE I.

To observe the performance of the controller during variation in reference voltage command, voltage reference changes from 48 volt 58 volt at 0.7sec, and it has changed again to 48 volt at 0.9secc.

TABLE I

Parameter Values		
Sl.No.	**Parameter**	**Value**
1	High Voltage Source	60 V
2	Low Voltage Source	30 V
3	Inductor	1 mH
4	Capacitor	470 μF
5	Switching Frequency	20 KHz
6	Load Resistance	19.2 ohm

During this period, the output voltage settles within 18 msec with an overshoot of 1.2%. Further, at 0.9 sec the output voltage reaches 48 V within 20msec with undershoot of 2.29%. The waveforms of output voltage, load current, source current of the low voltage source, duty ratio d_1 and d_2 have been shown in Fig 4.4, Fig 4.5, Fig 4.6 and Fig 4.7, respectively. The low voltage source current maintains the reference level, 1A, with some small disturbances, as shown in Fig. 4.6. The disturbances in low voltage source current, during increment and decrement in reference output voltage, reaches 10%, and settled within 16 msec. The decrement in d_2 in Fig. 4.7 ensures the maintenance of power delivery level of low voltage source. The increment in the output voltage and output power, thus, is supported by high voltage source only.

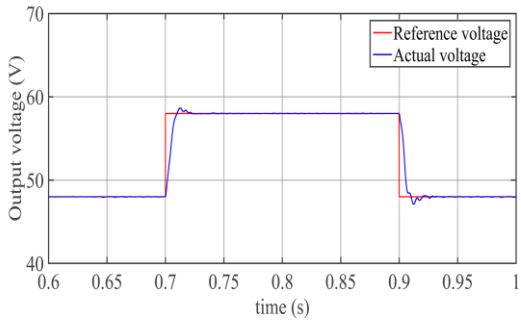

Fig. 4.4.. Reference voltage and output voltage during variation voltage command

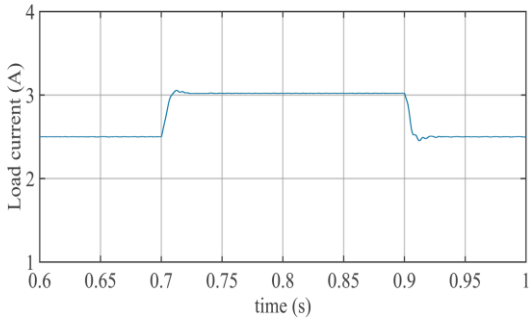

Fig. 4.5. Load current during variation voltage command

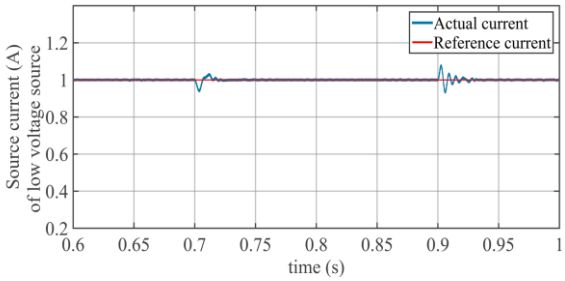

Fig. 4.6. Source current of low voltage input during variation of voltage command

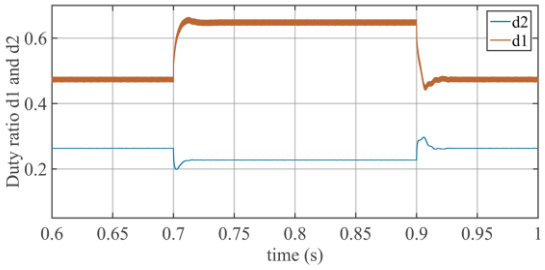

Fig. 4.7. Duty ratio d_1 and d2 during variation in voltage command

To verify the effectiveness of the controllers, 50% load variation is introduced keeping the voltage reference at 48V and current reference of low input source at 1A. The load current has been increased from 2.5A to 3.75A at 0.2 sec. Under this change, the output voltage undergoes a transient and settles to 48V at 18.2msec with an overshoot of 4.1%. At 0.4 sec the load is returned back to previous value. Consequently, the output voltage settles to 48V within 26msec with undershoot of 4.1%. The waveforms of voltage, load current, source current of the low voltage source, duty ratio d_1 and d_2 have been shown in Fig. 4.8, Fig. 4.9, Fig. 4.10 and Fig. 4.11 respectively. The increment in load power in this case also been supported by high voltage source only. The low voltage source current is maintained at the reference level, as shown in Fig. 4.10. The disturbances, created because of these load variations are settled within 28 msec. The duty ratio d_2 decreases as shown in Fig. 4.11.

It is thus clearly observed that the controller is performing successfully even under high load variation maintaining the output voltage as well as the current of the low voltage source at their corresponding reference value.

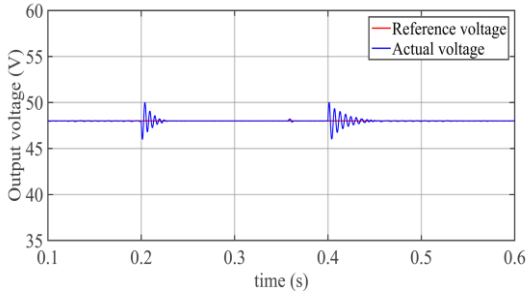

Fig. 4.8. Output voltage

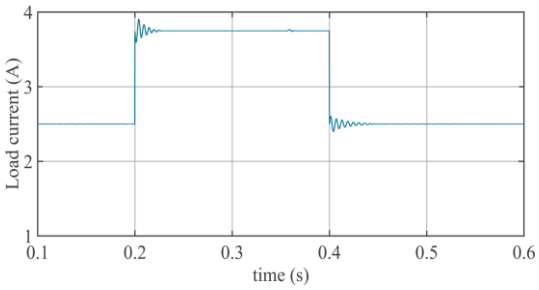

Fig. 4.9. Load current during variation in load

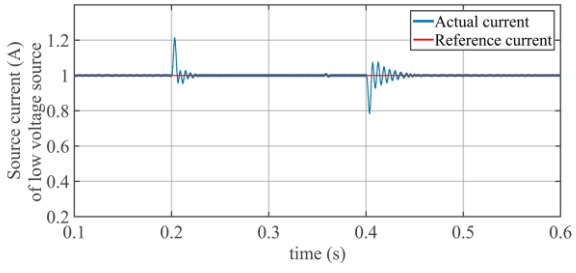

Fig. 4.10.Source current of low voltage input during variation in load

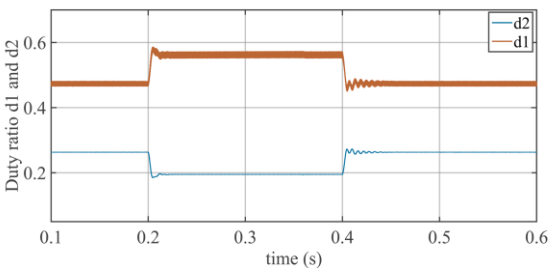

Fig. 4.11.Duty ratio d_1 during variation in load

4.2 Implementation of the PI Controller in real time platform

In closed loop control, first, variation in the reference of the output voltage is observed and the response is shown in Fig 4.12a. The low voltage source current experiences insignificant change in real-time which is shown in Fig. 4.12b. The duty ratios undergo similar change as obtained in simulation. The duty ratio curves are shown in Figs. 4.12c-4.12d. The output voltage reaches the reference value within 40ms which are depicted in zoomed view as well in Fig. 4.13.

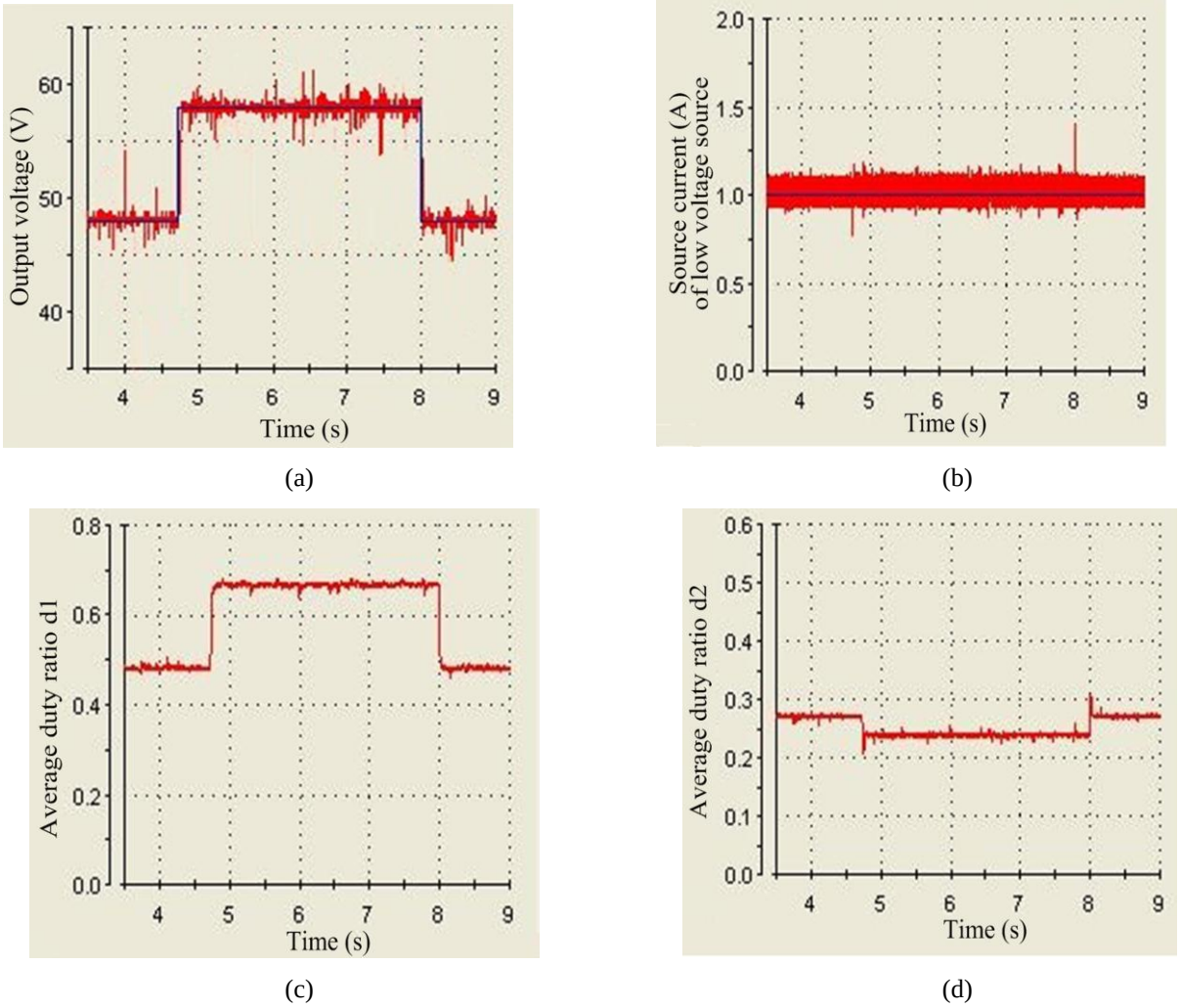

Fig. 4.12. Waveforms during variation in output voltage in real time

(**a)** Output voltage, (**b)** Source current of low voltage source, **(c)** duty ratio d1, **(d)** duty ratio d2

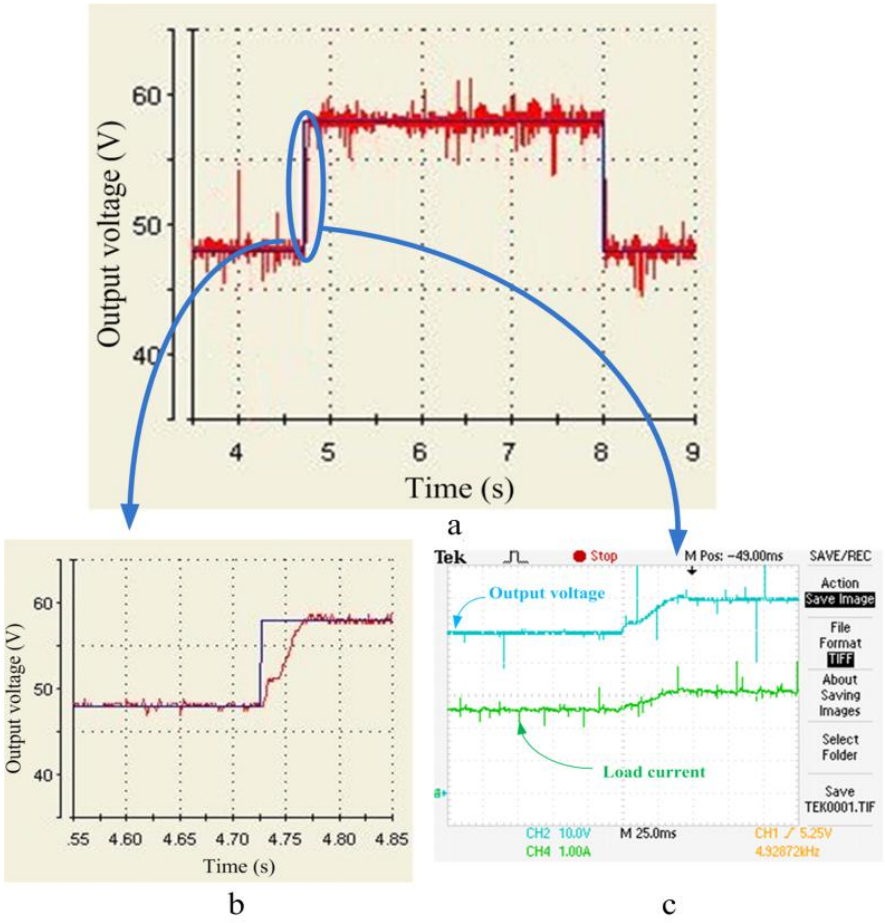

Fig. 4.13. Zoomed view of voltage variation have captured both in dSPACE abd DSO **(a)**Variation in output voltage **(b)**Zoomed view in dSPACE **(c)** Zoomed view in DSO

4.3 sliding mode controller (SMC)

A sliding mode controller (SMC) for the MIC has been developed here.

A hysteresis band (HB) based sliding mode controller is developed to control the proposed multi input converter. Its stability analysis also is performed to ensure the controlled variables, which are dependent on each other, to reach the desired band simultaneously.

This control scheme of the MIC is portrayed in Fig. 4.14.

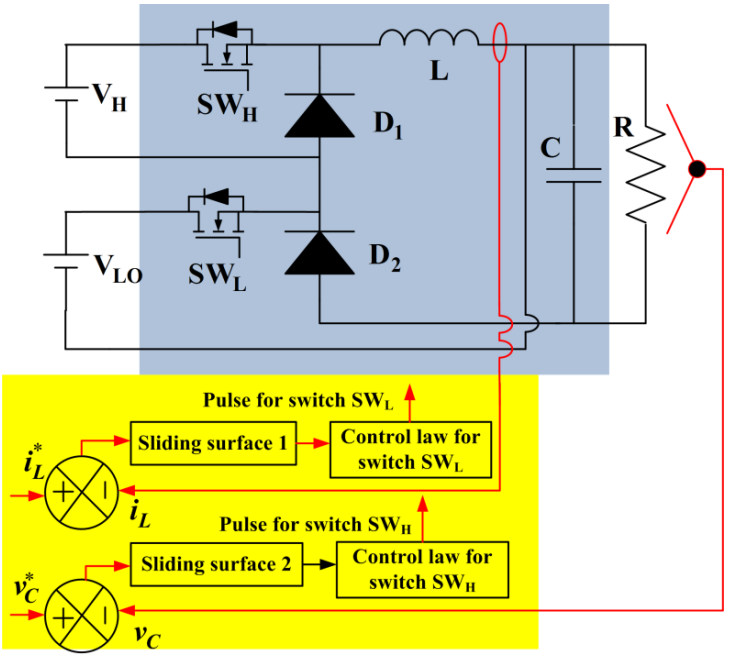

Fig. 4.14: Overall control strategy with hysteresis band based SMC controller for MIC

A. *Controller objectives*

The control scheme depicted in this work must achieve the desired level of controlled variables i.e. inductor current and output voltage very fast and simultaneously. These controlled variables must be maintained at reference band during increment in load and decrement in supply voltage.

B. *Control configuration*

Both inductor current and output voltage are compared with their corresponding reference value. The errors pass through sliding surface to generate the gate pulses according to the control law. The hysteresis bands are shown in Fig. 4.15.

In order to apply hysteresis band control for two switches of the selected converter, two sliding surfaces are chosen as:

$$S_1 = i_L^* - i_L$$

$$S_2 = v_C^* - v_C = v_O^* - v_O$$

Now the variable structure control for two switches is described as follows

$$u_1 = \begin{cases} \mathbf{1}, when\left(v_C^* - v_C\right) > \alpha \\ \mathbf{0}, when\left(v_C^* - v_C\right) < -\alpha \end{cases}$$

$$u_2 = \begin{cases} \mathbf{1}, when\left(i_L^* - i_L\right) > \beta \\ \mathbf{0}, when\left(i_L^* - i_L\right) < -\beta \end{cases}$$

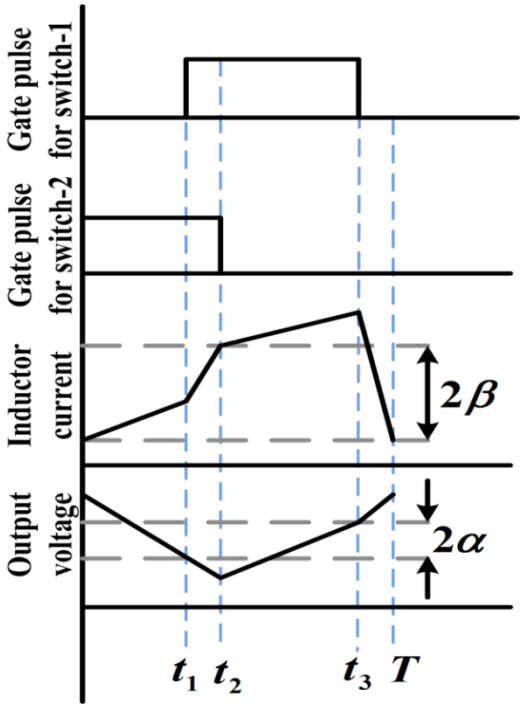

Fig. 4.15: Pattern of inductor current and output voltage during different durations in a switching time preoid

Analysis of sliding mode control

Stability of the Hysteresis modulation based sliding mode controlled DIBBFC

To examine the stability of the HM based sliding mode controlled DIBBFC Lyapunov approach, let consider a Lyapunov function

$$V(s,t) = 0.5s_1^2 + 0.5s_2^2$$

(1)

$$\dot{V}(s,t) = s_1\dot{s}_1 + s_2\dot{s}_2$$

(2)

Which, following eqns (1), (2), (14) and (15) yields $\dot{V}(s,t) = -\left[s_1\dot{i}_L + s_2\dot{v}_c\right]$.

Now each sliding surface has two polarities. So, two sliding surfaces give rise to four sets of sliding

possibilities.

Case I: $s_1 > \beta$ and $s_2 < -\alpha$

Therefore $u_1 = 0$ and $u_2 = 1$

$$\dot{V}(x) = -\left[s_1 \left(\frac{V_H + V_{LO}}{L} \right) + s_2 \left(-\frac{v_C}{RC} \right) \right]$$

Which $\dot{V}(x) < 0$

Case II when : $-\beta < s_1 < \beta$, $\frac{di_L}{dt} > 0$ and $s_2 > \alpha$

Therefore $u_1 = 1$ and $u_2 = 1$

$$\dot{V}(x) = -\left[s_1 \left(\frac{V_H + V_{LO}}{L} \right) + s_2 \left(-\frac{v_C}{RC} \right) \right]$$

To ensure $\dot{V} < 0$, one must satisfy the condition $\beta > \frac{L}{RC} \left(\frac{v_C}{V_H + V_{LO}} \right) \alpha$ (3)

Case III when $s_1 < -\beta$ and $s_2 > \alpha$

Therefore $u_1 = 1$ and $u_2 = 0$

$$\dot{V}(x) = -\left[s_1 \left(\frac{-v_C + V_H}{L} \right) + s_2 \left(\frac{i_L}{C} - \frac{v_C}{RC} \right) \right]$$
$$= -\left[s_1 \left(\frac{-v_C + V_H}{L} \right) + s_2 \left(\frac{i_L}{C} - \frac{i_O}{C} \right) \right]$$

To ensure $\dot{V} < 0$, the following condition is obtained $\beta < \frac{L}{RC} \left(\frac{i_L R - v_C}{V_H - v_C} \right) \alpha$ (4)

Case IV: when $s_1 < -\beta$ and $s_2 < -\alpha$

Therefore $u_1 = 0$ and $u_2 = 0$

$$\dot{V}(x) = -\left[s_1 \left(\frac{-v_C}{L} \right) + s_2 \left(\frac{i_L}{C} - \frac{v_C}{RC} \right) \right]$$

To ensure $\dot{V} < 0$, one must have $\beta > \frac{L}{RC} \left(\frac{i_L R - v_C}{v_C} \right) \alpha$ (5)

Following the equations it is evident that the variable β must be in the following range to ensure the stability of the system.

$$\frac{L}{RC}\left(\frac{i_L R - v_C}{v_C}\right)\alpha < \beta < \frac{L}{RC}\left(\frac{i_L R - v_C}{V_H - v_C}\right)\alpha \tag{6}$$

With the above condition satisfied for HM based SMC control algorithm, the system can be said to be asymptotically stable. With the proposed control law, the states are shown to reach their equilibrium points starting from their operating points. Both the sliding variables reach the hysteresis band and stay in the hysteresis band simultaneously.

Implementation of the control in simulation environment has been accomplished successfully.

The sliding mode controller is implemented and considerable improvement in the current controller is observed. The results are as below:

At 0.75 sec the reference of inductor current has changed from 3A to 4A.The current controller acts very fast to meet the reference with no overshoot. The output voltage maintain at desired level with negligible disturbances. Again the reference value of inductor current has changed from 4A to 3A at 1sec. The inductor current follows the change almost instantaneously. The output voltage is hardly suffered from any disturbances. As the load is purely resistive similar changes have observed in the load current as in output voltage. Differen waveorms during change in inductor current is shown in Fig. 4.16

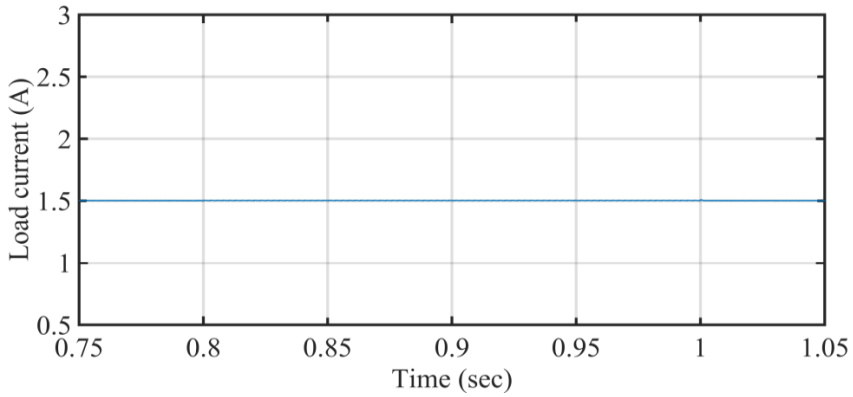

(a)

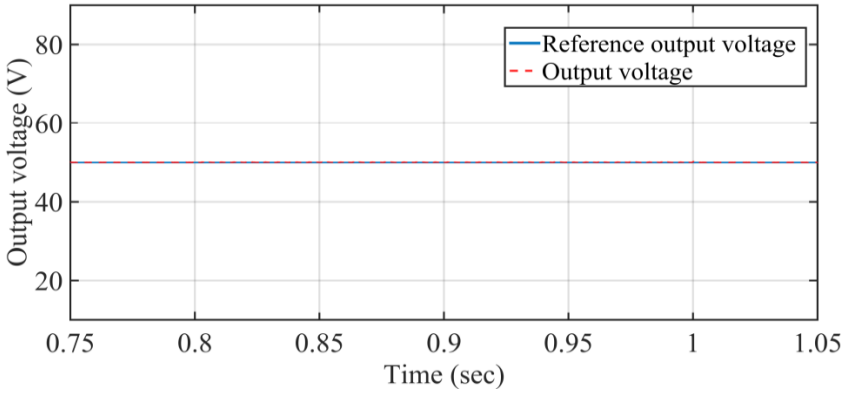

(b)

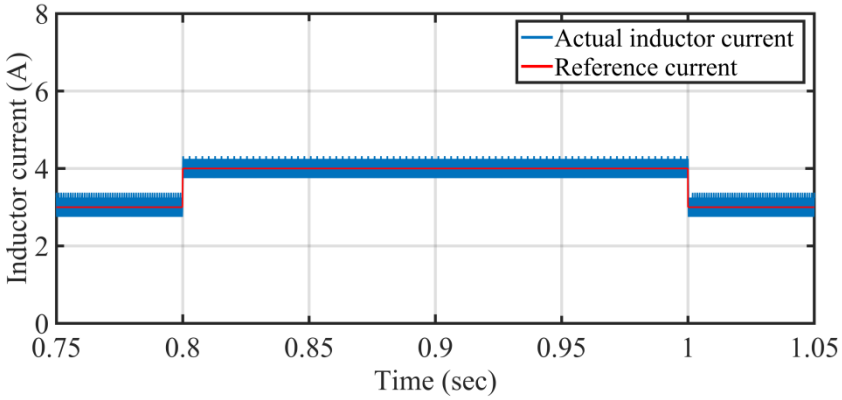

(c)

Fig. 4.16: Response of the converter during change in reference of inductor current: (a) Output voltage, (b) Load current, (c) inductor current

Implementation of SMC control

Some of the results are as follows.

The output voltage reaches the desired value in 10ms while the inductor current suffers a variation for 5ms. When the output voltage is decrased from 60V to 50V within 30ms,the inductor current hardly experiences any disturbances. Nature of inductor current and output voltageare presented in Fig. 4.17. during variation of outpur voltage in real time.

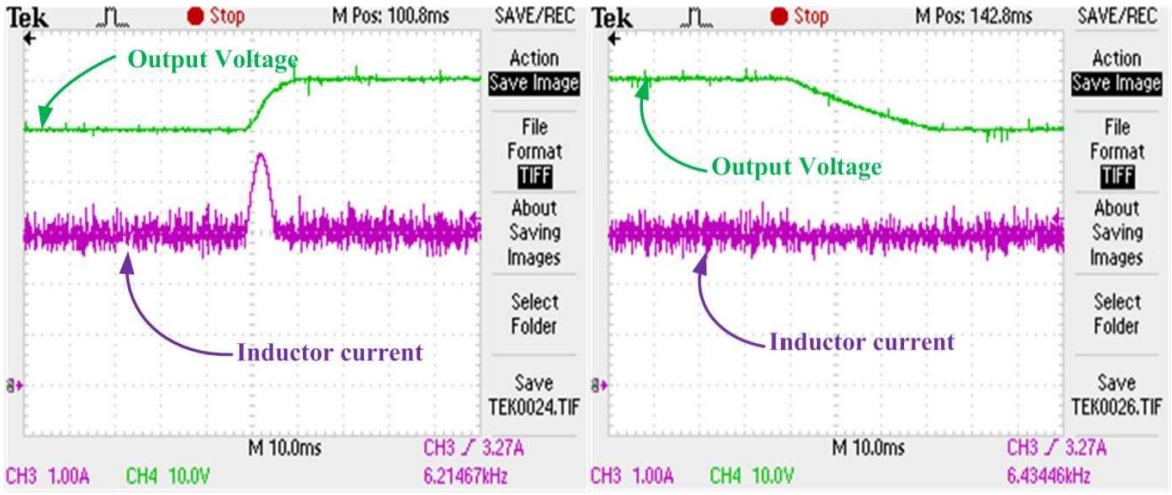

(a) (b)

Fig. 4.17: Variation in the output voltage in real time : (a) increament in output voltage, (b) decrement in output voltage

The inductor current is found to reach the increased reference of 4A from 3A almost instantaneously without affecting the other controlled variable, output voltage. The output voltage and the inductor current are portrayed in Fig. 4.18.

The load disturbances are introduced in the experimental setup. The load is increased by 33.33% almost in step. The inductor current and output voltage are fixed at their reference values. The waveforms of the output voltage, inductor current, load current during load disturbance are present in Fig. 4.19.

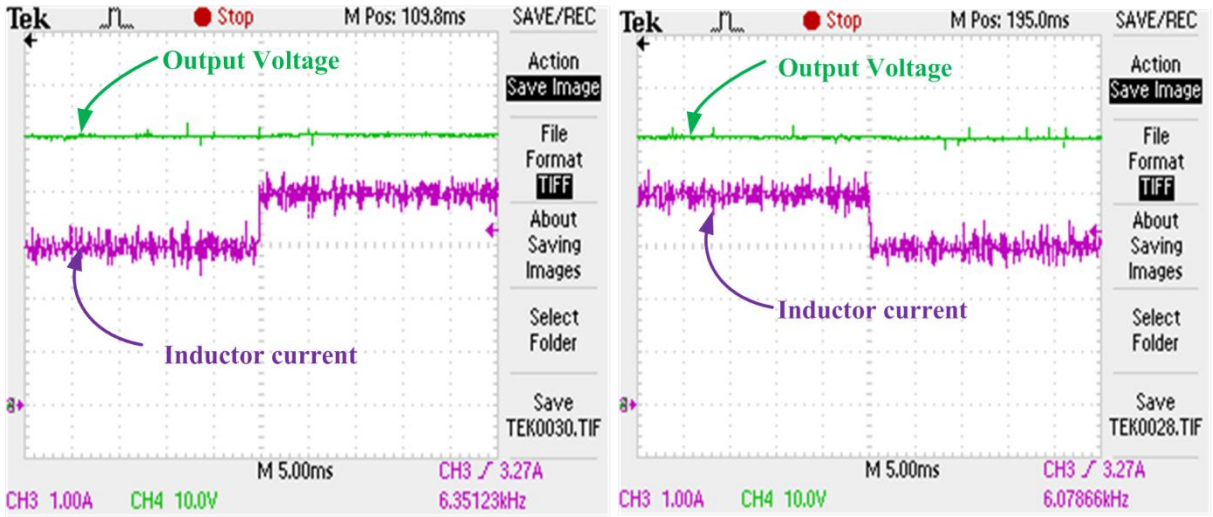

(a) (b)

Fig. 4.18: Variation in the inductor current in real time : (a) increment in inductor current , (b) decrement in inductor current

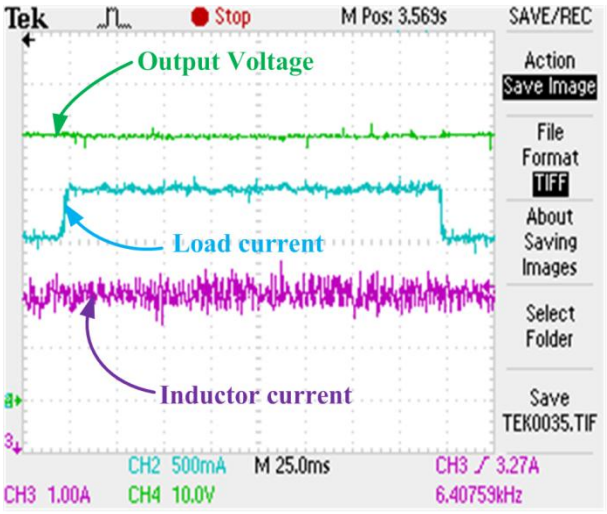

Fig. 4.19: Response of the converter during load disturbances in real time

Chapter 5: Control of Wind Energy Conversion System

The aforesaid converter will be using solar PV and wind energy sources at its two inputs, as presented in Fig. 2. Accordingly a control scheme is developed to utilise the generator at a stand-alone/ grid-connected system. The generator output in stand-alone will be taken from the AC output of the load side converter. The same generator output will be utilised by the MIC, by connecting the high voltage terminal of it, at the DC link of PMSG system. The scheme is as follows:

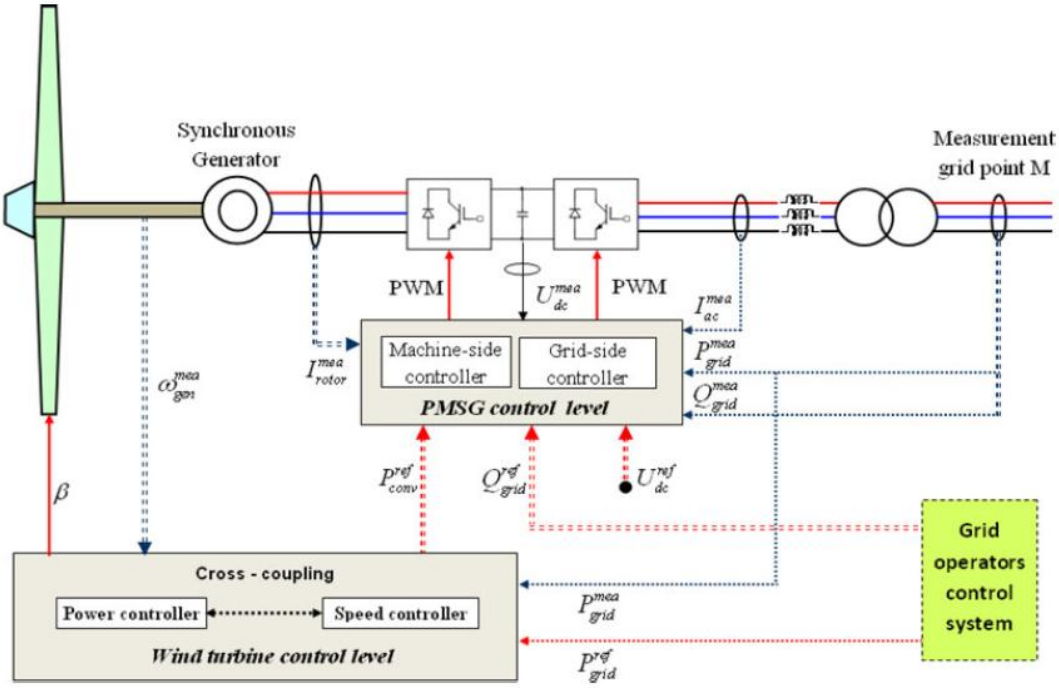

Fig 5.1: Scheme of Wind Energy Conversion System from PMSG

The Controllers are presented below:

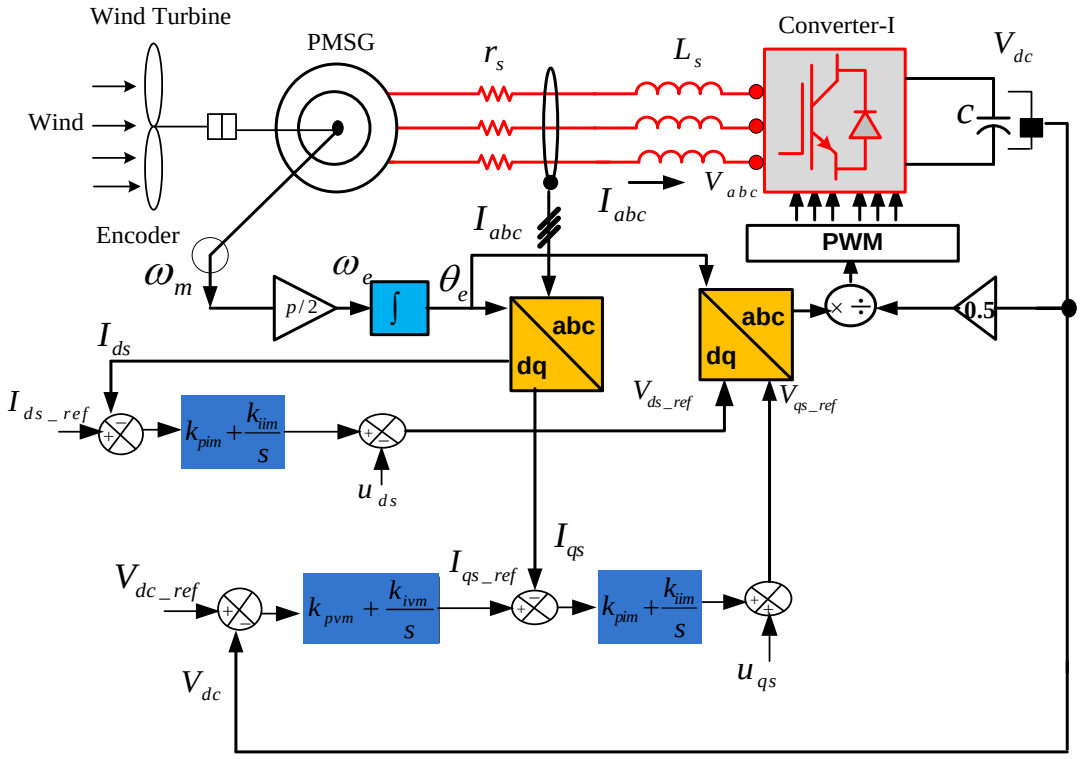

Fig. 5.2: DC Link Voltage Control Structure for Converter-I

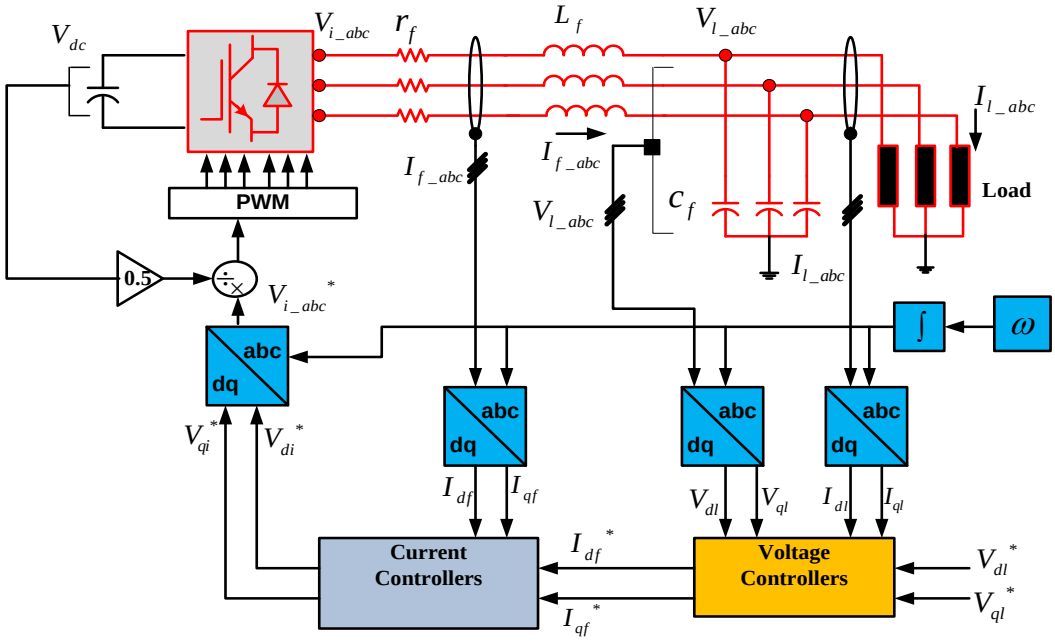

Fig. 5.3: Load side VSI control structure

The load side controller is analysed in frequency domain and are presented as:

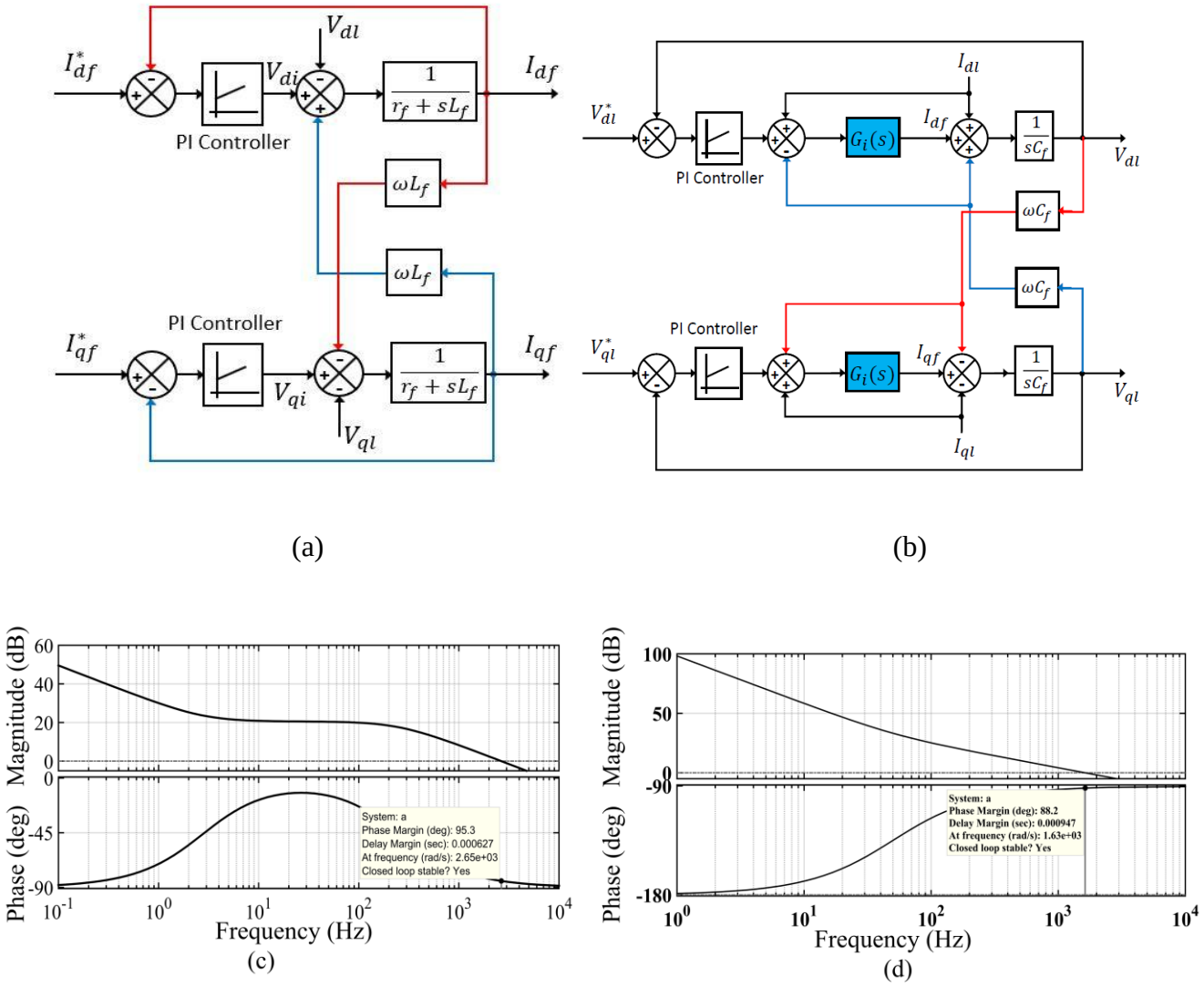

Fig. 5.4. The load side converter (a) Current control loop, (b) Voltage control loop, (c) Bode plot for compensated current loop, and (d) Bode plot for compensated voltage loop

The PMSG based system is implemented in simulation and real time environment)

The PMSG based wind energy conversion system has been implemented in stand-alone mode. Some results are as follows:

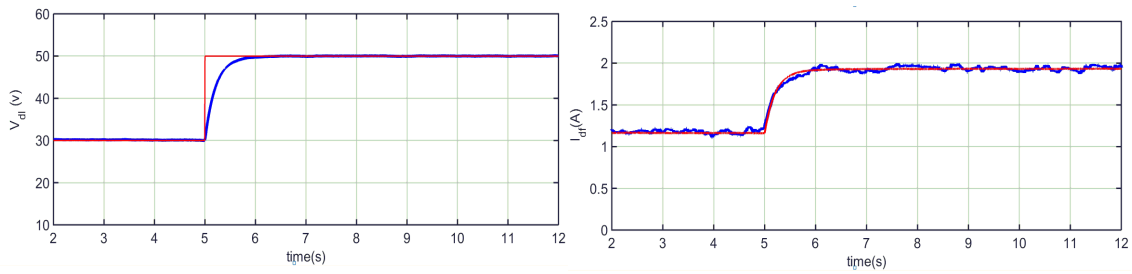

(a) (b)

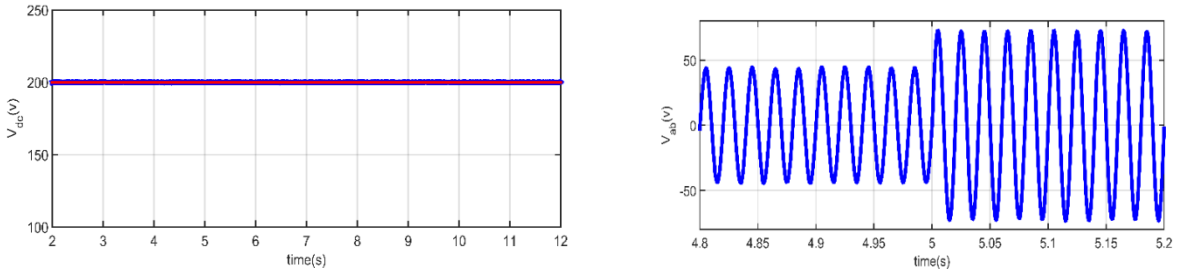

(c) (d)

Fig. 5.5: Simulation response of various parameters due to d-axis load voltage change (a)d-axis component of load voltage (b)d-axis filter current (c) dc-link voltage (d) AC load voltage

The d axis component of load voltage is changed for the PMSG in this case. The load voltage controller settles within 0.8 sec and the current controller is found to be tracking the reference throughout the operation.

The Speed of the wind generator has changed in both step and following the nature of change in wind. The nature of wind speed change is considered from the existing literature.

The controllers are found to accommodate the speed changes and successfully maintaining the DC link voltage and load voltages in these cases.

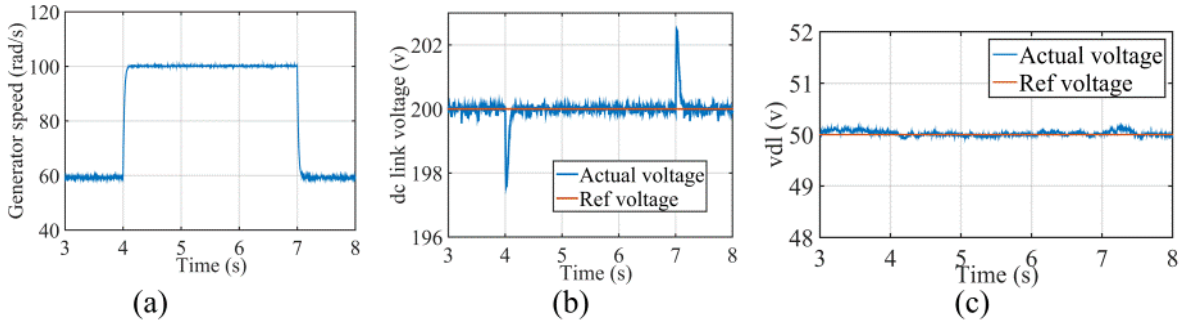

Fig. 5.6: Simulation response of various parameters due to speed change (a)generator speed, (b) dc link voltage, and (c) d -axis component of load voltage

A* novel approach on soft transition from stand-alone mode to grid-connected mode for uncontrolled prime mover driven squirrel cage induction generator (SCIG) *based wind energy conversion system and implementation is happening in simulation environments.

The power generation scheme presented in Fig. 5.7 operates both in stand-alone mode to grid-connected mode.

The transition from stand-alone mode to grid-connected mode is possible through a grid connecting switch. The is grid connecting switch operated by one block whose function is to detect the grid and synchronize the grid and load voltage after appearance of grid.

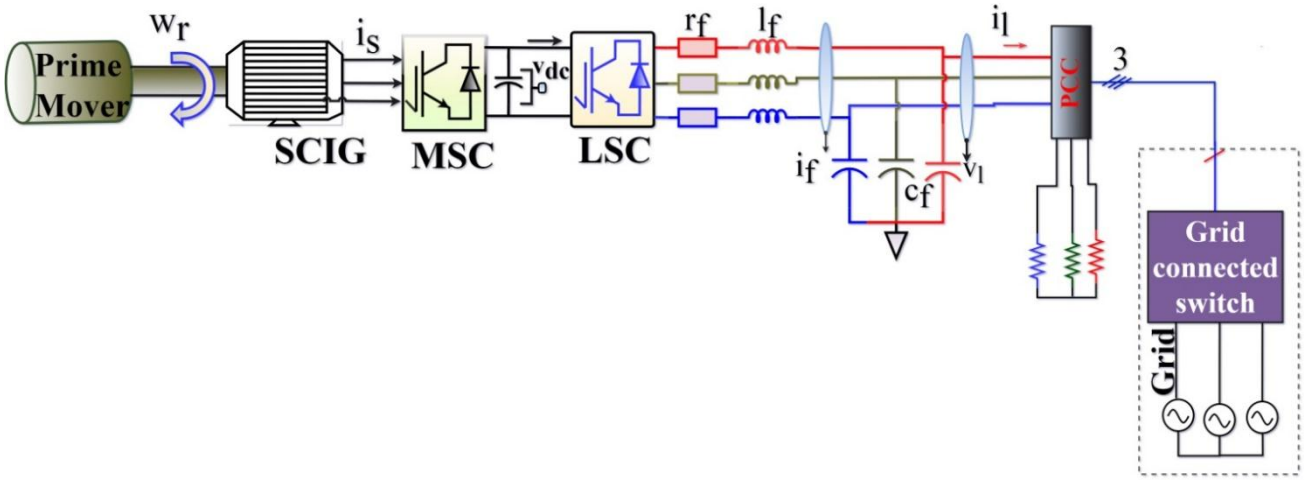

Figure: 5.7- System configuration

The aforesaid scheme is designed to achieve the following objectives as:

1. The machine side converter (MSC) and the load side converter (LSC) are controlled to maintain constant load voltage amplitude and frequency during stand-alone mode.
2. The smooth grid synchronisation is achieved with a novel virtual active and reactive power control technique. Additionally power regulation is made possible during grid connected mode of operation, with the help of this control.
3. The virtual power control is able to generate direct inverter voltage vector and its angle in synchronously rotating reference frame, without separate phase locked loop (PLL) and frequency measurement.
4. The MSC is controlled by three stage control technique, to maintain the dc link voltage, throughout the operation

The controllers for MSC and LSC are presented below as:

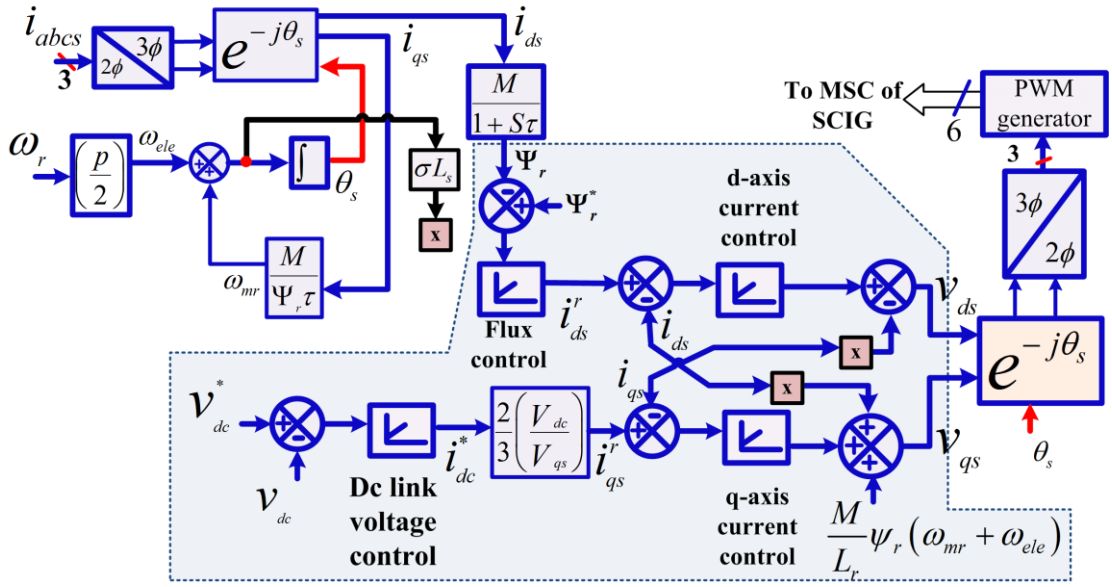

(a) Control strategy of MSC

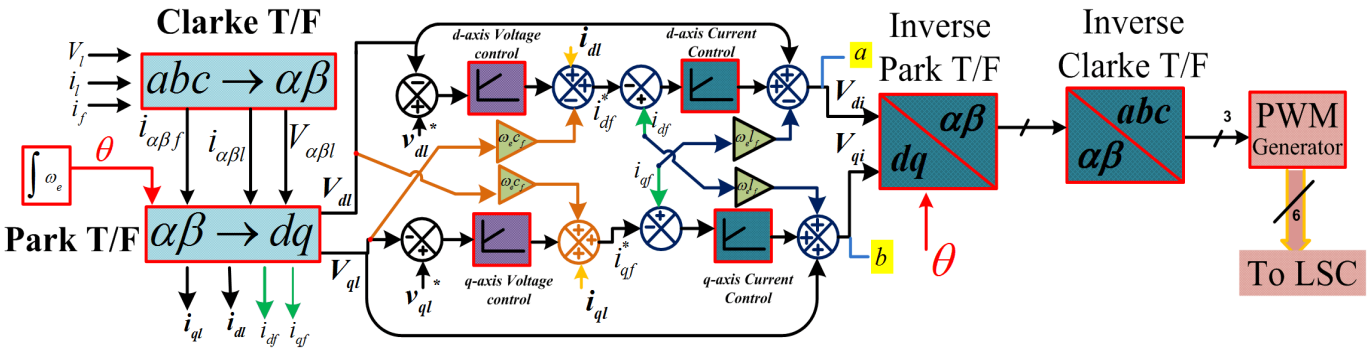

(b) Control strategy of LSC during stand-alone mode

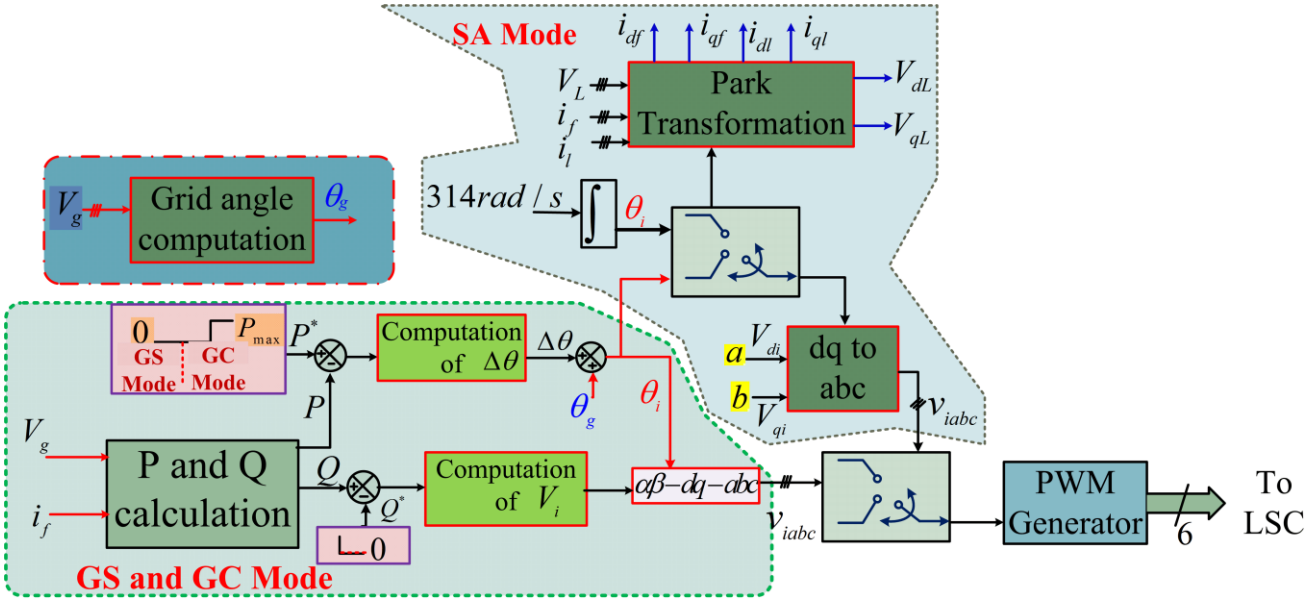

Figure: 5.8: Control strategy of LSC during grid synchronization (GS) and grid connected (GC) mode

The grid angle (θ_g) and inverter voltage angle (θ_i) is generated through the virtual power control depicted above. The application of controller ensures zero exchange of power between inverter and the

grid at 3.5 s as shown in Fig. 5.8. The corresponding inverter and grid angle are as shown in Fig.5.9. During GC mode zero exchange of active and reactive power between inverter and grid up to 9 s is shown in Fig 5.10. The increment in inverter angle is found in Fig. 7 (a) with the increase in active power command.

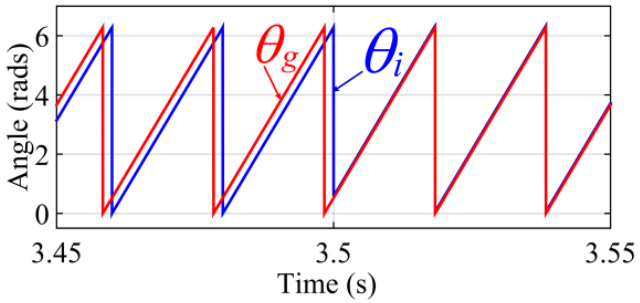

Fig. 5.9 Inverter and grid angle during transition from the SA mode angle to grid angle

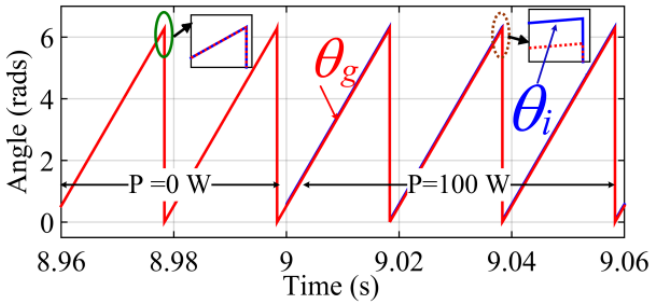

Fig. 5.10 Scenarios of inverter and grid angle during GC with virtual power and power regulation mode

The LSC controller is working successfully to keep the load voltage magnitude and angle fixed during stand-alone mode. The transient changes of the load and grid voltage during the process of synchronisation are as shown in Fig. 5.11 (b), Fig. 5.11 (c) respectively. Initially, the SA mode of operation is established with fixed magnitude and angle of load voltage vector. The change in the angle of load voltage vector is portrayed in Fig. 5.11 (b). The initial difference in angle between load voltage (Phase R) and the grid voltage (Phase R) diminishes within 10 ms. The action of power controller, at 5 s, is observed in Fig. 5.12 (a). The application of virtual controller has changed the load voltage to keep the power exchange between generation unit and grid at zero level. This is achieved by making $\Delta\theta$ to zero as shown in Fig 5.10. As explained before during this scenario active and reactive power reference is set to zero. Finally the synchronisation is done at 8 s and the smooth transition is portrayed in Fig 5.11(c).

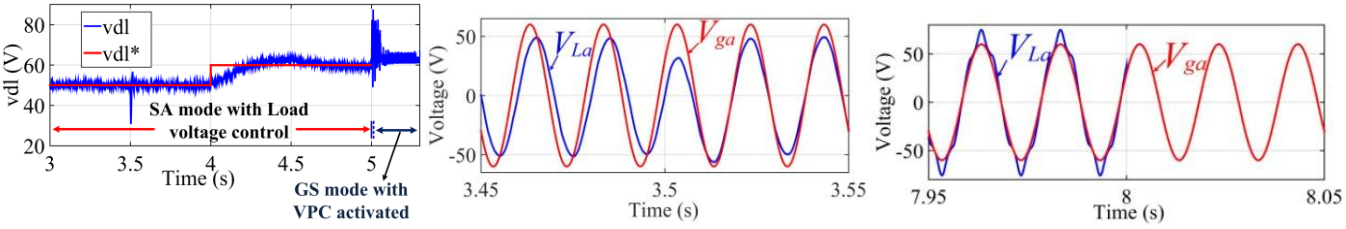

(a) (b) (c)

Fig. 5.11 Simulation Results for (a) Transient performance of load voltage during transition from fixed voltage reference to Vdg at 4 s, Responses of load and grid voltage during (b) Fixing the SA mode angle to grid angle (c) GS to GC mode

The virtual power control is operated to obtain desired power output by the distributed generation unit in this work in grid connected mode of operation. The initial value of reference power is set at 0 W as

shown in Fig.5.12. The actual power (P) reaches the set point 100 W immediately at 9 s, as shown in Fig. 5.12 (a). The angle difference between inverter and grid, as shown in Fig.5.9, and demand the generated voltage, is found to be leading to the grid voltage, as shown in Fig. 5.12.(b).

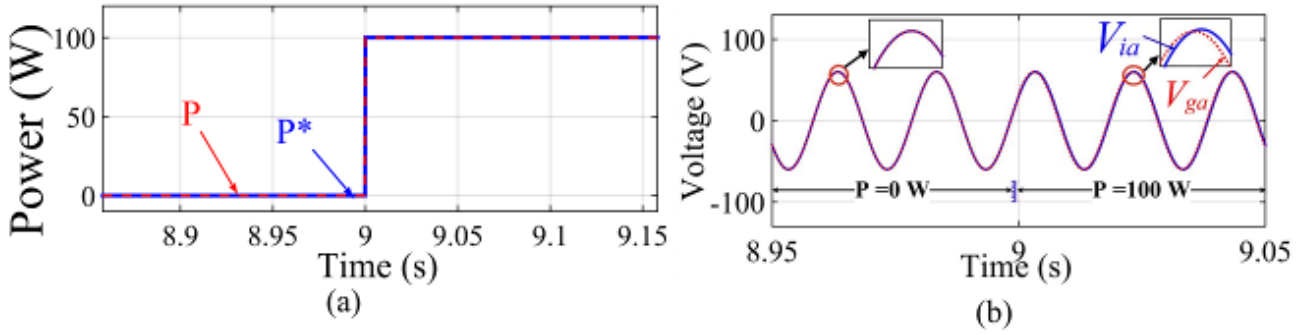

Fig. 5.12. Simulation Results during virtual power control implementation (a) step change in active power, (b) Response of inverter and grid voltage

The dynamic performances for the machine variables are depicted for all the three cases. The three stage control technique as is used for all the cases. The dc link voltage is maintained at 200 V throughout the operation as shown in Fig. 5.13

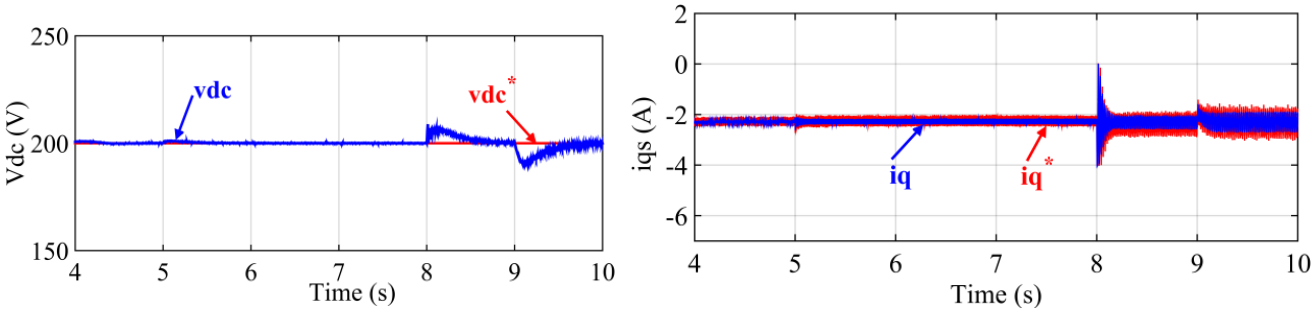

(a) (b)

Fig.5.13. Transient analysis of machine variables during three operating modes (a) dc link voltage (b) q-axis component of machine current

Development of PMSG based wind energy conversion system for grid in simulation

Structure of the grid connected based is presented in Fig 5.14

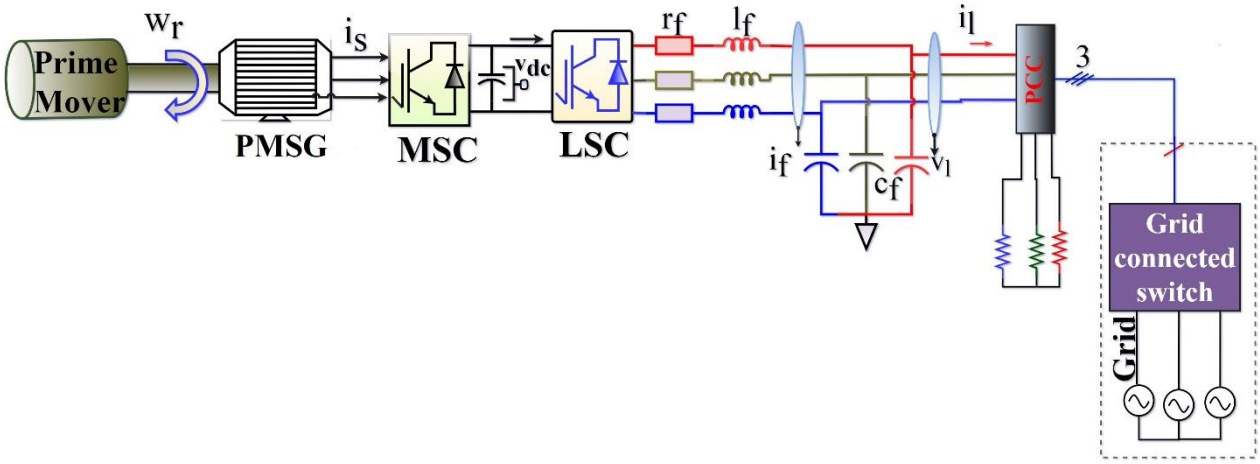

5.14.: Block diagram of PMSG based wind energy conversion system to Grid.

At 6 sec the active power is increased from 175W to 275 W and the reference level is brought back to nominal value at 9 sec. The DC link voltage maintains it reference level during this period. This smooth supply of power is maintained even at the presence of the random variation of the speed of prime mover.

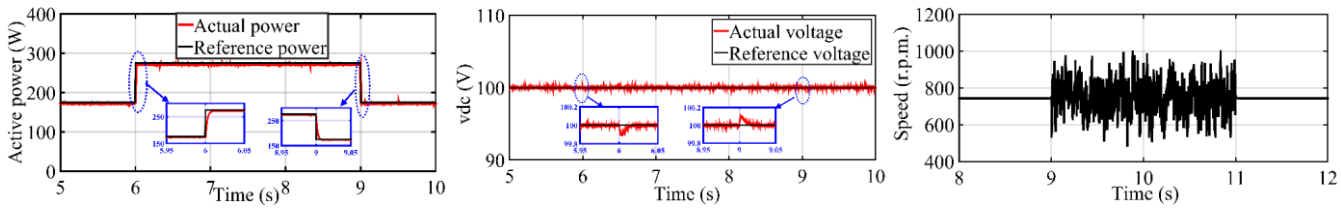

(a) (b) (c)

Fig 5.15: Active Power Change : (a)Active power, (b) DC link voltage, (c)Speed

The reactive power is changed from -200 VAr to -100 Var at 11 sec and is return back to nominal value at 15 sec. During this period the dc link voltage and reactive power is held at constant.

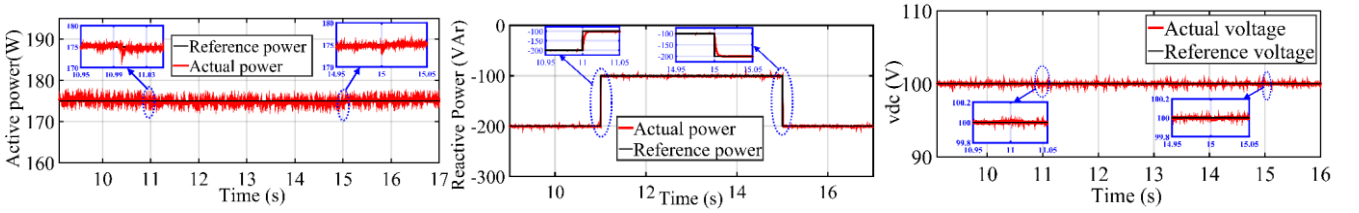

(a) (b) (c)

Fig 5.16. Reactive power change: (a) Active power, (b)Reactive power and (c) Dc link voltage

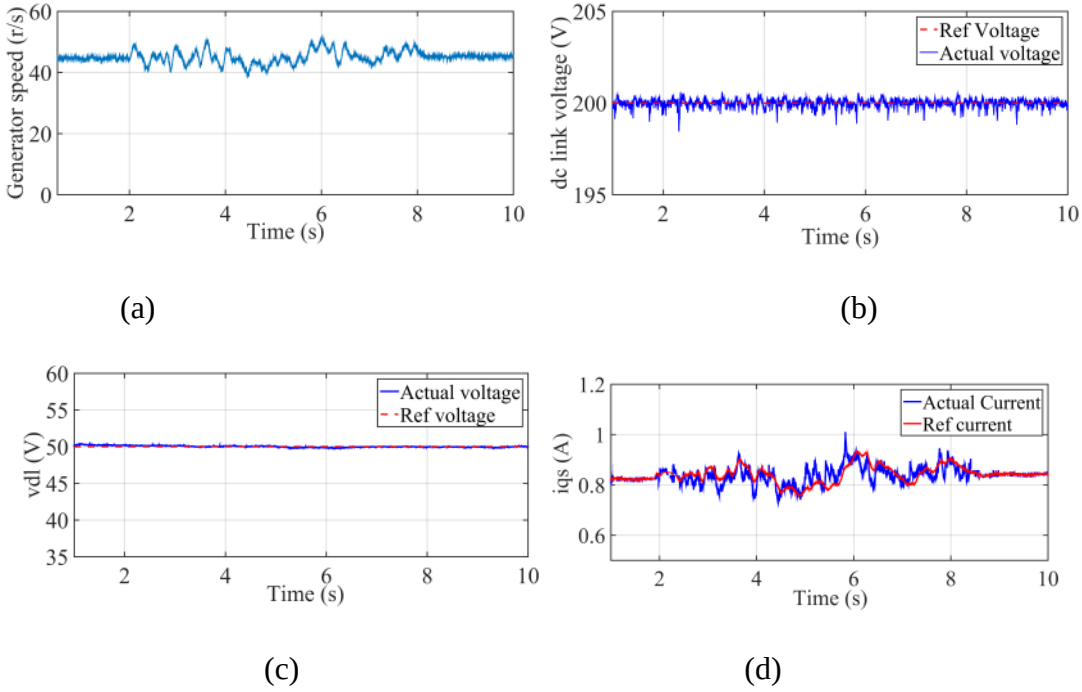

Fig.5.17: Simulation response of various parameters due to speed change (a) generator speed, (b) dc link voltage, (c) d -axis component of load voltage, and (d) q-axis component of machine current

The real time implementation of the same is presented here:

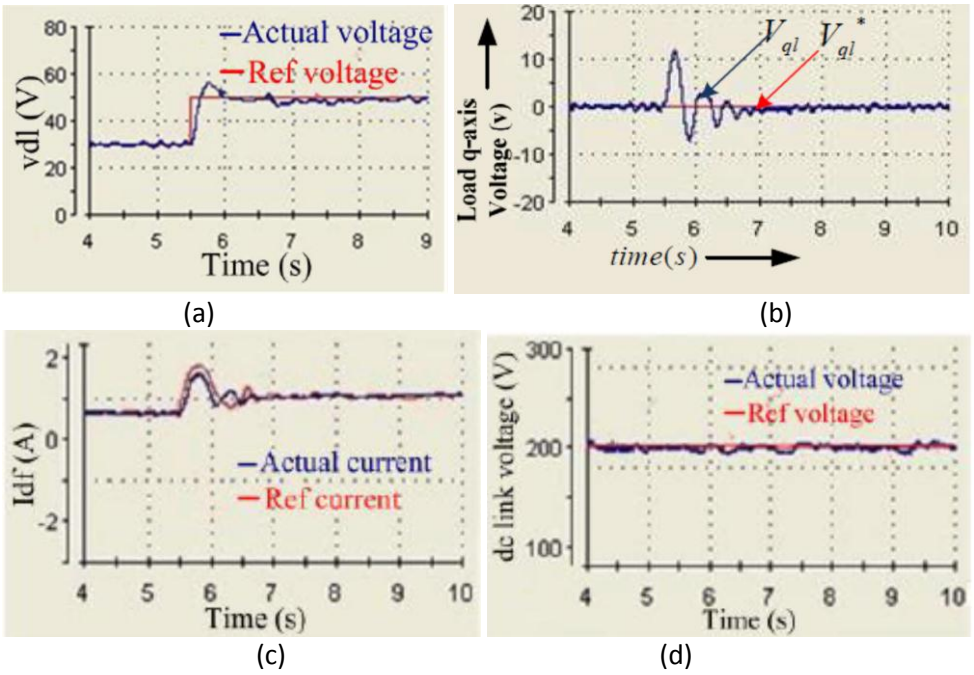

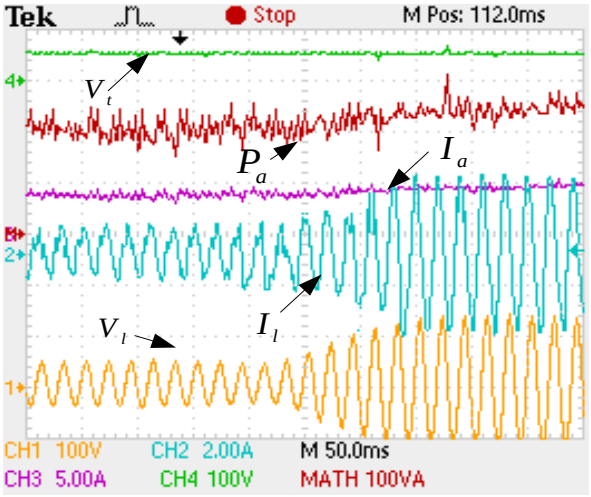

(e)

Fig.5.18. Experimental response of various parameters due to d-axis load voltage change (a)d-axis component and (b) q-axis component of load voltage,(c) d-axis component and (d) q-axis component of inverter current, (e) dc-link voltage, and (f) prime mover power.

Chapter 6: Control of the forward Inverter

The direct power control for the inverter is achieved with the following scheme.

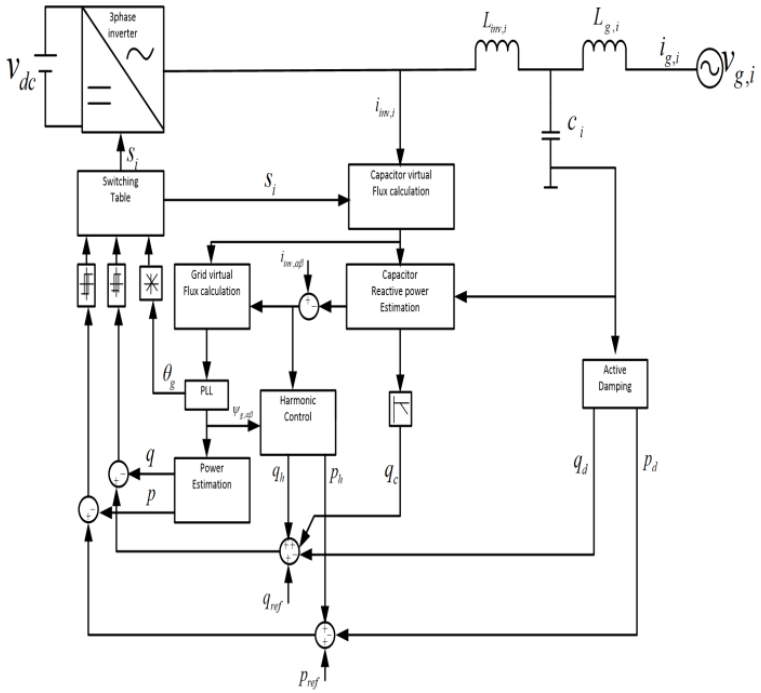

Figure: 6.1: Instantaneous active and reactive power control.

The system is implemented in simulation with scaled version. The change in active power flow is achieved as below:

In figure 5.19, the Active Power varies from 90w to 120w. The Active Power settles within 0.05sec in this case.

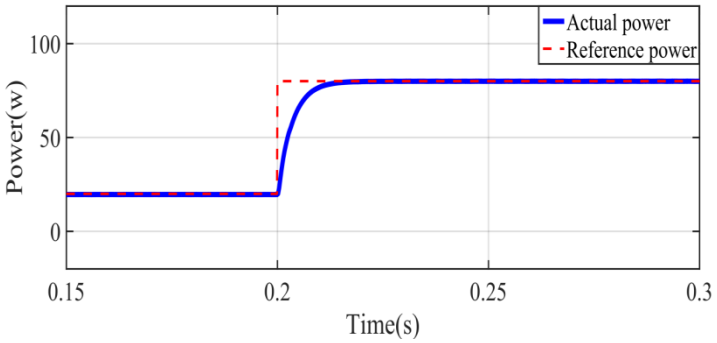

Figure: 6.2- Actual Active power and Reference Active power.

The reactive power is maintained at 20w throughout the operation.

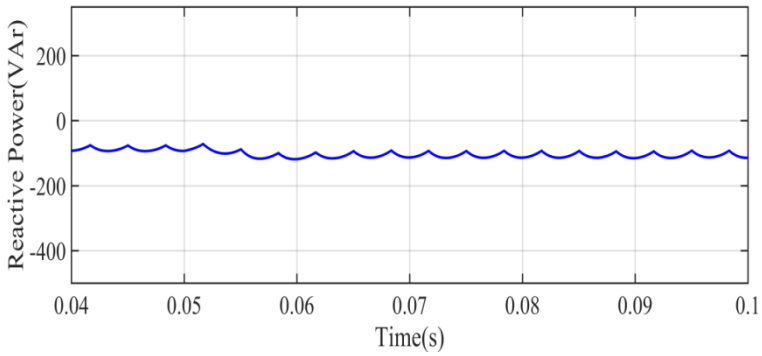

Figure: 6.3- DC to AC Reactive Power.

The space vectors to achieve the power control is shown in real time as follows:

The power has varied from 30w to 100w in a step, and the actual power reaches the reference within 0.05 sec. The nature of variation is portrayed in Fig. 6.4.

The sectors during low power supply and the corresponding vector selections for this direct power control are shown in Fig. 6.5 and Fig. 6.6, respectively.

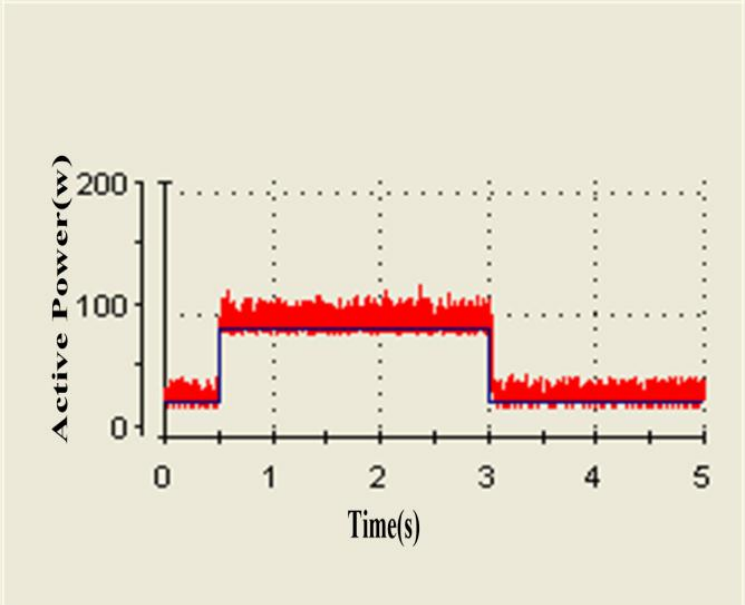

Figure: 6.4:- Active power variation for the inverter output.

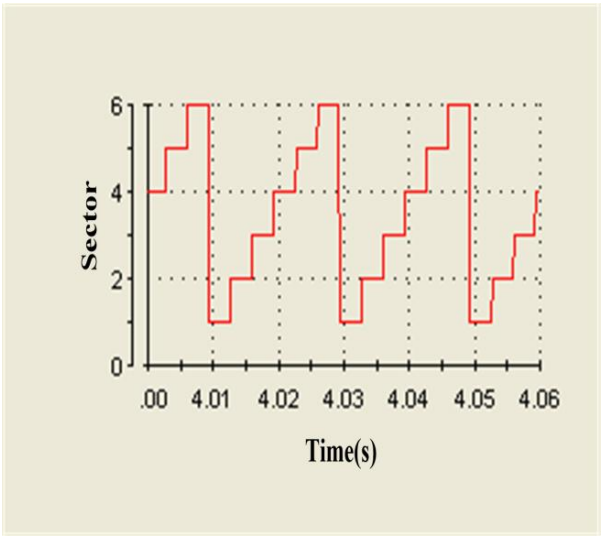

Figure: 6.5- Sectors at low power supply

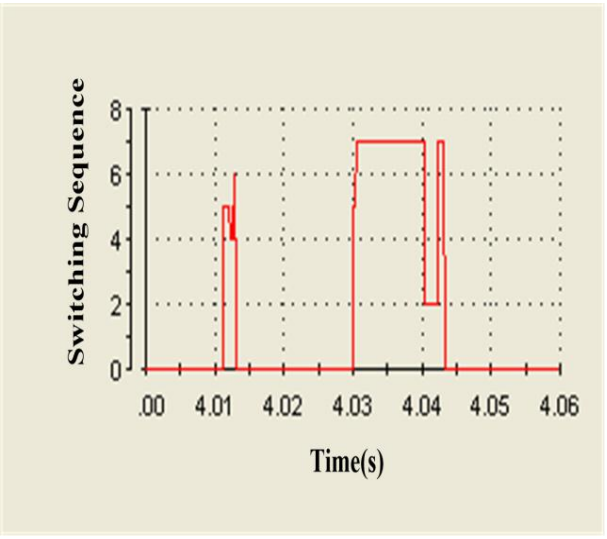

Figure: 6.6- Selection of vectors at low power supply

The sectors during high power supply and the corresponding vector selections for this direct power control are shown in Fig. 6.7 and Fig. 6.8 respectively.

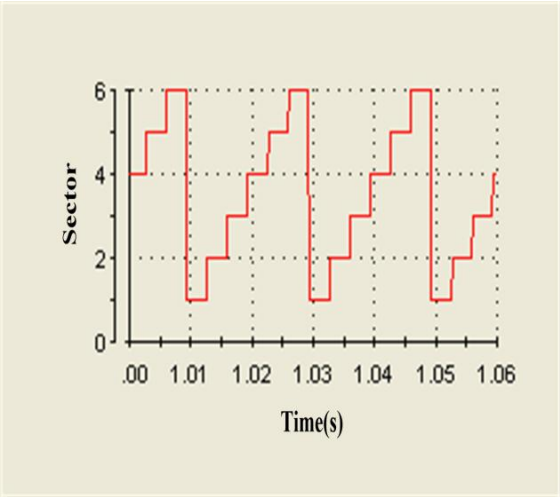

Figure: 6.7- Sectors at high power supply

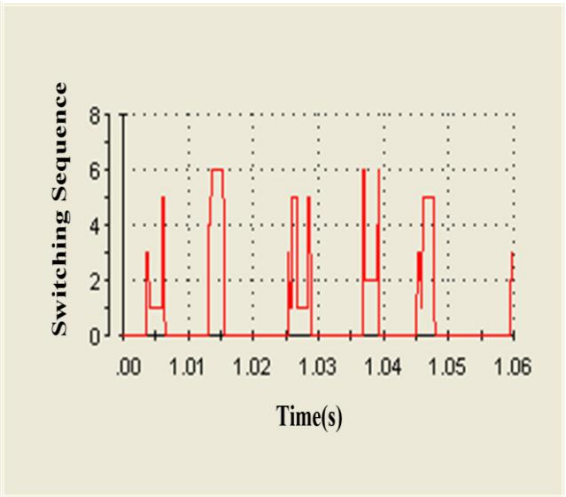

Figure: 6.8- Selection of vectors at high power supply

** It is observed that active vectors are mostly used in high power supply, supporting the logic of direct power control.

Chapter 7: MPPT operation of the PV for the converter

The completer structure of thre proposed MPPT scheme is presented below. The power circuit of DIBBFC is presented in Fig 7.1. The output voltage is controlled through a designed PI controller and is being implemented by using the upper switch (SW1). The PV voltage and current are taken as feedback and are fed to the PO based algorithm to generate the current reference corresponding to the MPP operation. The current control is achieved through the development of an SMC and is implemented through the lower switch (SW2). Switch (SW2) is performed the role of buck-boost operating part while switch (SW1) incorporating the buck nature in that buck-boost converterSince upper voltage source is integrating with the high voltage source and the lower switch is integrating with low voltage source, the output operating voltage is preferred to be a value within the range from the magnitude of low voltage source and the magnitude of high voltage. The PV voltage and current are observed and power is calculated in each specified instant and is being compared with the same of the previous instant. The flowchart is presented in Fig 7.2.The current reference is chosen instead of duty ratio to have the better resolution in operation. The selection of perturbation time and perturbation step size is very critical to achieve the satisfactory performance of the PV source. Larger perturbation time produces sluggish performance. While larger perturbation step size may improve the transient performance, but also increases the steady-state oscillation. For this work, the perturbation time is chosen as 0.05 sec and the step size is selected as 0.25.

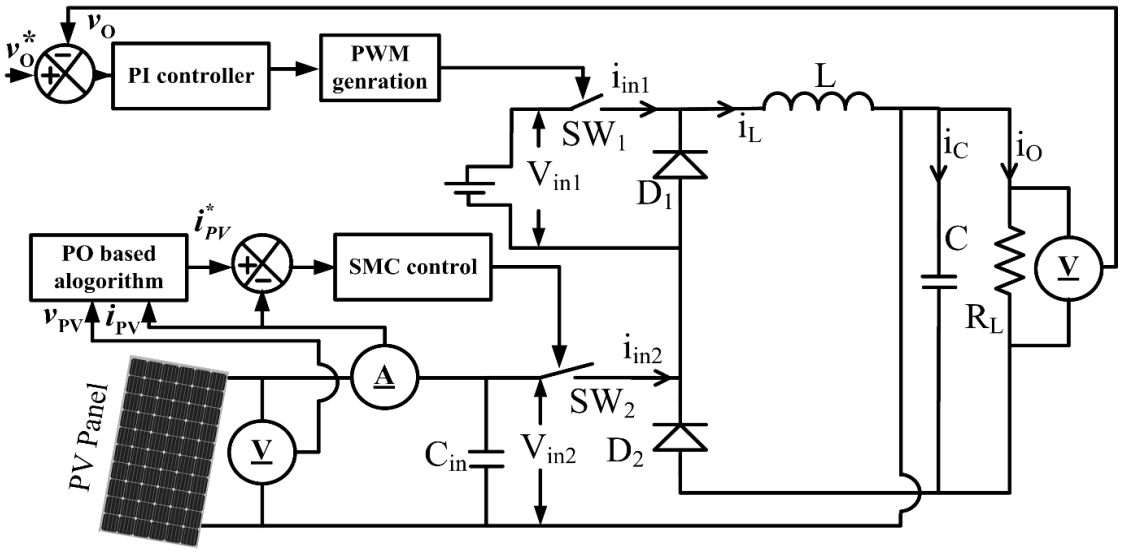

Fig 7.1: Overall control scheme of DIBBFC

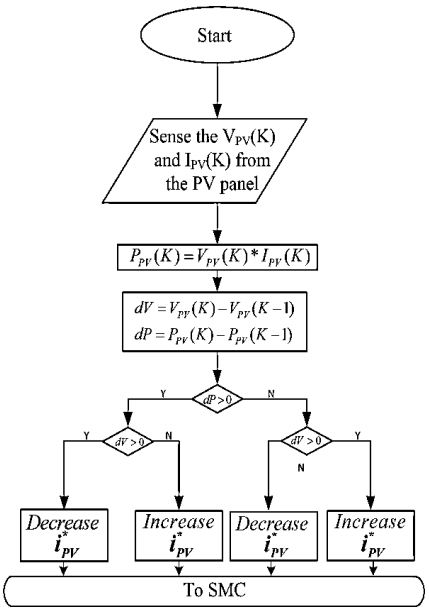

Fig 7.2: Algorithm of PO based MPPT to generate current reference of the SMC.

Results of MPPT operation:

Case1: Attainment of MPPT operation

The above-stated system is operated at the low voltage source current of 3.5A and the output voltage of 75 V. At 0.1 sec, the MPPT operation of PV panel is initiated. At the steady-state of MPPT operation of the PV panel, the PV current is in the band of 5.25A to 5.75A. The PV current at MPP is 5.55A at an irradiance of 1000W/m2. The output voltage maintains the reference of 75 V. Waveforms of the corresponding PV current, and output voltage are given in Fig 7.3.

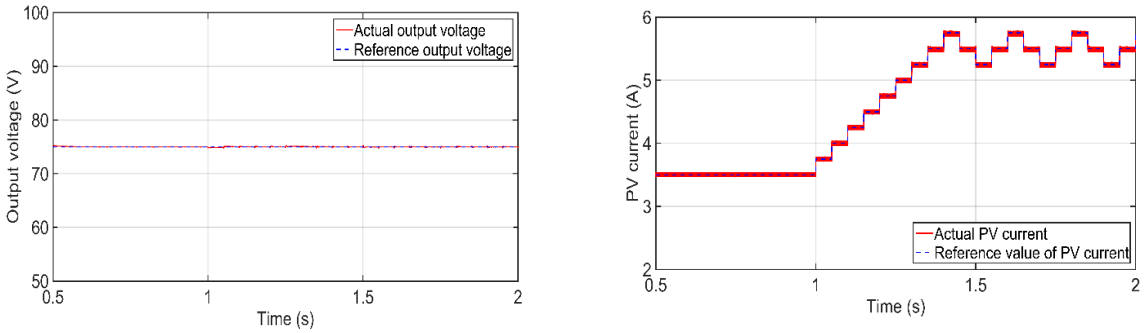

(a) (b)

Fig 7.3: Case1: Attainment of MPPT operation (a) output voltage (b) PV current.

Case2: Variation of the output voltage

At 3 sec, the reference value of the output voltage of the converter is changed from 75V to the 85V. The actual voltage flows the reference with 7% overshoot and settling time 39 msec. At 4sec, the reference is changed from 85 V to 75 V. The output voltage undergoes an undershoot of 1.33% and settling time of 33 msec. The PV panel is operated successfully at the MPP. Fig 7.4. displays the nature of PV Current, output voltage and load current. Therefore, it can be justified that different output voltages can be achieved while the PV panel operated at the maximum power point.

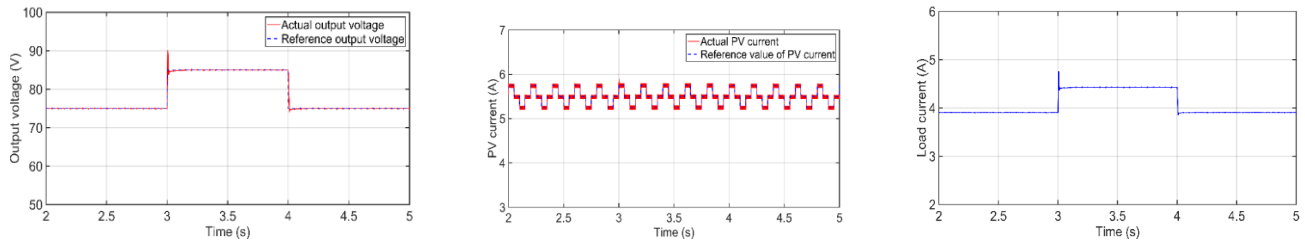

(a) (b) (c)

Fig 7.4: Case2: Variation of the output voltage (a) output voltage (b) PV current (c) Load current.

Case3: Increment of load increment

At 5.5 sec, the load demand is suddenly increased by 50%. The output voltage has suffered from an undershoot of 1.6% and settled within 11msec. The output voltage has an overshoot of 1.6% due to the sudden decrement of the load to the nominal operating point. During this, the MPP operation of PV panel remains unaffected. As the input power from the PV remains in a fixed band the excess power comes from the high voltage source. The waveforms of output voltage, PV current and load current are depicted in Fig 7.5. As maximum power generation is limited therefore the extra power is taken from the high voltage source

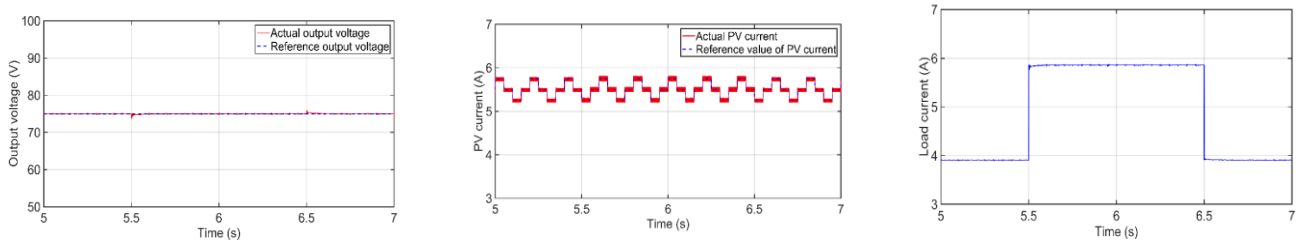

(a) (b) (c)

Fig. 7. 5: Case3: Load increment (a) output voltage (b) PV current (c) Load current.

Case4: Input disturbance at the high voltage source end

From 8 sec to 9 sec, the high voltage source is increased by 10%. This produces a very minimal effect on the MPP operation PV panel and the reference voltage. Since the power is delivered from PV source is at the fixed level, the input current from high voltage source has to reduce to support the load demand at the fixed level. The required waveforms of output voltage, PV current and voltage of high voltage source are presented in Fig 7.6.

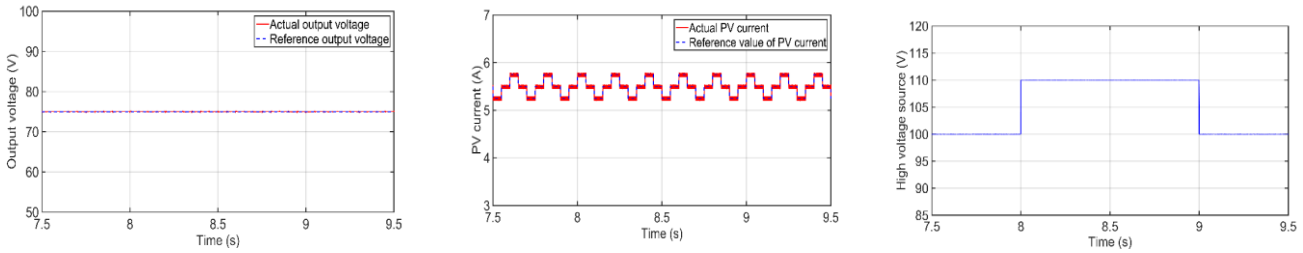

(a) (b) (c)

Fig 7.6: Case 4: Input disturbance at high voltage source end (a) output voltage (b) PV current (c) High voltage source.

Case5: Variation in solar radiation

The solar radiation is changed from 1000W/m^2 to 800 W/m^2, after some time it is reduced further at 600w/m^2 , after 1sec it is increased from 600 W/m^2 to 800 W/m^2, and after some more time, it is returned back to its nominal value. The pattern of solar radiation is presented in Fig 7(c). The PV current is settled at the current corresponding to MPP point for the respective irradiance. Thus, it ensured the maximum utilization of power, which is generated from the PV panel. The effect on the output voltage is almost negligible and it is maintained at the reference level. The condition of output voltage, PV current and irradiance level are presented in Fig 7.7.

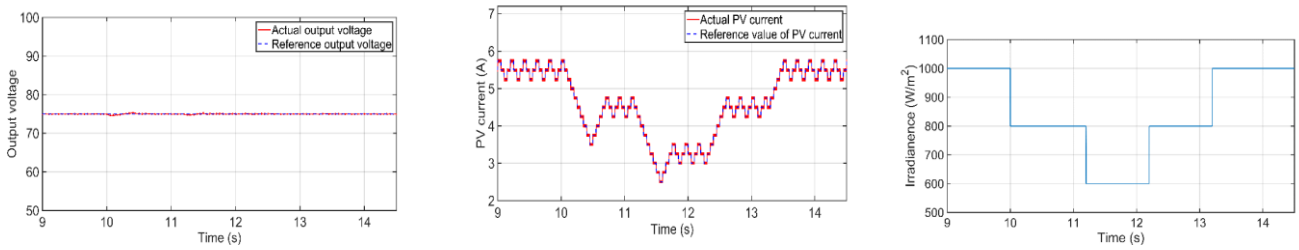

(a) (b) (c)

Fig 6.2.7: case 5: Variation in solar irradiance (a) output voltage (b) PV current (c) irradiance level of solar

Chapter 8: Conclusion

We do thank NIWE for providing the support to have the multi input converter model in this work.

The working system is presented in the following figure. The PV panel is on the roof of the laboratory.

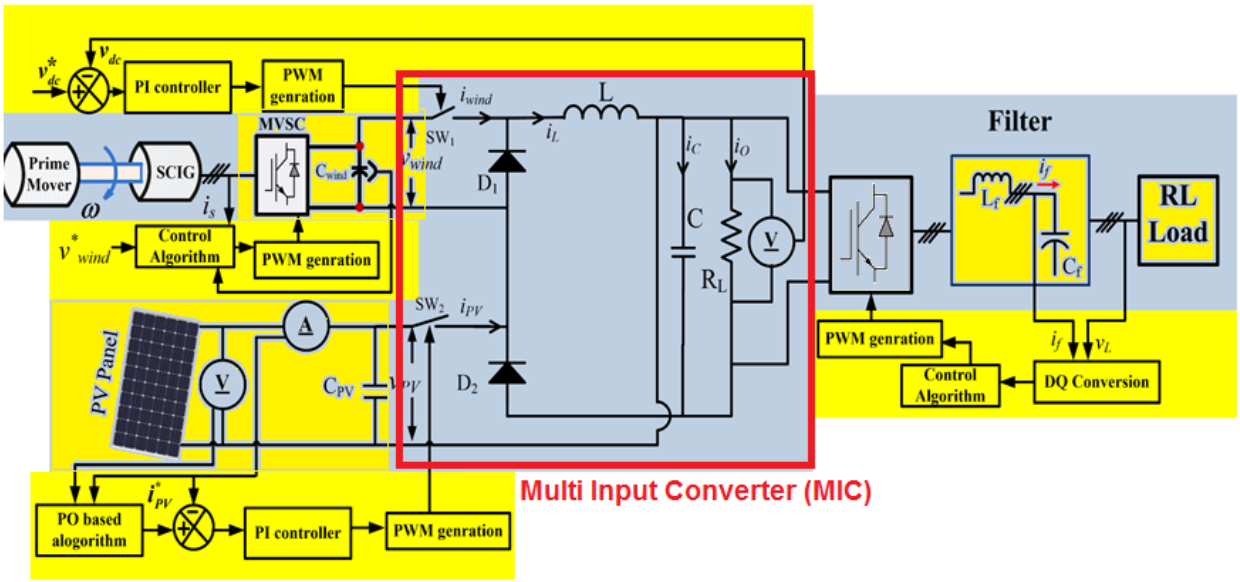

Fig. 8.1: Working System of the project

All of the equipment, purchased (the MIC, two machines, one DSO, and one PC for documentation) through this project, has been integrated with existing facility of the laboratory to make it workable. The Yellow highlighted areas of Fig.8.1 are available in the laboratory.

The existing facilities required to run the system are:

(i) Two digital controllers [dSPACE1104], connected at PCI slot of two computers,
(ii) Different power sources,
(iii) PV panels,
(iv) Semikron made rectifier-inverter model [Stack type no. MD 2* B6CI 440/220-27F]
(v) Interfacing circuits etc.

Following are the achievements of this project

1. Details of the decoupler-based pi controller is designed to control the DIBBFC (Double Input Buck Buck-boost Fused Converter).

2. A nonlinear control (Sliding mode control) is designed to control DIBBFC. Here, two different sliding surfaces are designed. These two sliding variable reaches to equilibrium point of operation simultaneously.

3. The bifurcation analysis of this double input converter is available for the first time in the literature.

4. In a standalone mode of operation, the PV panel is integrated at the low voltage source end. It operated at MPPT mode. The PMSG based generated DC is applied at the high voltage source end of this converter. This high voltage is utilized to keep the DC output voltage at a constant level.

5. The highlights of this work are that a single converter can integrate two different dc sources, and in standalone mode operation, one source can work at MPPT if the desired load power is greater than the source power.

References

[1]Yaow-Ming Chen, Yuan-Chuan Liu and Feng-Yu Wu, "Multi-input DC/DC converter based on the multiwinding transformer for renewable energy applications", IEEE Transactions on Industry Applications, vol. 38, no. 4, pp. 1096-1104, 2002. Available: 10.1109/tia.2002.800776.

[2]Y. Liu and Y. Chen, "A Systematic Approach to Synthesizing Multi-Input DC–DC Converters", IEEE Transactions on Power Electronics, vol. 24, no. 1, pp. 116-127, 2009. Available: 10.1109/tpel.2008.2009170.

[3]Y. Jiao, F. Luo and M. Zhu, "Generalised modelling and sliding mode control for n-cell cascade super-lift DC–DC converters", IET Power Electronics, vol. 4, no. 5, p. 532, 2011. Available: 10.1049/iet-pel.2010.0049.

[4]S. Danyali, S. Hosseini and G. Gharehpetian, "New Extendable Single-Stage Multi-input DC–DC/AC Boost Converter", IEEE Transactions on Power Electronics, vol. 29, no. 2, pp. 775-788, 2014. Available: 10.1109/tpel.2013.2256468.

[5]M. Banaei, H. Ardi, R. Alizadeh and A. Farakhor, "Non- isolated multi- input–single- output DC/DC converter for photovoltaic power generation systems", IET Power Electronics, vol. 7, no. 11, pp. 2806-2816, 2014. Available: 10.1049/iet-pel.2013.0977.

[6]B. Mangu, S. Akshatha, D. Suryanarayana and B. Fernandes, "Grid-Connected PV-Wind-Battery-Based Multi-Input Transformer-Coupled Bidirectional DC-DC Converter for Household Applications", IEEE Journal of Emerging and Selected Topics in Power Electronics, vol. 4, no. 3, pp. 1086-1095, 2016. Available: 10.1109/jestpe.2016.2544789.

[7]M. Azizi, M. Mohamadian and R. Beiranvand, "A New Family of Multi-Input Converters Based on Three Switches Leg", IEEE Transactions on Industrial Electronics, vol. 63, no. 11, pp. 6812-6822, 2016. Available: 10.1109/tie.2016.2581765.

[8]C. Chen, C. Liao, K. Chen and Y. Chen, "Modeling and Controller Design of a Semi-isolated Multi-input Converter for a Hybrid PV/Wind Power Charger System", IEEE Transactions on Power Electronics, vol. 30, no. 9, pp. 4843-4853, 2015. Available: 10.1109/tpel.2014.2367594.

[9]S. Dusmez, X. Li and B. Akin, "A New Multiinput Three-Level DC/DC Converter", IEEE Transactions on Power Electronics, vol. 31, no. 2, pp. 1230-1240, 2016. Available: 10.1109/tpel.2015.2424246.

[10]R. Ling, D. Maksimovic and R. Leyva, "Second-Order Sliding-Mode Controlled Synchronous Buck DC–DC Converter", IEEE Transactions on Power Electronics, vol. 31, no. 3, pp. 2539-2549, 2016. Available: 10.1109/tpel.2015.2431193.

[11]S. Zerkaoui, F. Druaux, E. Leclercq and D. Lefebvre, "Stable adaptive control with recurrent neural networks for square MIMO non-linear systems", Engineering Applications of Artificial Intelligence, vol. 22, no. 4-5, pp. 702-717, 2009. Available: 10.1016/j.engappai.2008.12.005.

[12]Lin Xu, Xinbo Ruan, Chengxiong Mao, Buhan Zhang and Yi Luo, "An Improved Optimal Sizing Method for Wind-Solar-Battery Hybrid Power System", IEEE Transactions on Sustainable Energy, vol. 4, no. 3, pp. 774-785, 2013. Available: 10.1109/tste.2012.2228509.

[13]P. Shanthi, G. Uma and M. Keerthana, "Effective power transfer scheme for a grid connected hybrid wind/photovoltaic system", IET Renewable Power Generation, vol. 11, no. 7, pp. 1005-1017, 2017. Available: 10.1049/iet-rpg.2016.0592.

[14] V. Mummadi and K. K. Sawant, "Control of Multi-Input Integrated Buck-Boost Converter," 2008 IEEE Region 10 and the Third international Conference on Industrial and Information Systems, 2008, pp. 1-6, doi: 10.1109/ICIINFS.2008.4798489.

The following references, though have not been cited in the report, are used to complete the work successfully.

[1]Yaow-Ming Chen, Yuan-Chuan Liu and Feng-Yu Wu, "Multi-input DC/DC converter based on the multiwinding transformer for renewable energy applications", *IEEE Transactions on Industry Applications*, vol. 38, no. 4, pp. 1096-1104, 2002. Available: 10.1109/tia.2002.800776.

[2]S. Danyali, S. Hosseini and G. Gharehpetian, "New Extendable Single-Stage Multi-input DC–DC/AC Boost Converter", *IEEE Transactions on Power Electronics*, vol. 29, no. 2, pp. 775-788, 2014. Available: 10.1109/tpel.2013.2256468.

[3]S. Danyali, S. Mozaffari Niapour, S. Hosseini, G. Gharehpetian and M. Sabahi, "New Single-Stage Single-Phase Three-Input DC-AC Boost Converter for Stand-Alone Hybrid PV/FC/UC Systems", *Electric Power Systems Research*, vol. 127, pp. 1-12, 2015. Available: 10.1016/j.epsr.2015.05.008.

[4]M. Banaei, H. Ardi, R. Alizadeh and A. Farakhor, "Non- isolated multi- input–single- output DC/DC converter for photovoltaic power generation systems", *IET Power Electronics*, vol. 7, no. 11, pp. 2806-2816, 2014. Available: 10.1049/iet-pel.2013.0977.

[5]B. Mangu, S. Akshatha, D. Suryanarayana and B. Fernandes, "Grid-Connected PV-Wind-Battery-Based Multi-Input Transformer-Coupled Bidirectional DC-DC Converter for Household Applications", *IEEE Journal of Emerging and Selected Topics in Power Electronics*, vol. 4, no. 3, pp. 1086-1095, 2016. Available: 10.1109/jestpe.2016.2544789.

[6]M. Azizi, M. Mohamadian and R. Beiranvand, "A New Family of Multi-Input Converters Based on Three Switches Leg", *IEEE Transactions on Industrial Electronics*, vol. 63, no. 11, pp. 6812-6822, 2016. Available: 10.1109/tie.2016.2581765.

[7]C. Chen, C. Liao, K. Chen and Y. Chen, "Modeling and Controller Design of a Semi isolated Multi input Converter for a Hybrid PV/Wind Power Charger System", *IEEE Transactions on Power Electronics*, vol. 30, no. 9, pp. 4843-4853, 2015. Available: 10.1109/tpel.2014.2367594.

[8]S. Dusmez, X. Li and B. Akin, "A New Multiinput Three-Level DC/DC Converter", *IEEE Transactions on Power Electronics*, vol. 31, no. 2, pp. 1230-1240, 2016. Available: 10.1109/tpel.2015.2424246.

[9]E. Babaei and O. Abbasi, "Structure for multi- input multi- output dc–dc boost converter", *IET Power Electronics*, vol. 9, no. 1, pp. 9-19, 2016. Available: 10.1049/iet-pel.2014.0985.

[10]J. Sebastian, P. Villegas, F. Nuno and M. Hernando, "High-efficiency and wide-bandwidth performance obtainable from a two-input buck converter", *IEEE Transactions on Power Electronics*, vol. 13, no. 4, pp. 706-717, 1998. Available: 10.1109/63.704143.

[11]K. Kobayashi, H. Matsuo and Y. Sekine, "Novel Solar-Cell Power Supply System Using a Multiple-Input DC–DC Converter", *IEEE Transactions on Industrial Electronics*, vol. 53, no. 1, pp. 281-286, 2006. Available: 10.1109/tie.2005.862250.

[12]A. Khaligh, Jian Cao and Young-Joo Lee, "A Multiple-Input DC–DC Converter Topology", *IEEE Transactions on Power Electronics*, vol. 24, no. 3, pp. 862-868, 2009. Available: 10.1109/tpel.2008.2009308.

[13]S. Khosrogorji, M. Ahmadian, H. Torkaman and S. Soori, "Multi-input DC/DC converters in connection with distributed generation units – A review", *Renewable and Sustainable Energy Reviews*, vol. 66, pp. 360-379, 2016. Available: 10.1016/j.rser.2016.07.023.

[14]Y. Liu and Y. Chen, "A Systematic Approach to Synthesizing Multi-Input DC–DC Converters", *IEEE Transactions on Power Electronics*, vol. 24, no. 1, pp. 116-127, 2009. Available: 10.1109/tpel.2008.2009170.

[15]L. Xian, G. Wang and Y. Wang, "Subproportion control of double input buck converter for fuel cell/battery hybrid power supply system", *IET Power Electronics*, vol. 7, no. 8, pp. 2141-2150, 2014. Available: 10.1049/iet-pel.2013.0353.

[16]C. Onwuchekwa and A. Kwasinski, "A Modified-Time-Sharing Switching Technique for Multiple-Input DC–DC Converters", *IEEE Transactions on Power Electronics*, vol. 27, no. 11, pp. 4492-4502, 2012. Available: 10.1109/tpel.2011.2180740.

[17]S. Hou, J. Chen, T. Sun and X. Bi, "Multi-input Step-Up Converters Based on the Switched-Diode-Capacitor Voltage Accumulator", *IEEE Transactions on Power Electronics*, vol. 31, no. 1, pp. 381-393, 2016. Available: 10.1109/tpel.2015.2399853.

[18]M. Jabbari and M. Dorcheh, "Resonant Multi-input/Multi-output/Bidirectional ZCS Step-Down DC--DC Converter With Systematic Synthesis for Point-to-Point Power Routing", *IEEE Transactions on Power Electronics*, vol. 33, no. 7, pp. 6024-6032, 2018. Available: 10.1109/tpel.2017.2749326.

[19]D. Yang, M. Yang and X. Ruan, "One-Cycle Control for a Double-Input DC/DC Converter", *IEEE Transactions on Power Electronics*, vol. 27, no. 11, pp. 4646-4655, 2012. Available: 10.1109/tpel.2011.2164582.

[20]Zhijun Qian, O. Abdel-Rahman, H. Al-Atrash and I. Batarseh, "Modeling and Control of Three-Port DC/DC Converter Interface for Satellite Applications", *IEEE Transactions on Power Electronics*, vol. 25, no. 3, pp. 637-649, 2010. Available: 10.1109/tpel.2009.2033926.

[21]W. Nwesaty, A. Iuliana Bratcu and O. Sename, "Power sources coordination through multivariable linear parameter- varying/ control with application to multi- source electric vehicles", *IET Control Theory & Applications*, vol. 10, no. 16, pp. 2049-2059, 2016. Available: 10.1049/iet-cta.2015.1163.

[22]M. Veerachary, "Two-Loop Controlled Buck–SEPIC Converter for Input Source Power Management", *IEEE Transactions on Industrial Electronics*, vol. 59, no. 11, pp. 4075-4087, 2012. Available: 10.1109/tie.2011.2174530.

[23]Y. Chen, Y. Liu, S. Hung and C. Cheng, "Multi-Input Inverter for Grid-Connected Hybrid PV/Wind Power System", *IEEE Transactions on Power Electronics*, vol. 22, no. 3, pp. 1070-1077, 2007. Available: 10.1109/tpel.2007.897117.

[24]C. Onwuchekwa and A. Kwasinski, "A Modified-Time-Sharing Switching Technique for Multiple-Input DC–DC Converters", *IEEE Transactions on Power Electronics*, vol. 27, no. 11, pp. 4492-4502, 2012. Available: 10.1109/tpel.2011.2180740.

[25]A. Sarikhani, B. Allahverdinejad, M. Hamzeh and E. Afjei, "A continuous input and output current quadratic buck-boost converter with positive output voltage for photovoltaic applications", *Solar Energy*, vol. 188, pp. 19-27, 2019. Available: 10.1016/j.solener.2019.05.025.

[26]H. Shi, X. Xiao, H. Wu and K. Sun, "Modeling and Decoupled Control of a Buck–Boost and Stacked Dual Half-Bridge Integrated Bidirectional DC–DC Converter", *IEEE Transactions on Power Electronics*, vol. 33, no. 4, pp. 3534-3551, 2018. Available: 10.1109/tpel.2017.2705131.

[27]W. Li, C. Xu, H. Luo, Y. Hu, X. He and C. Xia, "Decoupling-Controlled Triport Composited DC/DC Converter for Multiple Energy Interface", *IEEE Transactions on Industrial Electronics*, vol. 62, no. 7, pp. 4504-4513, 2015. Available: 10.1109/tie.2014.2385668.

[28]C. Zhao, S. Round and J. Kolar, "An Isolated Three-Port Bidirectional DC-DC Converter With Decoupled Power Flow Management", *IEEE Transactions on Power Electronics*, vol. 23, no. 5, pp. 2443-2453, 2008. Available: 10.1109/tpel.2008.2002056.

[29]Y. Chen, Y. Liu and S. Lin, "Double-Input PWM DC/DC Converter for High-/Low-Voltage Sources", *IEEE Transactions on Industrial Electronics*, vol. 53, no. 5, pp. 1538-1545, 2006. Available: 10.1109/tie.2006.882001.

[30]Z. Chen, "PI and Sliding Mode Control of a Cuk Converter", *IEEE Transactions on Power Electronics*, vol. 27, no. 8, pp. 3695-3703, 2012. Available: 10.1109/tpel.2012.2183891.

[31]N. Mukherjee and D. Strickland, "Control of Cascaded DC-DC Converter Based Hybrid Battery Energy Storage Systems: Part – I: Stability Issue", *IEEE Transactions on Industrial Electronics*, pp. 1-1, 2015. Available: 10.1109/tie.2015.2509911.

[32]A. Jaafar, A. Alawieh, R. Ortega, E. Godoy and P. Lefranc, "PI Stabilization of Power Converters With Partial State Measurements", *IEEE Transactions on Control Systems Technology*, vol. 21, no. 2, pp. 560-568, 2013. Available: 10.1109/tcst.2012.2186368.

[33]S. Kim, C. Park, J. Kim and Y. Lee, "A Stabilizing Model Predictive Controller for Voltage Regulation of a DC/DC Boost Converter", *IEEE Transactions on Control Systems Technology*, vol. 22, no. 5, pp. 2016-2023, 2014. Available: 10.1109/tcst.2013.2296508.

[34]L. Cavanini, G. Cimini and G. Ippoliti, "Model predictive control for pre-compensated power converters: Application to current mode control", *Journal of the Franklin Institute*, vol. 356, no. 4, pp. 2015-2030, 2019. Available: 10.1016/j.jfranklin.2019.01.032.

[35]Y. Chen, S. Zhao, Z. Li and Y. Kang, "Multi- object control of an isolated DC–DC modular multilevel converter", *IET Power Electronics*, vol. 11, no. 8, pp. 1338-1349, 2018. Available: 10.1049/iet-pel.2017.0151.

[36]S. Athikkal, G. Kumar, K. Sundaramoorthy and A. Sankar, "Performance Analysis of Novel Bridge Type Dual Input DC-DC Converters", *IEEE Access*, vol. 5, pp. 15340-15353, 2017. Available: 10.1109/access.2017.2734328.

[37]R. Saadi et al., "Dual loop controllers using PI, sliding mode and flatness controls applied to low voltage converters for fuel cell applications", *International Journal of Hydrogen Energy*, vol. 41, no. 42, pp. 19154-19163, 2016. Available: 10.1016/j.ijhydene.2016.08.171.

[38]F. Liu, Z. Wang, Y. Mao and X. Ruan, "Asymmetrical Half-Bridge Double-Input DC/DC Converters Adopting Pulsating Voltage Source Cells for Low Power Applications", *IEEE Transactions on Power Electronics*, vol. 29, no. 9, pp. 4741-4751, 2014. Available: 10.1109/tpel.2013.2257858.

[39]J. Hung, W. Gao and J. Hung, "Variable structure control: a survey", *IEEE Transactions on Industrial Electronics*, vol. 40, no. 1, pp. 2-22, 1993. Available: 10.1109/41.184817.

[40]V. Utkin, "Variable structure systems with sliding modes", *IEEE Transactions on Automatic Control*, vol. 22, no. 2, pp. 212-222, 1977. Available: 10.1109/tac.1977.1101446.

[41]J. Silva, "Sliding-mode control of boost-type unity-power-factor PWM rectifiers", *IEEE Transactions on Industrial Electronics*, vol. 46, no. 3, pp. 594-603, 1999. Available: 10.1109/41.767067.

[42]N. Kumar, T. Saha and J. Dey, "Sliding-Mode Control of PWM Dual Inverter-Based Grid-Connected PV System: Modeling and Performance Analysis", *IEEE Journal of Emerging and Selected Topics in Power Electronics*, vol. 4, no. 2, pp. 435-444, 2016. Available: 10.1109/jestpe.2015.2497900.

[43]A. Mallik, J. Lu and A. Khaligh, "Sliding Mode Control of Single-Phase Interleaved Totem-Pole PFC for Electric Vehicle Onboard Chargers", *IEEE Transactions on Vehicular Technology*, vol. 67, no. 9, pp. 8100-8109, 2018. Available: 10.1109/tvt.2018.2848238.

[44]Z. Tian, Z. Lyu, J. Yuan and C. Wang, "UDE-based sliding mode control of DC–DC power converters with uncertainties", *Control Engineering Practice*, vol. 83, pp. 116-128, 2019. Available: 10.1016/j.conengprac.2018.10.019.

[45]J. Liu, Y. Yin, W. Luo, S. Vazquez, L. Franquelo and L. Wu, "Sliding Mode Control of a Three-Phase AC/DC Voltage Source Converter Under Unknown Load Conditions: Industry Applications", *IEEE Transactions on Systems, Man, and Cybernetics: Systems*, vol. 48, no. 10, pp. 1771-1780, 2018. Available: 10.1109/tsmc.2017.2758598.

[46]Y. Jeung and D. Lee, "Voltage and Current Regulations of Bidirectional Isolated Dual-Active-Bridge DC–DC Converters Based on a Double-Integral Sliding Mode Control", *IEEE Transactions on Power Electronics*, vol. 34, no. 7, pp. 6937-6946, 2019. Available: 10.1109/tpel.2018.2873834.

[47]A. Momeneh, M. Castilla, M. Moradi Ghahderijani, J. Miret and L. Garcia de Vicuña, "Analysis, design and implementation of a DC/DC boost resonant- inductor converter with sliding- mode control", *IET Power Electronics*, vol. 11, no. 3, pp. 460-467, 2018. Available: 10.1049/iet-pel.2017.0234.

[48]M. Moradi Ghahderijani, M. Castilla, A. Momeneh, J. Miret and L. García de Vicuña, "Robust and fast sliding- mode control for a DC–DC current- source parallel- resonant converter", *IET Power Electronics*, vol. 11, no. 2, pp. 262-271, 2018. Available: 10.1049/iet-pel.2017.0033.

[49]A. Goudarzian, A. Khosravi and N. Abjadi, "Sliding mode current control of a NOCULL converter based on hysteresis modulation method in a wide range of operating conditions", *ISA Transactions*, vol. 85, pp. 214-225, 2019. Available: 10.1016/j.isatra.2018.10.007.

[50]S. Banerjee and K. Chakrabarty, "Nonlinear modeling and bifurcations in the boost converter", *IEEE Transactions on Power Electronics*, vol. 13, no. 2, pp. 252-260, 1998. Available: 10.1109/63.662832.

[51]J. Deane, "Chaos in a current-mode controlled boost DC-DC converter", *IEEE Transactions on Circuits and Systems I: Fundamental Theory and Applications*, vol. 39, no. 8, pp. 680-683, 1992. Available: 10.1109/81.168922.

[52]K. Cheng, M. Liu and J. Wu, "Chaos study and parameter-space analysis of the DC–DC buck–boost converter", *IEE Proceedings - Electric Power Applications*, vol. 150, no. 2, p. 126, 2003. Available: 10.1049/ip-epa:20030228.

[53]S. Maity, D. Tripathy, T. Bhattacharya and S. Banerjee, "Bifurcation Analysis of PWM-1 Voltage-Mode-Controlled Buck Converter Using the Exact Discrete Model", *IEEE Transactions on Circuits and Systems I: Regular Papers*, vol. 54, no. 5, pp. 1120-1130, 2007. Available: 10.1109/tcsi.2007.895526.

[54]W. Hu, B. Zhang, R. Yang and D. Qiu, "Dynamic behaviours of constant on- time one- cycle controlled boost converter", *IET Power Electronics*, vol. 11, no. 1, pp. 160-167, 2018. Available: 10.1049/iet-pel.2016.1013.

[55]H. Wu, V. Pickert, D. Giaouris and B. Ji, "Nonlinear Analysis and Control of Interleaved Boost Converter Using Real-Time Cycle to Cycle Variable Slope Compensation", *IEEE Transactions on Power Electronics*, vol. 32, no. 9, pp. 7256-7270, 2017. Available: 10.1109/tpel.2016.2626119.

[56]D. Yu, Y. Geng, H. Iu, T. Fernando and R. Xu, "Pulse Phase Shift Based Low-Frequency Oscillation Suppression for PT Controlled CCM Buck Converter", *IEEE Transactions on Circuits and Systems II: Express Briefs*, vol. 65, no. 10, pp. 1465-1469, 2018. Available: 10.1109/tcsii.2018.2863698.

[57]P. Deivasundari, G. Uma and R. Poovizhi, "Analysis and experimental verification of Hopf bifurcation in a solar photovoltaic powered hysteresis current- controlled cascaded- boost converter", *IET Power Electronics*, vol. 6, no. 4, pp. 763-773, 2013. Available: 10.1049/iet-pel.2012.0437.

[58]Y. Wang, J. Xu and D. Xu, "Effect of Circuit Parameters on the Stability and Boundaries of Peak Current Mode Single-Inductor Dual-Output Buck Converters", *IEEE Transactions on Industrial Electronics*, vol. 65, no. 7, pp. 5445-5455, 2018. Available: 10.1109/tie.2017.2774769.

[59]S. Zhou, G. Zhou, Y. Wang, X. Liu and S. Xu, "Bifurcation analysis and operation region estimation of current- mode- controlled SIDO boost converter", *IET Power Electronics*, vol. 10, no. 7, pp. 846-853, 2017. Available: 10.1049/iet-pel.2016.0539.

[60]F. Kardan, R. Alizadeh and M. Banaei, "A New Three Input DC/DC Converter for Hybrid PV/FC/Battery Applications", *IEEE Journal of Emerging and Selected Topics in Power Electronics*, vol. 5, no. 4, pp. 1771-1778, 2017. Available: 10.1109/jestpe.2017.2731816.

[61]S. Athikkal, G. Kumar, K. Sundaramoorthy and A. Sankar, "Performance Analysis of Novel Bridge Type Dual Input DC-DC Converters", *IEEE Access*, vol. 5, pp. 15340-15353, 2017. Available: 10.1109/access.2017.2734328.

[62]S. Athikkal, G. Kumar, K. Sundaramoorthy and A. Sankar, "Performance Analysis of Novel Bridge Type Dual Input DC-DC Converters", *IEEE Access*, vol. 5, pp. 15340-15353, 2017. Available: 10.1109/access.2017.2734328.

[63]A. Geetha, C. Subramani and V. Krithika, "Development and Analysis of Switched Capacitor Four Quadrant DC-DC Converter for Hybrid Electric Vehicle", *Indian Journal of Science and Technology*, vol. 9, no. 22, 2016. Available: 10.17485/ijst/2016/v9i22/93085.

[64]M. Cheng and Y. Zhu, "The state of the art of wind energy conversion systems and technologies: A review", *Energy Conversion and Management*, vol. 88, pp. 332-347, 2014. Available: 10.1016/j.enconman.2014.08.037.

[65]M. Cheng and Y. Zhu, "The state of the art of wind energy conversion systems and technologies: A review", *Energy Conversion and Management*, vol. 88, pp. 332-347, 2014. Available: 10.1016/j.enconman.2014.08.037.

[66]A. Shotorbani, B. Mohammadi-Ivatloo, L. Wang, M. Marzband and M. Sabahi, "Application of finite-time control Lyapunov function in low-power PMSG wind energy conversion systems for sensorless MPPT", *International Journal of Electrical Power & Energy Systems*, vol. 106, pp. 169-182, 2019. Available: 10.1016/j.ijepes.2018.09.039.

[67]A. Shotorbani, B. Mohammadi-Ivatloo, L. Wang, M. Marzband and M. Sabahi, "Application of finite-time control Lyapunov function in low-power PMSG wind energy conversion systems for sensorless MPPT", *International Journal of Electrical Power & Energy Systems*, vol. 106, pp. 169-182, 2019. Available: 10.1016/j.ijepes.2018.09.039.

[68]G. Marques and M. Iacchetti, "Stator Frequency Regulation in a Field-Oriented Controlled DFIG Connected to a DC Link", *IEEE Transactions on Industrial Electronics*, vol. 61, no. 11, pp. 5930-5939, 2014. Available: 10.1109/tie.2014.2311403.

[69]G. Marques and M. Iacchetti, "Stator Frequency Regulation in a Field-Oriented Controlled DFIG Connected to a DC Link", *IEEE Transactions on Industrial Electronics*, vol. 61, no. 11, pp. 5930-5939, 2014. Available: 10.1109/tie.2014.2311403.

[70]X. Qi and J. Holtz, "Modeling and Control of Low Switching Frequency High-Performance Induction Motor Drives", *IEEE Transactions on Industrial Electronics*, vol. 67, no. 6, pp. 4402-4410, 2020. Available: 10.1109/tie.2019.2924602.

[71]X. Qi and J. Holtz, "Modeling and Control of Low Switching Frequency High-Performance Induction Motor Drives", *IEEE Transactions on Industrial Electronics*, vol. 67, no. 6, pp. 4402-4410, 2020. Available: 10.1109/tie.2019.2924602.

[72]A. Gundavarapu, H. Misra and A. Jain, "Direct Torque Control Scheme for DC Voltage Regulation of the Standalone DFIG-DC System", *IEEE Transactions on Industrial Electronics*, vol. 64, no. 5, pp. 3502-3512, 2017. Available: 10.1109/tie.2016.2644623.

[73]A. Gundavarapu, H. Misra and A. Jain, "Direct Torque Control Scheme for DC Voltage Regulation of the Standalone DFIG-DC System", *IEEE Transactions on Industrial Electronics*, vol. 64, no. 5, pp. 3502-3512, 2017. Available: 10.1109/tie.2016.2644623.

[74]X. Zhang, Y. Li, K. Wang, W. Zhang and D. Gao, "Model Predictive Control of the Open-winding PMSG System Based on Three-Dimensional Reference Voltage-Vector", *IEEE Transactions on Industrial Electronics*, vol. 67, no. 8, pp. 6312-6322, 2020. Available: 10.1109/tie.2019.2938478.

[75]X. Zhang, Y. Li, K. Wang, W. Zhang and D. Gao, "Model Predictive Control of the Open-winding PMSG System Based on Three-Dimensional Reference Voltage-Vector", *IEEE Transactions on Industrial Electronics*, vol. 67, no. 8, pp. 6312-6322, 2020. Available: 10.1109/tie.2019.2938478.

[76]V. Phan, D. Nguyen, Q. Trinh, C. Nguyen and T. Logenthiran, "Harmonics Rejection in Stand-Alone Doubly-Fed Induction Generators With Nonlinear Loads", *IEEE Transactions on Energy Conversion*, vol. 31, no. 2, pp. 815-817, 2016. Available: 10.1109/tec.2016.2521331.

[77]V. Phan, D. Nguyen, Q. Trinh, C. Nguyen and T. Logenthiran, "Harmonics Rejection in Stand-Alone Doubly-Fed Induction Generators With Nonlinear Loads", *IEEE Transactions on Energy Conversion*, vol. 31, no. 2, pp. 815-817, 2016. Available: 10.1109/tec.2016.2521331.

[78]M. Cheng, Y. Jiang, P. Han and Q. Wang, "Unbalanced and Low-Order Harmonic Voltage Mitigation of Stand-Alone Dual-Stator Brushless Doubly Fed Induction Wind Generator", *IEEE Transactions on Industrial Electronics*, vol. 65, no. 11, pp. 9135-9146, 2018. Available: 10.1109/tie.2017.2779422.

[79]M. Cheng, Y. Jiang, P. Han and Q. Wang, "Unbalanced and Low-Order Harmonic Voltage Mitigation of Stand-Alone Dual-Stator Brushless Doubly Fed Induction Wind Generator", *IEEE Transactions on Industrial Electronics*, vol. 65, no. 11, pp. 9135-9146, 2018. Available: 10.1109/tie.2017.2779422.

[80]A. Naderipour, Z. Abdul-Malek, V. Ramachandaramurthy, A. Kalam and M. Miveh, "Hierarchical control strategy for a three-phase 4-wire microgrid under unbalanced and nonlinear load conditions", *ISA Transactions*, vol. 94, pp. 352-369, 2019. Available: 10.1016/j.isatra.2019.04.025.

[81]A. Satpathy, D. Kastha and K. Kishore, "Control of a STATCOM- assisted self- excited induction generator- based WECS feeding nonlinear three- phase and single- phase loads", *IET Power Electronics*, vol. 12, no. 4, pp. 829-839, 2019. Available: 10.1049/iet-pel.2018.5482.

[82]A. Giri, S. Arya, R. Maurya and B. Babu, "Mitigation of power quality problems in PMSG- based power generation system using quasi- Newton–based algorithm", *International Transactions on Electrical Energy Systems*, vol. 29, no. 11, 2019. Available: 10.1002/2050-7038.12102.

[83]J. Dannehl, C. Wessels and F. Fuchs, "Limitations of Voltage-Oriented PI Current Control of Grid-Connected PWM Rectifiers With LCL Filters", *IEEE Transactions on Industrial Electronics*, vol. 56, no. 2, pp. 380-388, 2009. Available: 10.1109/tie.2008.2008774.

[84]B. Singh and S. Sharma, "Voltage and frequency controllers for standalone wind energy conversion systems", *IET Renewable Power Generation*, vol. 8, no. 6, pp. 707-721, 2014. Available: 10.1049/iet-rpg.2013.0186.

[85]C. Tischer, J. Tibola, L. Scherer and R. Camargo, "Proportional- resonant control applied on voltage regulation of standalone SEIG for micro- hydro power generation", *IET Renewable Power Generation*, vol. 11, no. 5, pp. 593-602, 2017. Available: 10.1049/iet-rpg.2016.0857.

[86]B. Singh, R. Niwas and S. Dube, "Load Leveling and Voltage Control of Permanent Magnet Synchronous Generator-Based DG Set for Standalone Supply System", *IEEE Transactions on Industrial Informatics*, vol. 10, no. 4, pp. 2034-2043, 2014. Available: 10.1109/tii.2014.2341952.

[87]M. Liserre, R. Cardenas, M. Molinas and J. Rodriguez, "Overview of Multi-MW Wind Turbines and Wind Parks", *IEEE Transactions on Industrial Electronics*, vol. 58, no. 4, pp. 1081-1095, 2011. Available: 10.1109/tie.2010.2103910.

[88]Z. Alnasir and M. Kazerani, "An analytical literature review of standalone wind energy conversion systems from generator viewpoint", *Renewable and Sustainable Energy Reviews*, vol. 28, pp. 597-615, 2013. Available: 10.1016/j.rser.2013.08.027.

[89]Z. Zhang, F. Wang, J. Wang, J. Rodriguez and R. Kennel, "Nonlinear Direct Control for Three-Level NPC Back-to-Back Converter PMSG Wind Turbine Systems: Experimental Assessment With FPGA", *IEEE Transactions on Industrial Informatics*, vol. 13, no. 3, pp. 1172-1183, 2017. Available: 10.1109/tii.2017.2678500.

[90]F. Blaabjerg and Ke Ma, "Future on Power Electronics for Wind Turbine Systems", *IEEE Journal of Emerging and Selected Topics in Power Electronics*, vol. 1, no. 3, pp. 139-152, 2013. Available: 10.1109/jestpe.2013.2275978.

[91]F. Blaabjerg, R. Teodorescu, M. Liserre and A. Timbus, "Overview of Control and Grid Synchronization for Distributed Power Generation Systems", *IEEE Transactions on Industrial Electronics*, vol. 53, no. 5, pp. 1398-1409, 2006. Available: 10.1109/tie.2006.881997.

[92]T. Tran, T. Chun, H. Lee, H. Kim and E. Nho, "PLL-Based Seamless Transfer Control Between Grid-Connected and Islanding Modes in Grid-Connected Inverters", *IEEE Transactions on Power Electronics*, vol. 29, no. 10, pp. 5218-5228, 2014. Available: 10.1109/tpel.2013.2290059.

[93]P. Rodríguez, A. Luna, R. Muñoz-Aguilar, I. Etxeberria-Otadui, R. Teodorescu and F. Blaabjerg, "A Stationary Reference Frame Grid Synchronization System for Three-Phase Grid-Connected Power Converters Under Adverse Grid Conditions", *IEEE Transactions on Power Electronics*, vol. 27, no. 1, pp. 99-112, 2012. Available: 10.1109/tpel.2011.2159242.

[94]Y. Wang, B. Ren and Q. Zhong, "Robust Power Flow Control of Grid-Connected Inverters", *IEEE Transactions on Industrial Electronics*, vol. 63, no. 11, pp. 6887-6897, 2016. Available: 10.1109/tie.2016.2586439.

[95]F. Cai, D. Lu, Q. Lin and W. Wang, "Control Strategy Design of Grid-Connected and Stand-Alone Single-Phase Inverter for Distributed Generation", *Journal of Power Electronics*, vol. 16, no. 5, pp. 1813-1820, 2016. Available: 10.6113/jpe.2016.16.5.1813.

[96]J. Mohammadi, S. Vaez- Zadeh, E. Ebrahimzadeh and F. Blaabjerg, "Combined control method for grid- side converter of doubly fed induction generator- based wind energy conversion systems", *IET Renewable Power Generation*, vol. 12, no. 8, pp. 943-952, 2018. Available: 10.1049/iet-rpg.2017.0539.

[97]H. Nian, Y. Shen, H. Yang and Y. Quan, "Flexible Grid Connection Technique of Voltage-Source Inverter Under Unbalanced Grid Conditions Based on Direct Power Control", *IEEE Transactions on Industry Applications*, vol. 51, no. 5, pp. 4041-4050, 2015. Available: 10.1109/tia.2015.2428219.

[98]M. Zarei, C. Veganzones Nicolas and J. Rodriguez Arribas, "Improved Predictive Direct Power Control of Doubly Fed Induction Generator During Unbalanced Grid Voltage Based on Four Vectors", *IEEE Journal of Emerging and Selected Topics in Power Electronics*, vol. 5, no. 2, pp. 695-707, 2017. Available: 10.1109/jestpe.2016.2611004.

[99]Dawei Zhi, Lie Xu and B. Williams, "Model-Based Predictive Direct Power Control of Doubly Fed Induction Generators", *IEEE Transactions on Power Electronics*, vol. 25, no. 2, pp. 341-351, 2010. Available: 10.1109/tpel.2009.2028139.

[100]J. Hu, J. Zhu and D. Dorrell, "Predictive Direct Power Control of Doubly Fed Induction Generators Under Unbalanced Grid Voltage Conditions for Power Quality Improvement", *IEEE Transactions on Sustainable Energy*, vol. 6, no. 3, pp. 943-950, 2015. Available: 10.1109/tste.2014.2341244.

[101]X. Li, H. Zhang, M. Shadmand and R. Balog, "Model Predictive Control of a Voltage-Source Inverter With Seamless Transition Between Islanded and Grid-Connected Operations", *IEEE Transactions on Industrial Electronics*, vol. 64, no. 10, pp. 7906-7918, 2017. Available: 10.1109/tie.2017.2696459.

[102]T. Dragicevic, "Model Predictive Control of Power Converters for Robust and Fast Operation of AC Microgrids", *IEEE Transactions on Power Electronics*, vol. 33, no. 7, pp. 6304-6317, 2018. Available: 10.1109/tpel.2017.2744986.

[103]X. Wei, M. Cheng, J. Zhu, H. Yang and R. Luo, "Finite-Set Model Predictive Power Control of Brushless Doubly Fed Twin Stator Induction Generator", *IEEE Transactions on Power Electronics*, vol. 34, no. 3, pp. 2300-2311, 2019. Available: 10.1109/tpel.2018.2845129.

[104]M. Abdelrahem, C. Hackl, R. Kennel and J. Rodriguez, "Efficient Direct-Model Predictive Control With Discrete-Time Integral Action for PMSGs", *IEEE Transactions on Energy Conversion*, vol. 34, no. 2, pp. 1063-1072, 2019. Available: 10.1109/tec.2018.2872626.

[105]X. Liu, D. Wang and Z. Peng, "An improved finite control-set model predictive control for nested neutral point-clamped converters under both balanced and unbalanced grid conditions", *International Journal of Electrical Power & Energy Systems*, vol. 104, pp. 910-923, 2019. Available: 10.1016/j.ijepes.2018.07.046.

[106]N. Jin, C. Gan and L. Guo, "Predictive Control of Bidirectional Voltage Source Converter With Reduced Current Harmonics and Flexible Power Regulation Under Unbalanced Grid", *IEEE Transactions on Energy Conversion*, vol. 33, no. 3, pp. 1118-1131, 2018. Available: 10.1109/tec.2017.2781692.

[107]M. Liserre, R. Cardenas, M. Molinas and J. Rodriguez, "Overview of Multi-MW Wind Turbines and Wind Parks", IEEE Transactions on Industrial Electronics, vol. 58, no. 4, pp. 1081-1095, 2011. Available: 10.1109/tie.2010.2103910.

[108]K. Fischer et al., "Reliability of Power Converters in Wind Turbines: Exploratory Analysis of Failure and Operating Data From a Worldwide Turbine Fleet", IEEE Transactions on Power Electronics, vol. 34, no. 7, pp. 6332-6344, 2019. Available: 10.1109/tpel.2018.2875005.

[109]J. Mohammadi, S. Vaez- Zadeh, E. Ebrahimzadeh and F. Blaabjerg, "Combined control method for grid- side converter of doubly fed induction generator- based wind energy conversion

systems", IET Renewable Power Generation, vol. 12, no. 8, pp. 943-952, 2018. Available: 10.1049/iet-rpg.2017.0539.

[110]M. Achkar, R. Mbayed, G. Salloum, N. Patin and E. Monmasson, "Voltage Control of a Standalone Cascaded Doubly Fed Induction Generator", IEEE Transactions on Industrial Electronics, vol. 66, no. 1, pp. 762-771, 2019. Available: 10.1109/tie.2018.2856186.

[111]M. Pattnaik and D. Kastha, "Unbalance and harmonic voltage compensation for a standalone variable speed constant frequency double- output induction generator supplying nonlinear and unbalanced loads", IET Electric Power Applications, vol. 7, no. 1, pp. 27-38, 2013. Available: 10.1049/iet-epa.2012.0038.

[112]M. Haque, M. Negnevitsky and K. Muttaqi, "A Novel Control Strategy for a Variable-Speed Wind Turbine With a Permanent-Magnet Synchronous Generator", IEEE Transactions on Industry Applications, vol. 46, no. 1, pp. 331-339, 2010. Available: 10.1109/tia.2009.2036550.

[113]N. Mendis, K. Muttaqi, S. Sayeef and S. Perera, "Standalone Operation of Wind Turbine-Based Variable Speed Generators With Maximum Power Extraction Capability", IEEE Transactions on Energy Conversion, vol. 27, no. 4, pp. 822-834, 2012. Available: 10.1109/tec.2012.2206594.

[114]J. Leon, S. Kouro, L. Franquelo, J. Rodriguez and B. Wu, "The Essential Role and the Continuous Evolution of Modulation Techniques for Voltage-Source Inverters in the Past, Present, and Future Power Electronics", IEEE Transactions on Industrial Electronics, vol. 63, no. 5, pp. 2688-2701, 2016. Available: 10.1109/tie.2016.2519321.

[115]P. Karamanakos, P. Stolze, R. Kennel, S. Manias and H. du Toit Mouton, "Variable Switching Point Predictive Torque Control of Induction Machines", IEEE Journal of Emerging and Selected Topics in Power Electronics, vol. 2, no. 2, pp. 285-295, 2014. Available: 10.1109/jestpe.2013.2296794.

[116]M. Zarei, C. Veganzones Nicolas and J. Rodriguez Arribas, "Improved Predictive Direct Power Control of Doubly Fed Induction Generator During Unbalanced Grid Voltage Based on Four Vectors", IEEE Journal of Emerging and Selected Topics in Power Electronics, vol. 5, no. 2, pp. 695-707, 2017. Available: 10.1109/jestpe.2016.2611004.

[117]A. Bag, B. Subudhi and P. Ray, "Comparative Analysis of Sliding Mode Controller and Hysteresis Controller for Active Power Filtering in a Grid connected PV System", International Journal of Emerging Electric Power Systems, vol. 19, no. 1, 2018. Available: 10.1515/ijeeps-2017-0044.

[118]S. B and N. M, "DESIGN AND APPLICATION OF NEURO - FUZZY VECTOR CONTROL FOR RENEWABLE ENERGY DRIVEN DOUBLY - FED INDUCTION GENERATOR", Journal of Technological Advances and Scientific Research, vol. 1, no. 3, pp. 202-218, 2015. Available: 10.14260/jtasr/2015/25.

[119]X. Zhang, G. Foo, T. Jiao, T. Ngo and C. Lee, "A Simplified Deadbeat Based Predictive Torque Control for Three-Level Simplified Neutral Point Clamped Inverter Fed IPMSM Drives Using SVM", IEEE Transactions on Energy Conversion, vol. 34, no. 4, pp. 1906-1916, 2019. Available: 10.1109/tec.2019.2933465.

[120]X. Hao, X. Yang, T. Liu, L. Huang and W. Chen, "A Sliding-Mode Controller With Multiresonant Sliding Surface for Single-Phase Grid-Connected VSI With an LCL Filter", IEEE

Transactions on Power Electronics, vol. 28, no. 5, pp. 2259-2268, 2013. Available: 10.1109/tpel.2012.2218133.

[121]M. Kazmierkowski, "Predictive Control of Power Converters and Electrical Drives [Book News]", IEEE Industrial Electronics Magazine, vol. 6, no. 4, pp. 67-68, 2012. Available: 10.1109/mie.2012.2221371.

[122]M. Short and F. Abugchem, "A Microcontroller-Based Adaptive Model Predictive Control Platform for Process Control Applications", *Electronics*, vol. 6, no. 4, p. 88, 2017. Available: 10.3390/electronics6040088.

[123]T. Dragicevic, "Model Predictive Control of Power Converters for Robust and Fast Operation of AC Microgrids", *IEEE Transactions on Power Electronics*, vol. 33, no. 7, pp. 6304-6317, 2018. Available: 10.1109/tpel.2017.2744986.

[124]S. Cruz, G. Marques, P. Goncalves and M. Iacchetti, "Predictive Torque and Rotor Flux Control of a DFIG-DC System for Torque Ripple Compensation and Loss Minimization", *IEEE Transactions on Industrial Electronics*, vol. 65, no. 12, pp. 9301-9310, 2018. Available: 10.1109/tie.2018.2818667.

[125]R. Panigrahi, B. Subudhi and P. Panda, "Model predictive- based shunt active power filter with a new reference current estimation strategy", *IET Power Electronics*, vol. 8, no. 2, pp. 221-233, 2015. Available: 10.1049/iet-pel.2014.0276.

[126]"Enhanced Active Power Filter Action for Renewable Power Generation Systems", *International Journal of Science and Research (IJSR)*, vol. 5, no. 5, pp. 643-647, 2015. Available: 10.21275/v5i5.nov163394.

[127]X. KONG and X. LIU, "Nonlinear Model Predictive Control for DFIG-based Wind Power Generation", *Acta Automatica Sinica*, vol. 39, no. 5, pp. 636-643, 2014. Available: 10.3724/sp.j.1004.2013.00636.

[128]A. Kiselev, G. Catuogno, A. Kuznietsov and R. Leidhold, "Finite-Control-Set MPC for Open-Phase Fault-Tolerant Control of PM Synchronous Motor Drives", *IEEE Transactions on Industrial Electronics*, vol. 67, no. 6, pp. 4444-4452, 2020. Available: 10.1109/tie.2019.2931285.

[129]M. Abdelrahem, C. Hackl, R. Kennel and J. Rodriguez, "Efficient Direct-Model Predictive Control With Discrete-Time Integral Action for PMSGs", *IEEE Transactions on Energy Conversion*, vol. 34, no. 2, pp. 1063-1072, 2019. Available: 10.1109/tec.2018.2872626.

[130]X. Wei, M. Cheng, J. Zhu, H. Yang and R. Luo, "Finite-Set Model Predictive Power Control of Brushless Doubly Fed Twin Stator Induction Generator", *IEEE Transactions on Power Electronics*, vol. 34, no. 3, pp. 2300-2311, 2019. Available: 10.1109/tpel.2018.2845129.

[131]S. Li and J. Li, "Output Predictor-Based Active Disturbance Rejection Control for a Wind Energy Conversion System With PMSG", *IEEE Access*, vol. 5, pp. 5205-5214, 2017. Available: 10.1109/access.2017.2681697.

[132]J. Yan, H. Lin, Y. Feng, X. Guo, Y. Huang and Z. Zhu, "Improved sliding mode model reference adaptive system speed observer for fuzzy control of direct- drive permanent magnet synchronous generator wind power generation system", *IET Renewable Power Generation*, vol. 7, no. 1, pp. 28-35, 2013. Available: 10.1049/iet-rpg.2012.0081.

Conference Publication

SL. No.	Title of the paper	Authors	Conference Name	Conference place	Conference Date	Page No.	Doi
1.	Development and performance analysis of modified decoupler based control of double input DC-DC converter	Dibyendu Sen, Ruman Kalyan Mahapatra, Tapas Kumar Saha and Jayati Dey	International Conference on Power, Instrumentation, Control and Computing (PICC), IEEE conference	Thrissur, India	18-20 Jan. 2018	pp. 1-6	10.1109/ PICC.v 2018. 8384769.
2.	Control of Double Input Single Output Converter for Integration of PV Source	Dibyendu Sen, Tapas Kumar Saha and Jayati Dey	International Conference on Sustainable Energy Technologies and Systems (ICSETS), IEEE conference	Bhubaneswar, India, India	26 Feb.-1 March 2019	132-137	10.1109/ ICSETS. 2019. 8744907

Journal Publication

SL. No.	Title of the paper	Authors	Journal Name	Vol. No., Page No.	year	Doi	Impact Factor
1.	Development, implementation and performance analysis of decoupler based control of dual source DC-DC converter	Dibyendu Sen, Tapas Kumar Saha and Jayati Dey	International Journal of Electronics and Communications (AEÜ)	117, 153136	2020	10.1109/ PICC.v 2018. 8384769.	2.924
2.	Sliding mode control of double input buck buck–boost fused converter	Dibyendu Sen, Tapas Kumar Saha and Jayati Dey	Asian Journal of Control	Early view	2020	10.1002/asjc.2481	2.779